THE EVOLUTION OF THE PHYSICOCHEMICAL PROPERTIES OF AEROSOLS IN THE ATMOSPHERE

A Dissertation

by

JASON MICHAEL TOMLINSON

Submitted to the Office of Graduate Studies of
Texas A&M University
in partial fulfillment of the requirements for the degree of

DOCTOR OF PHILOSOPHY

December 2010

Major Subject: Atmospheric Sciences

The Evolution of the Physicochemical Properties of Aerosols in the Atmosphere

THE EVOLUTION OF THE PHYSICOCHEMICAL PROPERTIES OF AEROSOLS IN THE ATMOPSHERE

A Dissertation

by

JASON MICHAEL TOMLINSON

Submitted to the Office of Graduate Studies of
Texas A&M University
in partial fulfillment of the requirements for the degree of

DOCTOR OF PHILOSOPHY

Approved by:

Chair of Committee,	Donald R. Collins
Committee Members,	Kenneth P. Bowman
	Sarah D. Brooks
	Shari A. Yvon-Lewis
Head of Department,	Kenneth P. Bowman

December 2010

Major Subject: Atmospheric Sciences

ABSTRACT

The Evolution of the Physicochemical Properties of Aerosols in the Atmosphere.

(December 2010)

Jason Michael Tomlinson, B.S., Valparaiso University

Chair of Advisory Committee: Dr. Donald R. Collins

A Differential Mobility Analyzer/Tandem Differential Mobility Analyzer (DMA/TDMA) system was used to measure simultaneously the size distribution and hygroscopicity of the ambient aerosol population. The system was operated aboard the National Center for Atmospheric Research/National Science Foundation (NCAR/NSF) C-130 during the 2006 Megacity Initiative: Local and Global Research Observations (MILAGRO) field campaign followed by the 2006 Intercontinental Chemical Transport Experiment – Phase B (INTEX-B) field campaign.

The research flights for the MILAGRO campaign were conducted within the Mexico City basin and the region to the northeast within the pollution plume. The aerosol within the basin is dominated by organics with an average measured κ value of 0.21 +/- 0.18, 0.13 +/- 0.09, 0.09 +/- 0.06, 0.14 +/- 0.07, and 0.17 +/- 0.04 for dry particle diameters of 0.025, 0.050, 0.100, 0.200, and 0.300 μm, respectively. As the aerosols are transported away from the Mexico City Basin, secondary organic aerosol formation through oxidation and condensation of sulfate on the aerosols surface rapidly

increases the solubility of the aerosol. The most pronounced change occurs for a 0.100 μm diameter aerosol where, after 6 hours of transport, the average κ value increased by a factor of 3 to a κ of 0.29 +/- 0.13. The rapid increase in solubility increases the fraction of the aerosol size distribution that could be activated within a cloud.

The research flights for the INTEX-B field campaign investigated the evolution of the physicochemical properties of the Asian aerosol plume after 3 to 7 days of transport. The Asian aerosol within the free troposphere exhibited a bimodal growth distribution roughly 50% of the time. The more soluble mode of the growth distribution contributed between 67-80% of the overall growth distribution and had an average κ between 0.40 and 0.53 for dry particle diameters of 0.025, 0.050, 0.100, and 0.300 μm. The secondary mode was insoluble with an average κ between 0.01 and 0.05 for all dry particle diameters. Cloud condensation nuclei closure was attained at a supersaturation of 0.2% for all particles within the free troposphere by either assuming a pure ammonium bisulfate composition or a binary composition of ammonium bisulfate and an insoluble organic.

DEDICATION

To my family who always encouraged me to pursue my dreams.

And to my wife for her support and encouragement.

ACKNOWLEDGEMENTS

I would like to thank my advisor and committee chair, Dr. Collins, for his support and the opportunities he afforded me throughout my time as a graduate student at Texas A&M University. I also would like to thank my committee members, Dr. Bowman, Dr. Brooks, and Dr. Yvon-Lewis, for their guidance.

Thanks also to my colleagues, the faculty, and the staff within the Department of Atmospheric Sciences at Texas A&M University for their support. I also want to extend my gratitude to the National Science Foundation who funded this research under grant ATM-0514401. I also would like to thank the pilots, mechanics, and support crew for the National Science Foundation and National Center for Atmospheric Research C-130 aircraft. Without their dedicated efforts, the research presented within this dissertation would not have been possible.

Additional thanks to my employer, Pacific Northwest National Laboratory, manager, Dr. Schmid, and team members within the Atmospheric Radiation Measurement Aerial Facility. Without their support, the completion of this dissertation would not have been possible.

Thanks to my mother, father, and brother for their encouragement. Lastly, but most importantly, I owe a huge debt of gratitude to my wife, Michelle Niemeyer, for her patience, support, motivation, and love throughout this long and arduous process.

TABLE OF CONTENTS

Page

LIST OF FIGURES

Page

LIST OF TABLES

`

Page

Page

1. INTRODUCTION

1.1 Overview of Aerosols and Their Effects

Anthropogenically emitted aerosols and greenhouse gases alter the radiative budget of the Earth. Over the past twenty years, research has unraveled the effects of greenhouse gases on the Earth's radiative budget; however, the exact effects of aerosols are still debatable. Aerosols directly affect the magnitude of the incoming solar radiation by scattering and absorption depending on the composition. Aerosols composed of sulfate or organic carbon tend to scatter the incoming solar radiation back towards the top of the atmosphere. This tends to cool both the atmosphere and the surface of the Earth through the extinction of solar radiation [*Charlson et al.*, 1992; *Coakley et al.*, 1987; *Foster et al.*, 2007; *Schwartz*, 1996]. Aerosols composed of black carbon or dust tend to absorb the incoming solar radiation. At the level where absorption is occurring, the atmosphere is heated, which can suppress the formation of clouds. This is known as the "semidirect effect" [*Ackerman et al.*, 2000; *Cook and Highwood*, 2004; *Hansen et al.*, 1997; *Huang et al.*, 2007; *Jacobson*, 2002; *Johnson et al.*, 2004; *Menon et al.*, 2003]. The magnitude of the scattering or absorption is dependent on the aerosol optical properties, size distribution, sphericity, degree of internal mixing, and environmental conditions such as ambient relative humidity or extent of cloud cover above or below the aerosol layer [*Menon*, 2004].

This dissertation follows the style of the *Journal of Geophysical Research.*

Hydrophilic aerosols can indirectly affect the radiative budget of the Earth by altering the properties of clouds. The first indirect effect theorizes the increase in hydrophilic aerosols leads to an increase in the concentration of cloud condensation nuclei. Assuming constant liquid water content, this would lead to a decreased cloud droplet diameter and increased cloud albedo [*Twomey*, 1974; 1977]. A second indirect effect results from the decreased cloud droplet diameter, which lowers the efficiency of the collision and coalescence process. The decreased efficiency reduces the formation of precipitation and extends the lifetime of the cloud [*Albrecht*, 1989; *Lohmann and Feichter*, 2005] and cloud thickness [*Pincus and Baker*, 1994]. The magnitude of the indirect effect is dependent on a particle's ability to act as a cloud condensation nuclei (CCN), which is a function of the size, chemical composition, mixing state, and ambient environment [*Penner et al.*, 2001].

The current estimated magnitude of the direct and indirect effect is shown in Figure 1. The direct effect is estimated to have a net radiative forcing of -0.50 +/- 0.40 W/m^2, and the indirect effect is currently estimated to have a net radiative forcing of -0.7 W/m^2 as the median, with a 5 to 95% range of -0.3 to -1.8 W/m^2 [*Foster et al.*, 2007]. The total aerosol radiative forcing is estimated to have a cooling effect on the Earth's climate; however, there is still a large error in the estimation of the magnitude of this effect. The most uncertain effect of aerosols is the aerosol indirect effect.

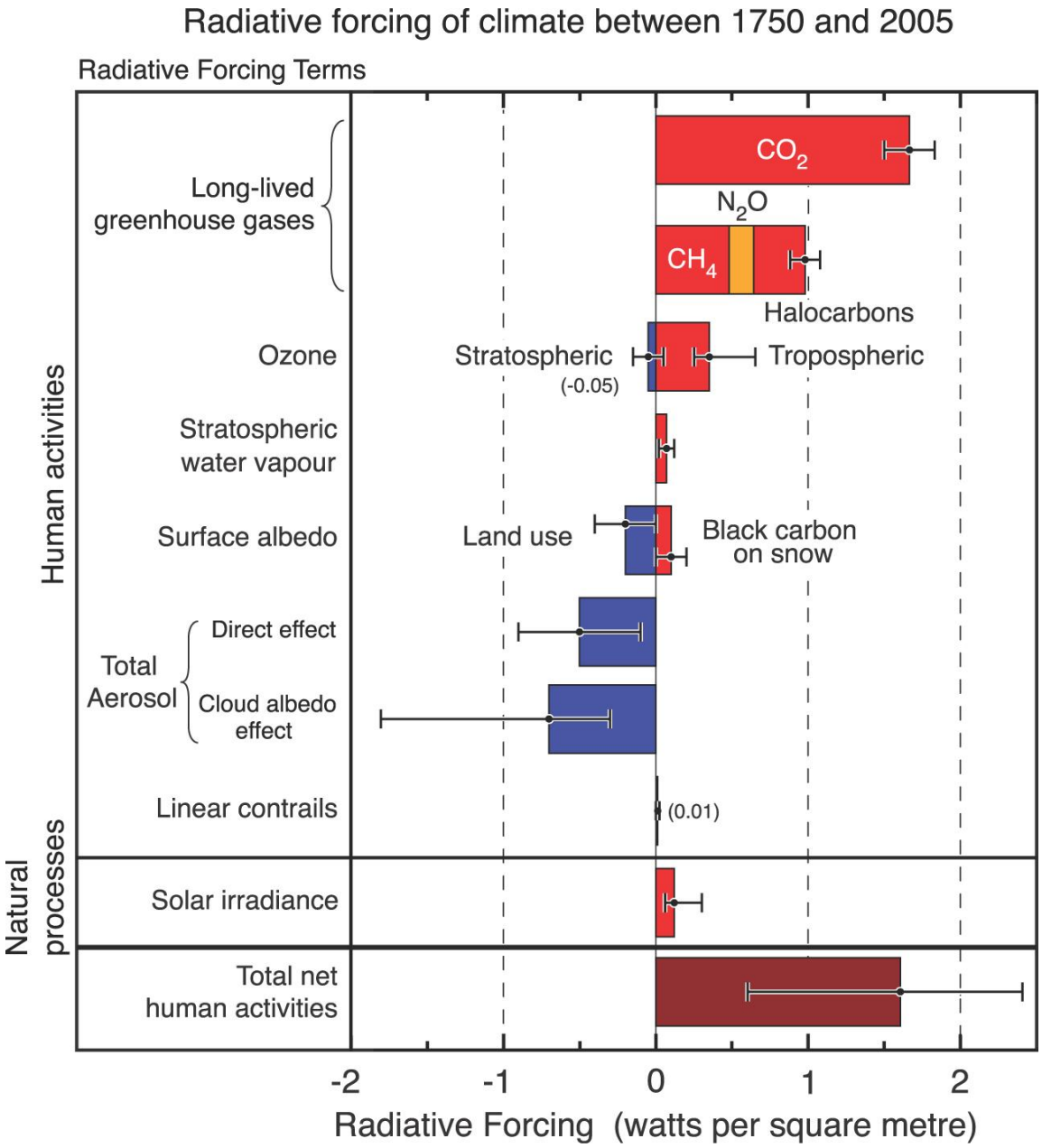

Figure 1. Summary of the principal components of the radiative forcing of climate change as reported in "Climate Change 2007", the IPCC Fourth Assessment Report [*Foster et al.*, 2007]. The forcings in 2005 are relative to the start of the industrial era in 1750.

Observations have presented evidence of an increase in reflectance with increased cloud droplet concentration [*Feingold et al.*, 2003; *Kim et al.*, 2003; *Penner et al.*, 2004], and heavy smoke from biomass burning within the Amazon has been shown to increase cloud droplet concentration and decrease cloud droplet size [*Andreae and Merlet*, 2001; *Mircea et al.*, 2005; *Reid et al.*, 1999]. However, the link between aerosols and cloud microphysics may not be as simple as indicated above. The previous studies were conducted in environments where one type of aerosol was dominant. Over the continents in close proximity to urban areas, the aerosol is a complex internal and external mixture of organics; black carbon; sulfates and nitrates either fully or partially neutralized by ammonia; sulfuric acid; and even dust or sea salt could be present. The solubility of inorganic aerosol has been well characterized [*Tang*, 1976; *Tang and Munkelwitz*, 1977; 1994] and therefore their impact on clouds can be reasonably predicted. However, organic carbon aerosols are a complex mixture of compounds emitted into the atmosphere anthropogenically by the burning of fossil fuels and biomass and through natural biogenic emissions. Hundreds of primary compounds exist, and thousands of secondary organic aerosols [*Hallquist et al.*, 2009] can be formed, which makes it difficult to determine their direct and indirect effects.

The presence of organics alone could reduce surface tension and lead to a significant increase in cloud droplet concentration [*Facchini et al.*, 1999; *Facchini et al.*, 2000; *Lohmann and Feichter*, 2005; *McFiggans et al.*, 2006; *Ming et al.*, 2005; *Nenes et al.*, 2002; *Rissler et al.*, 2004]. However, other studies have shown that an organic coating can delay the activation of aerosols into CCN, which would reduce the cloud

droplet concentration [*Feingold and Chuang*, 2002; *Shantz et al.*, 2003]. Another possible scenario is the ability of a particle to activate is largely dependent on size, not composition [*Dusek et al.*, 2006]. Recent laboratory studies have indicated an increase in the solubility of organic aerosols with increasing oxidation [*Duplissy et al.*, 2008].

The large uncertainty in the aerosol indirect effect is the motivating factor behind the research presented within this dissertation. The data presented within were collected by a Differential Mobility Analyzer/Hygroscopic Tandem Differential Mobility Analyzer (DMA/TDMA) system designed and built at Texas A&M that can simultaneously measure the aerosol size distribution and hygroscopicity. The DMA/TDMA was deployed aboard the National Center for Atmospheric Research/National Science Foundation (NCAR/NSF) C-130 during the 2006 Megacity Initiative: Local and Global Research Observations (MILAGRO) field campaign followed by the 2006 Intercontinental Chemical Transport Experiment – Phase B (INTEX-B) field campaign. The MILAGRO campaign was conducted within the Mexico City basin, which is dominated by organic aerosol, and investigated the evolution of the physicochemical properties of the aerosol plume as it was advected out of the Mexico City basin. The INTEX-B field campaign investigated the evolution of the physicochemical properties of the Asian aerosol plume after 3 to 7 days of transport. Data from both field campaigns will be used to investigate the impact of the evolution of the aerosol plumes on the aerosol's ability to activate and become CCN.

1.2 Instrumentation

The Texas A&M University Differential Mobility Analyzer/Tandem Differential Mobility Analyzer (DMA/TDMA) was designed and built by the Aerosol Research Group within the Department of Atmospheric Sciences. The instrument is unique because of the inclusion of three differential mobility analyzers allowing for simultaneous operation of a single DMA to measure the aerosol size distributions every ninety seconds and the operation of a TDMA to measure the hygroscopic properties of the aerosol population every fifteen minutes. With the simultaneous operation, the instrument has much higher temporal resolution than previous versions, which only measured a size distribution every fifteen minutes. A flow diagram is shown in Figure 2.

The ambient aerosol sampled by the TAMU DMA/TDMA instrument is pulled into the aircraft through a passive solid diffuser inlet mounted on the starboard side of the NCAR/NSF C-130. The inlet is designed by the University of Hawaii and has been shown to have better than 50% efficiency for particles with dry geometric particle diameters of 3.1 μm [*McNaughton et al.*, 2007]. The inlet has almost 100% efficiency for submicron aerosols. Within the DMA/TDMA, the aerosol is first dried to a relative humidity (RH) less than 15% using a Nafion tube and then charged using Po-210 to achieve a predictable charging state. The dried and charged aerosol sample flow is then split into the DMA and TDMA sample flows.

The DMA operates in a scanning mode where the voltage is ramped from a low to high value to select particles with increasingly larger mobility diameters that

correspond to dry diameters from 0.012 μm to 0.670 μm. The number of selected particles at each specified mobility diameter is counted using a condensation particle counter (CPC TSI 3760A) across 75 logarithmically spaced bins. The voltage is then decreased, allowing a second size distribution to be measured.

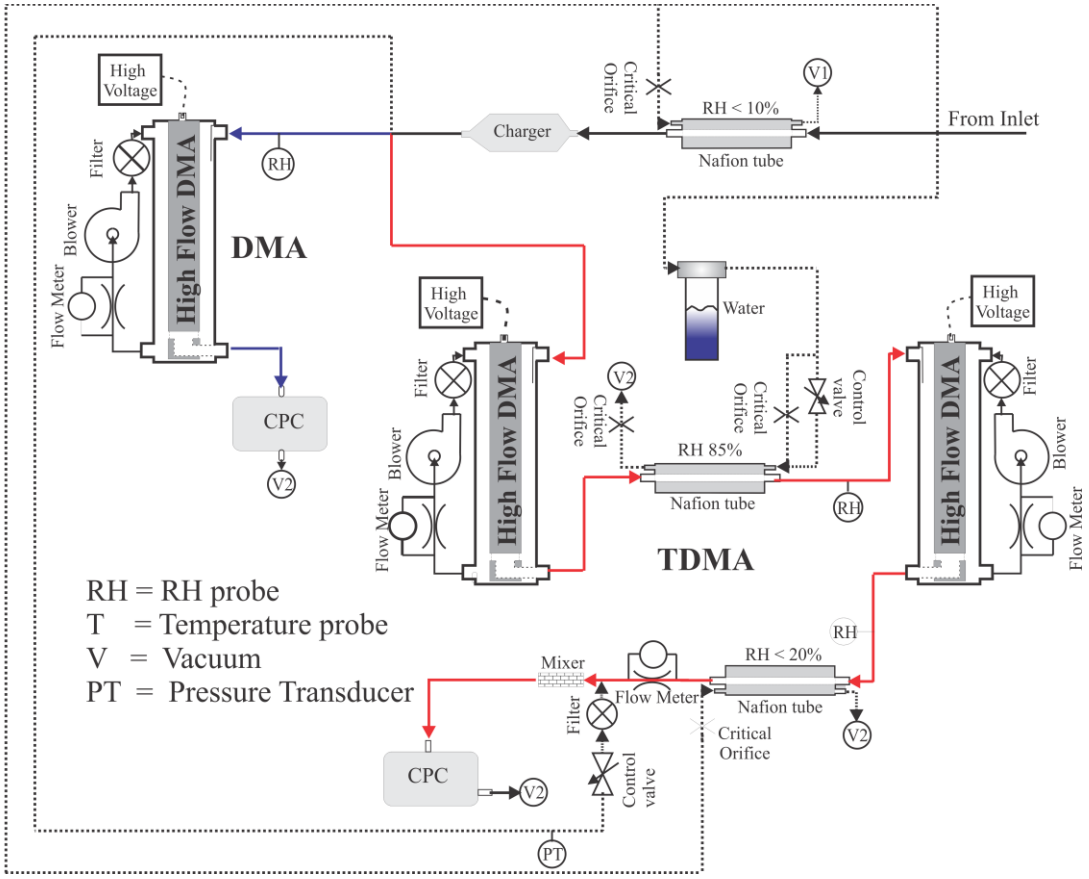

Figure 2. A flow schematic for the DMA/TDMA system. The flow for the DMA is highlighted in blue and the flow for the TDMA is highlighted in red. The dashed line represents makeup and vacuum flows used by the system.

Within the TDMA, the aerosol first passes through a DMA maintained at a constant voltage which selects a monodisperse aerosol population of a specified dry

diameter (D_p*). Throughout both projects, aerosols with dry diameters of 0.025, 0.050, 0.100, and 0.300 μm were selected. For the MILAGRO campaign 0.200 μm is selected and during times of possible dust 0.600 μm is selected during the INTEX-B campaign. The monodisperse aerosol population then passes through a Nafion tube maintained at a RH of 85%. An aerosol will take up water within the Nafion tube and grow if hygroscopic. The hygroscopicity of an aerosol is dependent on the chemical composition. The now modified aerosol population passes through a second DMA that scans from low to high voltage and then back down to a low voltage. The separated particles at each voltage are counted by a CPC (TSI 3762). The modified aerosol size distribution is then divided by the D_p* to calculate the growth distribution.

The TDMA within the instrument is calibrated daily by maintaining a relative humidity of less than 20% within the Nafion tube. At this relative humidity, the ambient aerosol will not grow, and therefore the growth distributions are centered at one. Any deviations from unity are used in the reprocessing of the data to correct the measured growth distributions. The humidity probes are calibrated once during each field campaign. The relative humidity is maintained at 85% while atomized ammonium sulfate is sampled by the TDMA. A monodisperse distribution of 0.100 μm particles is selected, and the growth of the particle is measured by the TDMA. If the relative humidity is truly 85%, the ammonium sulfate will grow 1.55 times its initial diameter according to a derived empirical relationship by *Tang and Munkelwitz* [1994]. The DMA is calibrated once during each field campaign by injecting PSL with a diameter of 0.300 μm.

1.3 Methodology

All data collected in the field are subsequently reprocessed. The main step in the reprocessing is the recovery of the size distribution through the use of a Twomey Algorithm [*Berg et al.*, 1998; *Collins et al.*, 2002; *Twomey*, 1975]. The algorithm accounts for the penetration efficiency of the particles, the counting efficiency of the condensation particle counter, the charging probability of the aerosol, and the DMA transfer function [*Collins et al.*, 2004]. The inversion is applied to both the DMA and TDMA data. The distributions are subsequently manually checked to ensure quality. Distributions that contain poor counting statistics are discarded.

After the initial inversion and quality control check of the TDMA data, the growth distributions are fitted using a log-normal distribution. One or two distributions, referred to as modes, are normally adequate to correctly fit the distribution; however, on rare occasions a third mode is needed. The log-normal fit obtains the useful statistics of the geometric mean of the mode, referred to as the growth factor (GF); the contribution of the mode to the overall distribution represented as a percentage (ε_i); and the standard deviation.

Traditionally, the solubility of aerosol is reported as the growth factor, which is dependent on the relative humidity the instrument was operating at when the growth factor was measured. This relative humidity dependency can cause difficulty when one is trying to compare the measured growth factor across several studies or to incorporate the measurements into modeling studies. Recently, a single variable parameter kappa,

κ, has been used to describe the solubility of an aerosol [*Petters and Kreidenweis,* 2007]. *Petters and Kreidenweis* [2007] defined the "κ-Kohler" equation below:

$$S(D) = \frac{D^3 - D_d^3}{D^3 - D_d^3(1-\kappa)} \exp\left(\frac{4\sigma_{s/a} M_w}{RT\rho_w D}\right), \quad (1)$$

where *S(D)* is the saturation ratio and is the relative humidity the aerosol was exposed to (85%), *D* is the measured diameter of the humidified aerosol, D_d is the dry diameter of the aerosol, $\sigma_{s/a}$ is the surface tension (0.072 J m^{-2}) of the solution/air interface, M_w is the molecular weight of water, *R* is the universal gas constant, *T* is temperature (298.15 K), and ρ_w is the density of water. The GF is defined as:

$$GF = \frac{D}{D_d} \quad . \quad (2)$$

Solving equation (2) for D and substituting into equation (1) yields:

$$RH = \frac{(GF * D_d)^3 - D_d^3}{(GF * D_d)^3 - D_d^3(1-\kappa)} \exp\left(\frac{4\sigma_{s/a} M_w}{RT\rho_w GF * D_d}\right). \quad (3)$$

Equation 3 can be solved for κ:

$$\kappa = \left(GF^3 - 1\right)\left(\frac{\exp\left(\frac{4\sigma_{s/a} M_w}{RT\rho_w GF * D_d}\right) - 1}{RH}\right). \quad (4)$$

The average measured RH throughout the measurement of a growth distribution and the GF for each mode is used to calculate κ for each mode within a growth distribution. For a multi-modal distribution, a weighted κ_w is calculated using the equation below:

$$\kappa_w = \sum_i \varepsilon_i \kappa_i \quad . \quad (5)$$

Laboratory measurements indicate κ values between 0.5 and 1.4 for hygroscopic inorganic species, between 0.01 and 0.5 for organic species, and less than 0.01 for insoluble species. More specifically, Ammonium Sulfate on average has a κ value of 0.53, sodium chloride has an average value of 1.12, and sulfuric acid has an average value of 1.19 [*Petters and Kreidenweis*, 2007].

The measured solubility of a particle at a specified dry diameter permits the use of modified Kohler theory to predict the critical supersaturation (S_c) of the particle. Unlike κ, the GF is a direct measurement of the volume of the aqueous aerosol and therefore will be used in the prediction of the S_c. The GF value is dependent on the mass fraction of solute, x_s, within the aqueous solution. The GF was measured at an RH of 85% and will be referred to as G(85). The soluble material is usually assumed to be ammonium sulfate or ammonium bisulfate. The discussion below will assume ammonium bisulfate. The diameter of the particle at 85%, $D_{p(85)}$, is the product of its dry diameter and its G(85) value. The volume of the particle at 85%, V_{85}, and its dry volume, V_{dry}, are proportional to the volume of insoluble material, V_i, the volume of soluble material, V_s, and the volume of aqueous solution V_{as}.

$$V_{85} = \frac{\pi}{6} D_{p(85)}^3 = V_i + V_{as} \tag{6}$$

$$V_{dry} = \frac{\pi}{6} D_p^{*3} = V_i + V_s \tag{7}$$

Subtracting (6) from (7) yields:

$$\frac{m_s}{x_s \rho_{as}(x_s)} - \frac{m_s}{\rho_s} = \frac{\pi}{6}\left(D_{p(85)}^3 - D_p^{*3}\right), \tag{8}$$

where m_s and ρ_s represent the mass and density of soluble material respectively. The density of the aqueous ammonium bisulfate solution, ρ_{as}, is calculated using an empirical relationship from *Tang and Munkelwitz* [1994]:

$$\rho_{as} = 0.9971 + \sum_i A_i x_s^i = \rho_{as}(x_s), \tag{9}$$

where the coefficients A_1, A_2, and A_3 are 5.87 X 10^{-3}, -1.89 X 10^{-6}, and 1.763 X 10^{-7} respectively.

The Köhler Theory relates the composition and water activity of a particle to its $D_{p(85)}$

$$0.85 = a_w \exp\left[\frac{4M_w\sigma_{as}}{RT\rho_w\left(G(85) * D_p^*\right)}\right], \tag{10}$$

where T is temperature, σ_{as} is the surface tension of the aqueous solution, M_w and ρ_w are the molecular weight and density of water respectively, and $G(85)*D_p^*$ has been substituted for $D_{p(85)}$ [*Seinfeld and Pandis*, 2006]. The surface tension of the aqueous solution is dependent on temperature and the molarity of the solution:

$$\sigma_{as} = \sigma_w(T) + \frac{0.000002 x_s \rho_{as}(x_s)}{M_s} = \sigma_{as}(x_s). \tag{11}$$

Equation (9) is substituted for the density of the aqueous solution. An empirical relationship for the water activity of ammonium sulfate is provided by [*Tang and Munkelwitz*, 1994]:

$$a_w = 1.0 + \sum_i C_i x_s^i = a_w(x_s), \tag{12}$$

where the coefficients C_1, C_2, and C_3 are -3.05 X 10^{-3}, -2.94 X 10^{-5}, and -4.43 X 10^{-7} respectively. The effect of any insoluble material on the activity of the water is assumed to be negligible. Using equations (8) and (10), the mass of the solute, m_s, within the aqueous solution can be found through iteration until both equations are satisfied.

In supersaturation conditions, one can assume ideal behavior of the solution, and the empirically calculated water activity can be replaced by a mole fraction based representation:

$$a_w = \frac{n_w}{n_w + in_s} = \frac{1}{\frac{iM_w}{M_s}\left(\frac{x_s}{1-x_s}\right)+1}. \tag{13}$$

Substituting equation (13) into equation (10) and manipulating the equation for supersaturation (S=RH-1) yields the following equation:

$$S\left[D_p^*, G(85)\right] = \frac{1}{\frac{iM_w}{M_s}\left(\frac{x_s}{1-x_s}\right)+1} * \exp\left[\frac{4M_w\sigma_{as}(x_s)}{RT\rho_w\left(G(85)*D_p^*\right)}\right] - 1 \tag{14}$$

with assumed values of 3 for the van't Hoff Factor, i, and 115 g mol^{-1} for the molecular weight of ammonium bisulfate. For a specified G(85) and D_p*, the x_s is increased until a maximum is found for S. This value is considered the activation supersaturation, and it describes when the solution droplet is in thermodynamic equilibrium. Once at equilibrium the aerosol will activate and become a cloud droplet.

1.4 Experiment Overview

Eastern Asia (China, Japan, and South Korea) and Mexico City are currently undergoing a phase of rapid urbanization and industrialization leading to an increase in the production of anthropogenic aerosols. The effects of the aerosols from both these areas occur on regional and intercontinental scales that could possibly have a profound effect on air quality and visibility within North America and the overall radiative balance of the atmosphere. To ascertain these effects, two field campaigns were conducted in 2006. The first was the Megacity Initiative: Local and Global Research Observations (MILAGRO) field campaign, which studied the local and regional effects of the pollution from Mexico City. The Intercontinental Chemical Transport Experiment – Phase B (INTEX-B) was the second project, which focused on the pollution plume from Asia as it entered the far northeastern edges of the Pacific Ocean and the West Coast of the United States.

Texas A&M University deployed a Differential Mobility Analyzer/Tandem Differential Mobility Analyzer (DMA/TDMA) aboard the National Center for Atmospheric Research/National Science Foundation (NCAR/NSF) C-130 for both projects. This platform awarded a unique opportunity to study aerosols as they have been transported over a period of zero to several days from Mexico City and to study a more aged aerosol transported over a period of one week from East Asia.

The discussion within this dissertation will use the above methodology to describe the physiochemical properties of the aerosol over Mexico City, within the Mexico City plume, and within the Asian plume. A study of the evolution of the

physiochemical properties will be conducted, and the modified Kohler theory will be used to investigate how the evolution and resulting changes in the physicochemical properties of the aerosol could affect the properties of clouds.

2. RESULTS FROM THE MILAGRO FIELD CAMPAIGN

2.1 Overview of Mexico City Air Pollution

Mexico City is one the most populated urban areas in the world with a population approaching twenty million people. The city is situated in the middle of ancient lake bed at an elevation over 2000 m surrounded by mountains on all sides expect to the north and a narrow opening to the southeast. The city receives intense solar radiation at this elevation and subtropical latitude that causes an increase in the production of photochemical pollutants compared to cities in the United States. More than three million vehicles and five thousand industries emit more than 28 metric tons per day of particulate matter smaller than 10 μm (PM-10), including 17 tons per day of particulate matter smaller than 2.5 μm (PM-2.5) [*SMADF*, 2002]. A more detailed breakdown of emissions is included in Table 1. In addition to anthropogenic sources, the nearby volcano of Popocatepetl is considered a high-emission rate, passively degassing eruptive volcano with continuous SO_2 emissions in the absence of any visible eruptions [*Delgado-Granados et al.*, 2001].

Table 1. Emission from within the Mexico City Metropolitan Area reported as Gg per year. [*SMADF*, 2002].

Sector	Emissions (Gg/yr)								
	PM_{10}	$PM_{2.5}$	SO_2	CO	NO_x	COT	CH_4	COV	NH_3
Point Sources	2.81	0.57	10.29	10	24.72	22.79	0.18	22.01	0.22
Area Sources	0.51	0.49	0.05	6.63	10.64	418.6	168.6	197.8	12.97
Mobile Sources	5.29	4.59	4.35	2019	157.2	210.8	11.59	194.5	2.26
Natural	1.74	0.38	N/A	N/A	0.86	15.43	N/A	15.43	N/A
Total	10.34	6.03	14.68	2035	193.5	667.6	180.3	429.8	15.45

Over the past 40 years, the air pollution within Mexico City has been sporadically studied. *Bravo* [1960] was the first, with measurements focusing on particles and SO_2. Subsequently, gas phase measurements have been conducted routinely; however, aerosols received little attention until the 1990s [*Raga et al.*, 2001]. Measurements of the aerosols within Mexico City with high volume samplers and cascade impactors have led researchers to identify three dominant sources for fine mass: (a) ammonium sulfate or sulfuric acid, (b) automotive emissions, and (c) industrial emissions *[Raga et al., 2001]*. Secondary ammonium nitrate and ammonium sulfate were determined to be distributed homogenously and estimated to constitute 15–30 % of PM-2.5, while carbon-containing aerosols accounted for 25–50 % of PM-2.5 *[Raga et al., 2001]*. In April 2003 an Aerodyne Aerosol Mass Spectrometer (AMS) was deployed along with a nanoparticle Differential Mobility Analyzer (nano-DMA) within the Mexico City Metropolitan Area (MCMA) at the CENICA supersite to investigate particle concentrations, sources, and processes [*Dunn et al.*, 2004; *Salcedo et al.*, 2006]. The Aerodyne AMS determined the PM-2.5 was composed of 54.6% organic compounds versus 27.5% inorganic compounds, in agreement with the previous cascade impactors measurements. The black carbon mass concentration was about 11.0 %, while soil represented the remaining 6.7% [*Salcedo et al.*, 2006].

The observed inorganics were mainly ammonium nitrate, sulfate/ammonium salts, and a small amount of ammonium chloride. A majority of the time the chloride, sulfate, and nitrate present were neutralized by the ammonium. However, there were periods of high sulfate concentrations that led to the formation of ammonium bisulfate.

Overall, sulfate seems to be formed on a regional scale from the oxidation of SO_2 and has enhanced concentrations during high relative humidity. Nitrate exhibited a diurnal cycle consistent with local photochemical production of nitric acid. The accumulation mode exhibited an internal mixture of organic and inorganic species. However, smaller size modes exhibited in external mixture of these species raise the question of what time and length scales are important in the evolution before they eventually reach a uniform mixing state [*Salcedo et al.,* 2006].

New particle formation was also observed with a scanning mobility particle sizer consisting of a nano-DMA at the CENICA supersite. The nucleation events were observed during daylight hours and corresponded with enhanced ambient concentrations of SO_2, suggesting an important role for sulfuric acid in the new particle formation [*Dunn et al.*, 2004].

These measurements, however, have offered very little information on the size distribution of the PM-2.5 aerosol. Without this, the ability to understand the formation processes of the aerosol and the effect on human health is diminished. There have been no measurements of the aerosol in the vertical dimension, which is crucial to the understanding of the vertical mixing and eventually evacuation of the aerosols from the Mexico City basin.

In addition, the hygroscopicity of the aerosol has never been explicitly measured. However. in April of 1984, the average maximum concentration of cloud condensation nuclei (CCN) was measured to be approximately 6000 cm^{-3} at a 1% supersaturation [*Herrera and Castro,* 1988]. A subsequent study in 1985 measured CCN concentrations

of the same magnitude [*Montanez and Garciagarcia*, 1993]. In 2000, the CCN concentrations were measured to be from 2000 to 3000 cm^{-3} at 0.5% supersaturation, and the condensation nuclei with diameters greater than 0.01 μm were measured to be from 30,000 to 60,000 cm^{-3} [*Baumgardner et al.*, 2004]. The similar values for CCN concentrations imply the hygroscopicity of the aerosol has changed little over the past 20 years

In 2006, the largest and most extensive field campaign, MILAGRO, was conducted. This study entailed ground measurements within the city and at two separate measurement sites to the north of the city to enable the measurement of the evolution of the aerosol proprieties during transport. The study also included the use of several aircraft including the NCAR-C130 and NASA's DC-8 Airborne Laboratory.

2.2 MILAGRO Overview

MILAGRO was composed of five field campaigns occurring simultaneously within and in the vicinity of Mexico City. The Mexico City Metropolitan Area-2006 (MCMA-2006) campaign examined the emissions and boundary layer concentration within the Mexico City Basin. The Department of Energy (DOE) Atmospheric Science Program (ASP) led the Megacity Aerosol Experiment in Mexico (MAX-Mex), which examined the evolution of aerosols and gas phase species, and the interaction between the two. The DOE campaign made airborne measurements using a G-1 aircraft and made ground-based measurements. The NASA led Intercontinental Chemical Transport Experiment-Phase B (INTEX-B) studied the evolution and transport of pollution from Mexico City on a more global scale. A USDA sponsored Twin Otter sampled biomass

burning plumes within and near Mexico City. Finally, the Megacity Impacts on Regional and Global Environments (MIRAGE-Mex) campaign led by the National Center for Atmospheric Research (NCAR) used a C-130 aircraft to make airborne measurements of the aerosol and gas-phase species within the Mexico City basin and within the pollution plume.

MIRAGE-Mex was conducted throughout March 2006. Twelve research flights for a total of 86 research flight hours were conducted and are displayed in Figure 3. The majority of flights were in the vicinity of Mexico City or within the pollution plume being advected away from the Mexico City Basin. The lone exception was March 22, when the C-130 flew to the Yucatan Peninsula to sample biomass burning. The C-130 frequently flew over three heavily instrumented surface sites that were operated throughout the campaign. T0 (19.49°N, 99.15°W) was situated within Mexico City and T1 (19.70°N, 99.98°W) and T2 (20.01°N, 98.91°W) were located to the northeast of Mexico City as shown in Figure 4.

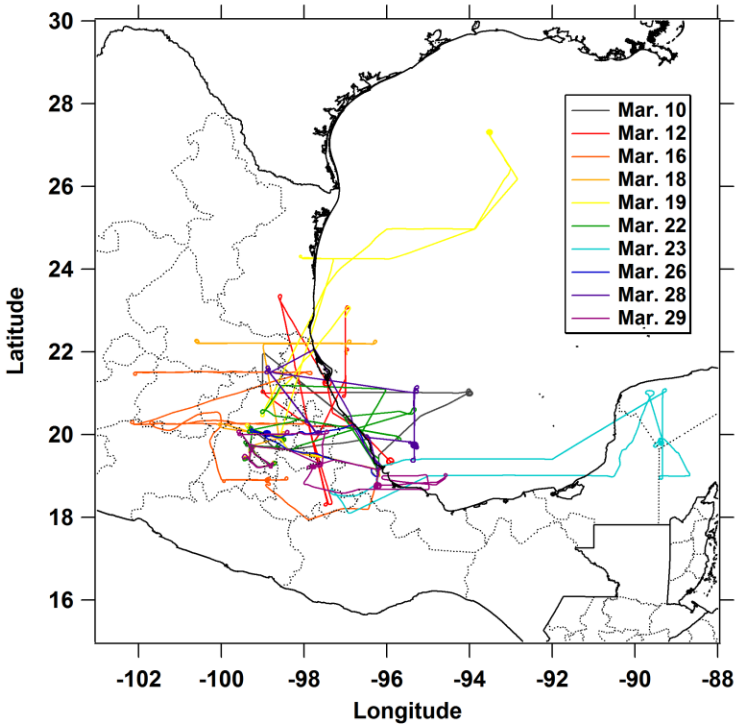

Figure 3. NCAR C-130 flight paths for all research flights flown during MIRAGE.

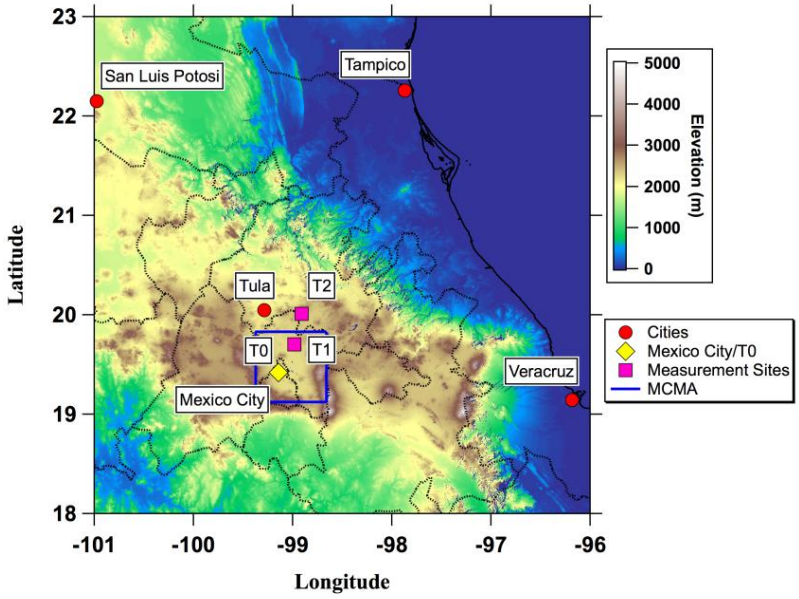

Figure 4. A terrain map of the MILAGRO operations area. The surface measurement sites along with several major Mexican cities are shown. In addition, the industrial area of Tula is indicated. The blue box encompasses the Mexico City Metropolitan Area.

The basin has a synoptically weak meteorological pattern, but the solar radiation is intense, leading to a complex weather pattern influenced by mountain-valley and urban-induced wind patterns [*de Foy et al.*, 2008]. This results in local circulations that cause convergence zones within the basin [*Fast and Zhong*, 1998]. An overview of the meteorology during MILAGRO is presented in *Fast et al.* [2007]. The field campaign can be broken down into three regimes. The first regime prior to March 14 was mostly sunny and dry. The second regime between March 14 and 23 began with a sharp increase in humidity and deep convection that slowly diminished over subsequent days

as the atmosphere dried down. The third regime after March 23 followed the passage of cold surge that brought increased humidity, deep convection, and precipitation.

2.3 Instrumentation

The DMA/TDMA status and the number of size and growth distributions measured are shown in Table 2. The DMA did not operate on the first flight, operated intermittently on the second flight, and shut down two-thirds of the way through the flight on March 12. Otherwise, the instrument performed normally. The TDMA experienced problems on the first two flights and worked flawlessly throughout the rest of the field campaign.

The aerosol drawn into the DMA/TDMA instrument was first dried by passing through a Nafion tube maintained at 3.7 ± 2.9 % RH throughout the MIRAGE campaign. The aerosol flow was then split between the DMA and TDMA. On average, the DMA measured one size distribution from 0.012 μm to 0.670 μm every 90 seconds for a total of 2487 size distributions throughout the campaign. The TDMA cycled through the dry diameters 0.025, 0.050, 0.100, 0.200, and 0.300 μm roughly every 15 minutes and measured over 200 growth distributions for each dry diameter throughout MIRAGE. The TDMA relative humidity was set to 85% and on average was maintained at 84.2 ± 2.3% throughout the campaign.

The cloud condensation nuclei (CCN) concentration was measured by a Droplet Measurement Technology continuous-flow stream-wise thermal-gradient CCN counter (CCNc) [*Lance et al.*, 2006; *Roberts and Nenes*, 2005]. A stream-wise temperature

gradient establishes a supersaturation within the column. Activated particles are detected by an optical particle counter at the base of the column. The supersaturation was maintained at 0.18± 0.09% and only data from level legs will be used in this analysis.

Table 2. An overview of the number of flight hours and the number of measurements made by the DMA and TDMA.

	Flight Hours	DMA	TDMA 0.025 mm	TDMA 0.50 mm	TDMA 0.100 mm	TDMA 0.200 mm	TDMA 0.300 mm
March 4, 2006	7.4	0	0	0	0	0	0
March 8, 2006	6.8	262	0	0	0	0	0
March 10, 2006	8.1	292	25	26	26	23	23
March 12, 2006	8.1	200	24	24	24	23	19
March 16, 2006	8.8	305	28	28	28	25	23
March 18, 2006	8.5	289	25	26	26	26	23
March 19, 2006	8.8	298	27	27	27	25	25
March 22, 2006	7.0	265	24	25	25	25	25
March 23, 2006	6.1	209	17	18	18	17	16
March 26, 2006	2.3	92	9	9	9	9	9
March 28, 2006	7.4	279	26	27	27	27	27
March 29, 2006	6.8	258	26	26	26	26	26
Total	86.4	2749.0	231.0	236.0	236.0	226.0	216.0

The High Resolution Time of Flight Aerosol Mass Spectrometer (HR-ToF-AMS) used during MILAGRO was capable of directly separating most ions from inorganic and organic species at the same nominal m/z, quantifying several types of organic fragments, and directly identifying organic nitrogen and organosulfur content [*DeCarlo et al.*, 2006]. This was an improvement over previous versions of the AMS [*Canagaratna et al.*, 2007; *Drewnick et al.*, 2005; *Jayne et al.*, 2000]. The isokinetic inlet was installed towards the rear of the C-130 on the belly of the aircraft [*DeCarlo et al.*, 2008].

A Thermo Environmental Instruments 43S SO2 instrument was operated by NOAA aboard the C-130 to measure the concentration of ambient SO_2. The instrument

utilizes pulsed ultraviolent fluorescence at 294 nm to measure the concentration of SO_2 and has been modified to increase the instrument's temporal resolution [*Ryerson et al.*, 1998]. The instrument had a sample frequency of 1 HZ.

2.4 Back Trajectory Model

The analysis of the origin of the measured aerosol was determined using seven-day kinematic back trajectories calculated by the Fuelberg research group at Florida State University (http://fuelberg.met.fsu.edu/research/intexb). The wind fields are calculated from the u, v, and w wind components of the European Centre for Medium-Range Weather Forecasts (ECMWF) analysis. The back trajectories were modeled at one-second intervals along the C-130 flight path. Every DMA distribution and TDMA growth distribution was tagged with the back trajectory calculated nearest to the midpoint time of the measurement. A back trajectory passing through the blue box shown in Figure 4 was determined to be the measurement of Mexico City Metropolitan Area (MCMA) emissions.

2.5 Data Discussion

The physiochemical properties of the aerosol within the MCMA will be discussed in the first and second sections. This will establish a starting point for the aerosol when it has been recently emitted. The third section will analyze the emission to the northeast of the MCMA. The fourth section will examine the transformation of the aerosol that occurs as it is being advected out of the MCMA towards the North and

Northeast. Finally, the fifth section will conclude the discussion by investigating the aerosol and cloud interactions.

2.5.1 Size distributions and concentrations within MCMA

The C-130 conducted five flights within the MCMA, and the DMA operated during the flights conducted on March 10, 18, 22, and 29. The flights were within the boundary layer with an average altitude above ground level of 1.26 ± 0.50 km. A size distribution was measured from 0.012 to 0.67 μm every 90 seconds with a total of 194 measured during the MCMA research flights. Figure 5 shows a probabilistic size distribution measured during each research flight within the MCMA. The calculation of the probabilistic size distribution is as follows. For a specified dry diameter bin, a normalized histogram of all measured $dN/dLogD_p$ or $dV/dLogD_p$ values for given research flight within the MCMA is calculated. The normalized histograms for each of the 75 dry diameter bins are compiled to form a probabilistic size distribution that indicates the probability of measuring a value of $dN/dlogD_p$ or $dV/dlogD_p$. Probabilities greater than 0.04 are shaded in Figure 5. The cumulative frequency of the $dN/dLogD_p$ or $dV/dlogD_p$ values equal to or greater than 0.04 for each bin is displayed in the chart below each probabilistic size distribution. On average, the probabilistic size distributions in Figure 5 represent greater than or equal to 75% of all possible size distributions.

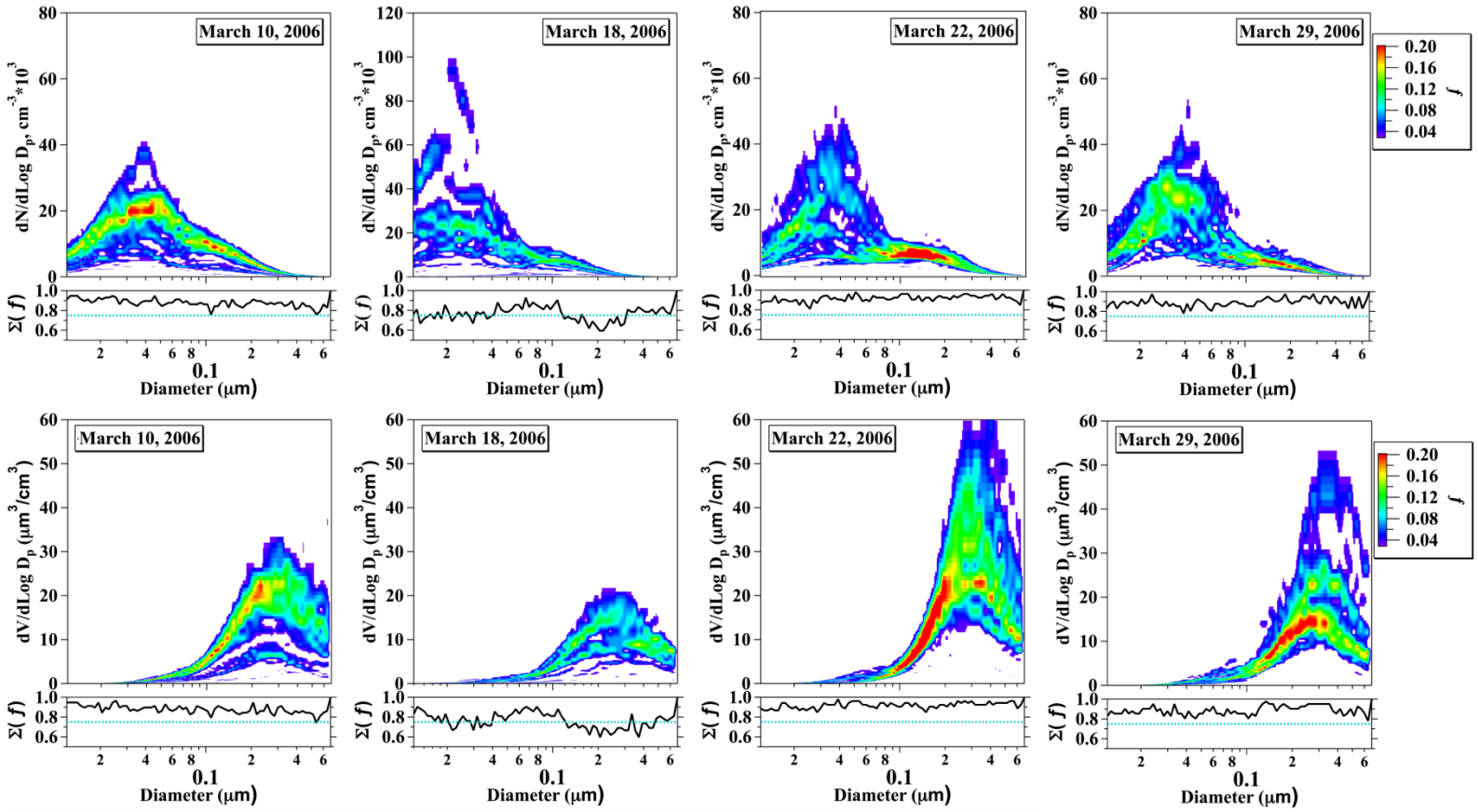

Figure 5. The probabilistic size distributions within the MCMA for each research flight. The probabilistic number distributions are shown along the top row with the flight date annotated. The corresponding probabilistic volume distributions are shown along the bottom row. The strip chart below each size distribution indicates the percentage of all probable values that is displayed in the corresponding size distribution.

The probabilistic number distributions are similar in shape and magnitude on March 10, 22, and 29. However, the March 18 probabilistic number distribution exhibits an elevated amplitude and high variability versus the aforementioned dates. On March 10, 22, and 29, the magnitude of the probabilistic volume distribution varies; however, the geometric mean diameter was on average 0.283 ± 0.002 μm. On March 18, the probabilistic volume distribution was shifted to the left with a geometric mean diameter of 0.238 μm, and the magnitude was the lowest of all research flights. Between the research flight on the March 10 and March 18, scattered convection and rainfall occurred through the central plateau following the first Norte on March 14. This removed a considerable fraction of the large particles in the atmosphere through precipitation scavenging. Therefore, the corresponding volume and surface concentrations were anomalously lower on March 18. This reduction in surface area concentration could enable nucleation because the small particles do not have particles with larger surface area to condense onto and instead interact, resulting in a high rate of nucleation [*Dunn et al.*, 2004; *Kulmala et al.*, 2004]. The airborne observation is corroborated by the observation of a Type II nucleation event by scanning mobility particle sizers, a radial differently mobility analyzer, and an inclined grid mobility analyzer at Tecamac, Mexico, 35 km NW of the center of Mexico City [*Iida et al.*, 2008]. Type II events generate a significantly higher number of particles in the 3 to 6 nm size range, and the concentration remains higher for a longer period of time when compared to Type I nucleation events. The growth rate for this event was the highest reported during MILAGRO at 39 +/- 9.0 nm/h, and the event occurred over a 1.2 hour period.

The probabilistic number and volume distribution compiled from all measured size distribution within the MCMA is shown in Figure 6**.** On average, over 80% of the more probable size distributions are represented in Figure 6. The dashed line represents the most probable value of $dN/dlogD_p$ or dV/dlogD. The parameters of the fit of three lognormal modes to the size distribution are shown in Table 3. The number distribution indicates that on average, the aerosol within the boundary layer has already undergone some aging and typically does not display a strong nucleation mode. However as discussed above, there are instances when a nucleation mode could form.

The size distributions measured by the DMA are integrated to calculate a number and volume concentration. Throughout the data discussion, the integrated number or volume concentration will be referred to as the number or volume concentration. The measured number concentration from the flights is shown in Figure 7. What is readily apparent is that the location of the highest aerosol concentrations varies from day to day. The variance is the result of the location of the convergence zone that varies daily and the strength of the advection of the pollution away from the MCMA

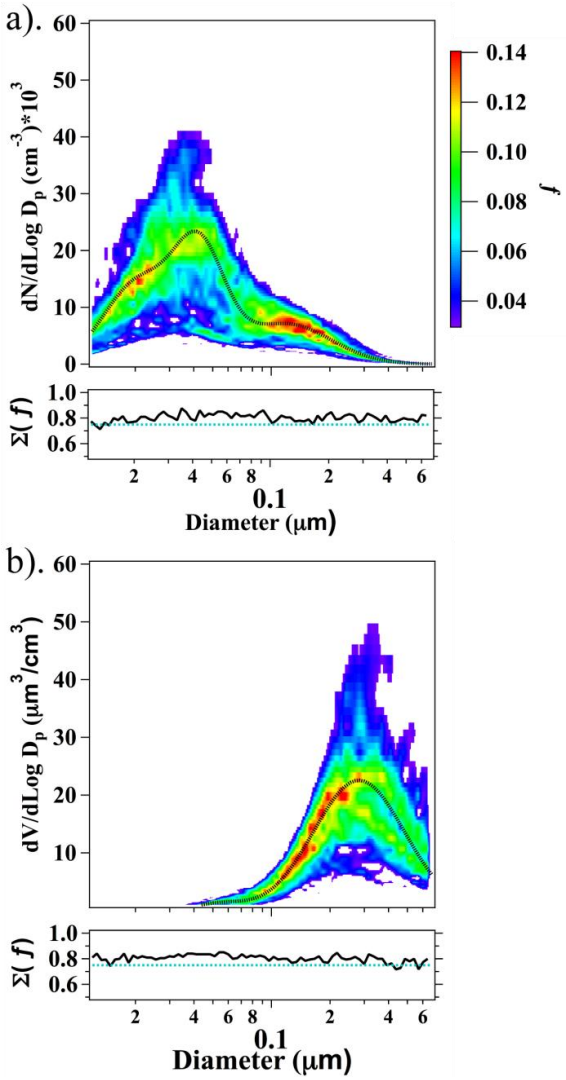

Figure 6. The most probable size distribution within the MCMA. The number distribution is on the left (a), and volume distribution (b) is on the right. The strip chart below each size distribution indicates the percentage of all probable values that are displayed in the corresponding size distribution. The dashed line on each distribution indicates the concentration with the highest probability.

Table 3. The log-normal fit parameters for the dashed line in Figure 6.

Mode I			Mode II			Mode III		
N (cm^{-3})	D_p	s	N (cm^{-3})	D_p	s	N (cm^{-3})	D_p	s
5238	0.019	1.45	7494	0.041	1.39	4008	0.121	1.70

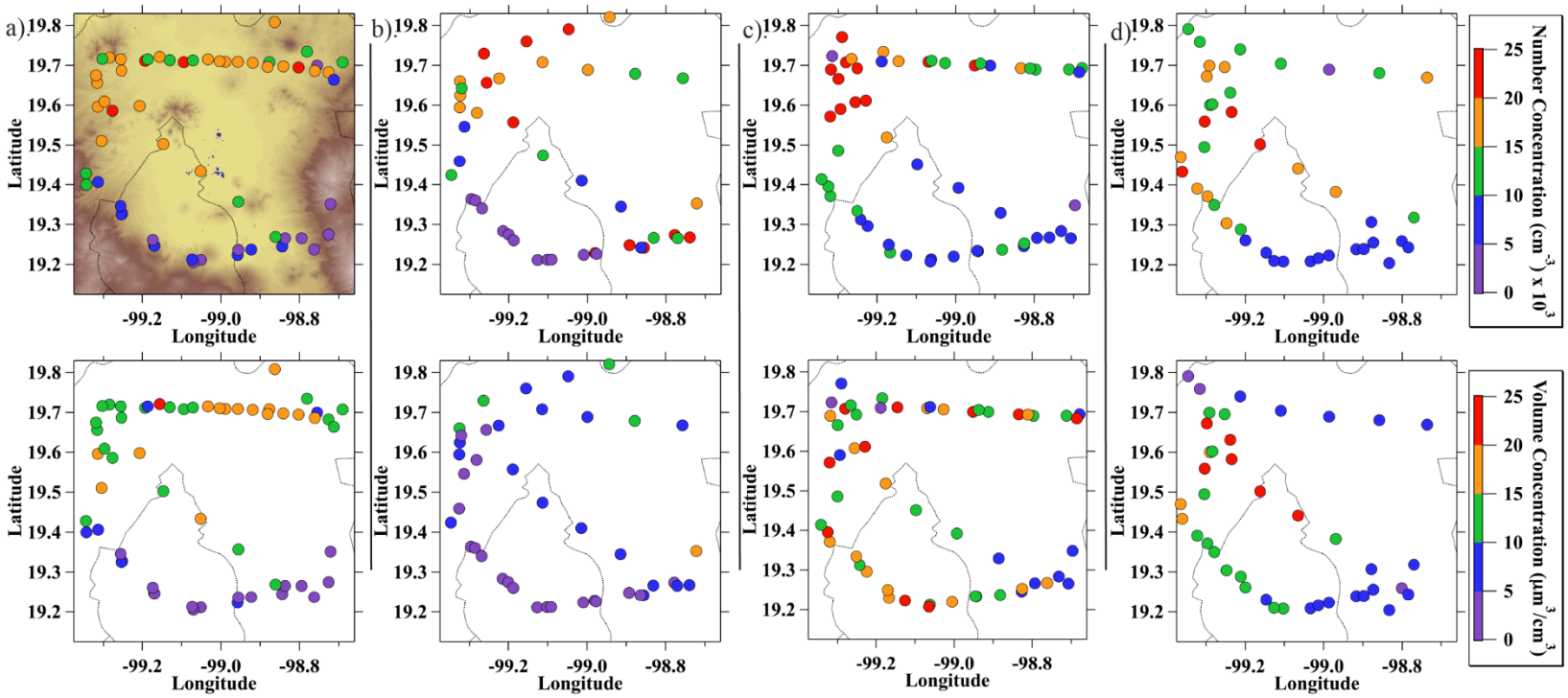

Figure 7. The integrated number and volume concentration within the MCMA. The figures are arranged by flight date: (a) March 10, (b) March 18, (c) March 22, and (d) March 29. The terrain is only shown in the top left figure.

However, taking the average of the aerosol number concentration across the MCMA indicates that the number concentration may not be as variable from day to day as it first appears (Table 4). The average number concentration for all research flights was 13,100 ± 7715 cm^{-3}. This is in reasonable agreement with the average number concentration of 18,000 cm^{-3} measured at the mountain site of Altzomoni, 4010 m ASL, located 60 km to the southeast of Mexico City [*Baumgardner et al.*, 2009]. This site is roughly the same altitude above the Mexico City basin as the aircraft measurements. A Student t-test found no statistically significant differences (α=0.05) between the number concentrations for each research flight within MCMA. As discussed above, the larger variability on March 18 can be attributed to the nucleation event. Peak number concentrations within the plume of nucleated aerosols were in excess of 38,000 cm^{-3}, whereas number concentrations were below 1,000 cm^{-3} outside of the plume. This is readily visible in Figure 7 in the northwest corner of the MCMA. A Student t-test found that the average volume concentration was statistically lower (α=0.05) for the research flight on March 18 and higher on March 22 compared to the other measurements. The large volume on March 22 could be a result of condensational growth following the nucleation event. The average volume concentration was 10.8 ± 6.6 $\mu m^3/cm^3$ for all research flights. The variability in the volume concentration is most likely a result of the variability in meteorological conditions. As discussed earlier, the decrease in volume concentration was most likely caused by wet deposition removal. The high volume concentration on March 22 was measured during the passage of a very strong Norte, which potentially could have lofted large particles into the atmosphere.

Table 4. The average number and volume concentration measured during each research flight within the MCMA.

	Number Conc. (cm^{-3})	σ	Volume Conc. ($\mu m^3/cm^3$)	σ	N
3/10/2006	12291	5979	10.4	5.8	58
3/18/2006	14067	11020	5.3	4.3	42
3/22/2006	13634	7738	15.0	6.0	53
3/29/2006	12919	5476	12.0	6.3	40
AVERAGE	13100	7715	10.8	6.6	193

2.5.2 Kappa values within the MCMA

The solubility of the aerosol measured during the MCMA research flights is shown in Figure 8. A total of 20, 19, 20, 18, and 18 TDMA measured growth distributions were respectively measured at dry diameters of 0.025, 0.050, 0.100, 0.200, and 0.300 μm. The κ value is indicated by the color of the circle, where higher values are represented by blue and the size of the circle represents ε_i. The average κ_w is indicated for each dry diameter. The low values of κ_w indicate the aerosol is mostly composed of organic species. However, the TDMA growth distributions begin to exhibit some bimodality for D_d of 0.100 μm, and for D_d of 0.200 and 0.300 μm they are almost exclusively bimodal. The second more soluble mode has κ values exceeding 0.40, indicating a mixture of organics and most likely ammonium sulfate. A High Resolution Time of Flight Aerosol Mass Spectrometer aboard the C-130 [*DeCarlo et al.,* 2008] and at T0 [*Aiken et al.,* 2009] measured an aerosol composition dominated by oxidized organic aerosol (mostly secondary organic aerosol [SOA]) within the MCMA. Large concentrations of inorganic aerosol composed of sulfate, ammonium, ammonia, and nitrate were also measured. [*DeCarlo et al.,* 2008]. The oxidization of organics has been

observed in laboratory smog chamber experiments [*Duplissy et al.*, 2008; *Hallquist et al.*, 2009] to increase the hygroscopicity of the aerosol and could explain why the κ_w were slightly elevated. The bimodality is a result of a multitude of chemical processing occurring within the MCMA, including the formation of SOA by oxidation, condensational growth of the aerosols, and growth of the aerosols through coagulation involving a complex mixture of insoluble and soluble organic and soluble inorganic aerosol species within the MCMA. The 0.100 μm dry diameter is the least soluble of all measured dry sizes, as indicated in Figure 8 and shown in Figure 9a.

In Figure 9a, the κ_w value decreases between dry diameters of 0.025 to 0.100 μm and increases between 0.100 to 0.300 μm. This u-shaped behavior further illustrates the occurrence of coagulation, growth by condensation of soluble gas phase species, and potentially cloud processing. The u-shaped behavior is fairly consistent from day to day; however, the relative magnitude of the measured κ_w has some daily variation (Figure 9b). The variability in the magnitude appears driven by local nucleation events and meteorological conditions. The sharp uptick in solubility on March 18 at 0.025 and 0.050 μm can be attributed to the nucleation event that converted gas phase sulfate into the particle phase. Subsequently these small (< 0.010 μm) almost pure sulfate particles coagulated together with the 0.025 and 0.050 μm diameter particles resulting in a rapid increase in their hygroscopicity. After the El Norte passage on March 18, the RH increased along with the presence of clouds. This was followed by a decrease in solubility at 0.025 and 0.050 μm and an increase in solubility at 0.200 and 0.300 μm. This trend is indicative that the more soluble species 0.025 and 0.050 μm coagulated

onto the surface of the larger particles, thus effectively removing the more soluble species at the smaller diameters. In addition, the increase in cloudiness most likely enabled cloud processing of the aerosols with diameters larger than 0.100 μm.

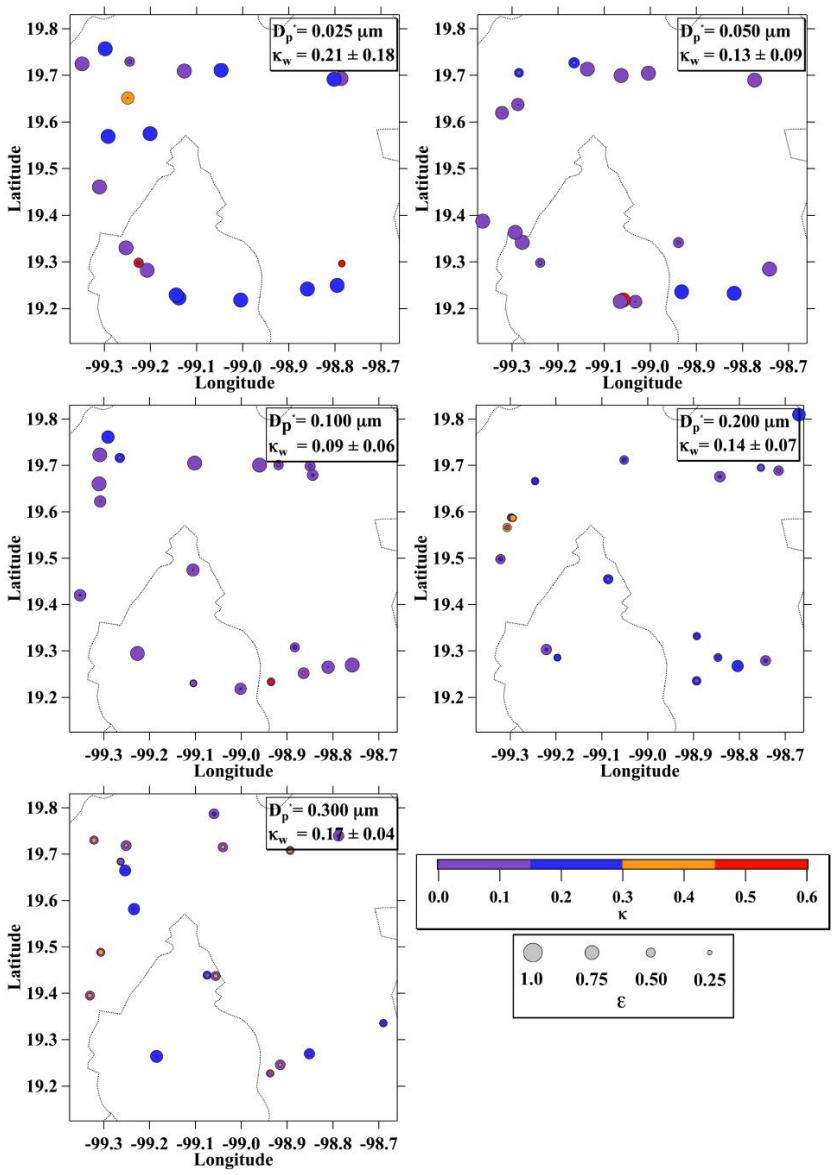

Figure 8. The measured κ values within the MCMA. The color of the marker indicates the κ value and the size of the marker indicates its overall contribution to the measured growth distribution. The annotation indicates the dry diameter and the average κ_w.

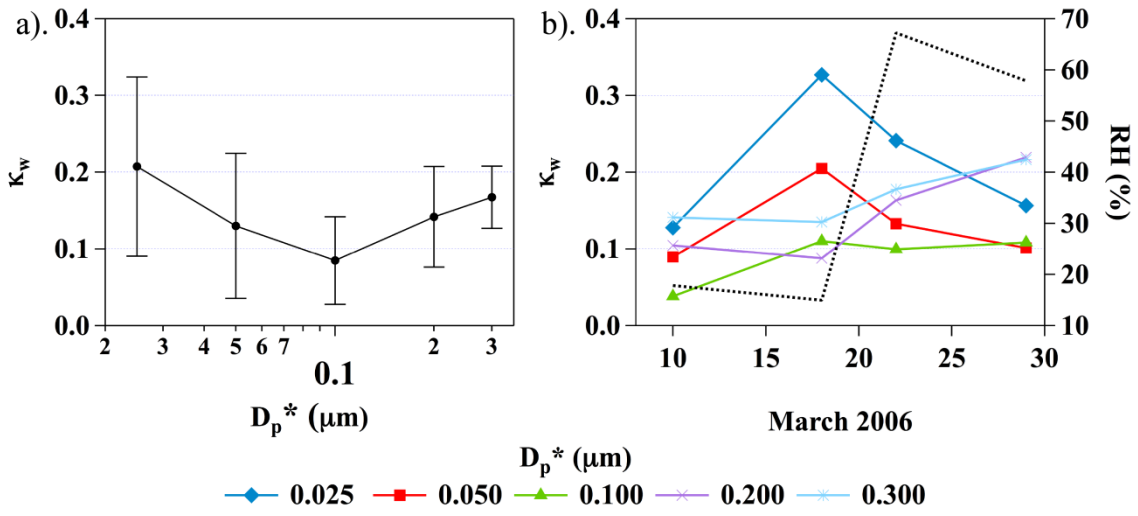

Figure 9. Average κ_w versus dry diameter and date within the MCMA. The average κ_w within the MCMA (a) exhibits a minimum at 0.100 μm. The average κ_w for each dry diameter is plotted by the research flight date (b). Also plotted is the average ambient RH (%) measured within the MCMA aboard the NCAR C-130.

Throughout the nucleation event and meteorological transition, the solubility of the 0.100 μm particles stayed almost constant, with only a slight increase between the March 10 and March 18 flights. This consistency is to be expected, because the very soluble smaller particles formed from the nucleation have a much higher probability to collide and coagulate onto the largest particles. As the diameter decreases, so does the probability. With the very low κ_w value, the 0.100 μm particle is not favored for CCN activation, and the diameter is too small for the Kelvin effect to compensate.

2.5.3 DMA/TDMA measurements to the northeast of Mexico City

One of the primary goals of MILAGRO was to investigate the evolution of the physiochemical properties of the aerosol advected towards the northeast away from

Mexico City. To examine this on a more local scale, the T0, T1, and T2 research sites were operated. The location of the sites is shown in Figure 2.

The average values of κ_w measured within 15 km of each site are shown in Table 5. The sparse data for T0 resulted from few flights occurring near the site. The measured κ_w for all dry diameters increased from T1 to T2; however, only the κ_w for the 0.100 μm dry diameters is significantly different (α=0.05). The measured number and volume concentration decreases as the plume is advected from T0 to T1 than on to T2. The measured number and volume concentration at T2 is significantly different (α=0.05) from the concentrations measured at T0 and T1. This is a promising sign that the aerosol on local scale is undergoing transformation as it is advected away from Mexico City.

Measurements near Tula were also included in Table 5. This is a major industrial complex located to the north and slightly west of Mexico City. The high number concentrations, relatively low volume concentrations, and high κ_w values indicate that Tula is dominated by primary emissions. The measured κ_w for 0.025 and 0.050 μm particles are the highest of anywhere in the Mexico City area, although the difference is not significant (α=0.05) when compared to T2. The measured number concentration is also the highest, but only significantly different than the concentration measured at T2. The volume concentration is significantly lower (α=0.05) than the measured volume concentration at T0 and T1.

Table 5. The average κ_w measured within 15 km of T0, T1, T2, and Tula. The average number and volume concentration are indicated in the bottom 2 rows.

	Mexico City			T1			T2			Tula		
D_p* (μm)	κ_w	σ	N	κ_w	σ	N	κ_w	σ	N	κ_w	σ	N
0.025	0.24		1	0.27		1	0.30	0.12	3	0.35	0.16	5
0.05			0	0.14		1	0.19	0.05	4	0.38	0.21	4
0.1	0.03		1	0.05	0.04	5	0.14	0.08	8	0.13	0.03	3
0.2	0.21		1	0.07	0.01	2	0.18	0.08	6	0.18	0.08	2
0.3	0.18	0.04	3	0.14	0.04	3	0.20	0.08	4	0.25	0.08	3
	Average	σ	N	**Average**	σ	N	**Average**	σ	N	**Average**	σ	N
Number (cm^{-3})	17905.9	5378.1	10	15364.2	4567.1	24	9041.9	7022.2	48	22682.2	18082.6	33
Volume ($\mu m^3/cm^3$)	15.7	7.0	10	13.4	4.7	24	6.4	4.6	48	8.3	4.3	33

The measurements in the vicinity of Mexico City indicate that the aerosol is undergoing both physical and chemical changes on a local scale. To examine this evolution on a more regional scale with better counting statistics, a study domain with a 300 km radius from the center of the MCMA but excluding the MCMA was used and is shown as the light blue line in Figure 10. The distance of 300 km was chosen because the average wind speed measured aboard the C-130 to the northeast of the MCMA was 25 km/hr. Therefore, at the edge of the domain, the aerosol has roughly been in transport for 12 hours.

A total of 954 size distributions were measured within this domain. The average number and volume concentration for each research flight are shown in Table 6. The standard deviation is large for the number and volume concentration. This is a result of the difference in the concentrations within the plume versus outside of the plume. Also, there is a very large and dominant source of aerosol from the Tula, which was overflown on many research flights. A more detailed analysis that breaks out the MCMA emissions from the background will be discussed in the following section.

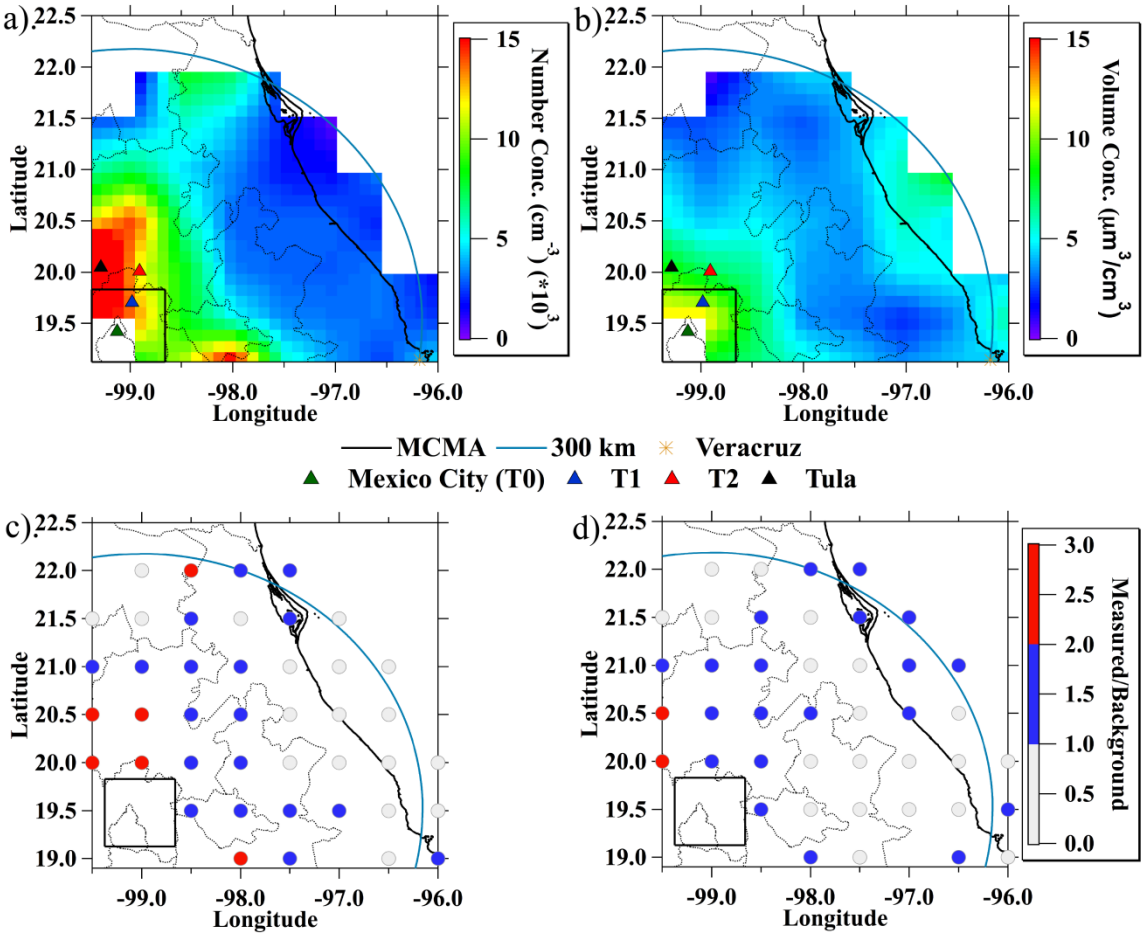

Figure 10. The average number (a) and volume (b) concentration northeast of the MCMA. The ratio of measured number concentration to background (c) and measured volume concentration to background (d) is also shown. The extent of the 300 km domain is indicated by the blue arc.

Table 6. The average number and volume concentration measured within the 300 km domain to the northeast of Mexico City.

	Number Conc. (cm^{-3})	σ	Volume Conc. ($\mu m^3/cm^3$)	σ	N
3/10/2006	4619	4355	6.1	5.1	137
3/12/2006	1845	1964	3.9	4.9	113
3/16/2006	5739	5055	2.7	1.9	81
3/18/2006	9572	9178	3.9	4.1	70
3/19/2006	10152	10579	4.9	2.6	85
3/22/2006	7177	10995	7.3	4.4	148
3/26/2006	5138	7446	2.9	1.7	65
3/28/2009	2501	811	3.5	1.2	162
3/29/2006	9804	10890	5.6	2.6	93
AVERAGE	5820	7983	4.8	3.9	954

Even with the large standard deviations, the mean number and volume concentration gives further insight into the daily variability of the aerosol. The Meteorological overview paper by *Fast et al.* [2007] indicated isolated convection occurring on March 13 and 14 ahead of the first Norte, scattered convection during the frontal passage on March 15, scattered convection on the backside of the front on March 16, and isolated convection on March 17. On the first research flight, the average volume concentration was 6.1 +/- 5.1 $\mu m^3/cm^3$; however, after convective activity and passage of the Norte, the average volume concentration decreased to 2.9 +/- 1.9 $\mu m^3/cm^3$ on March 16. This difference is statistically significant (α=0.05). However, this drop in volume and surface area (not shown) concentration as discussed in the previous section appears to have enabled nucleation to occur, with the number concentration almost doubling from 5739 +/- 5055 cm^{-3} on March 16 to 9572 +/- 9178 on March 18. This difference is statistically significant (α=0.05). During the same time period, the volume

concentration increased to 3.9 +/- 4.1 $\mu m^3/cm^3$. This difference is also statistically significant (α=0.05). Condensational growth appears to have then occurred from March 18 to March 22 as the number concentration decreased and the volume concentration significantly increased. The next two Nortes came in quick succession with a frontal passage occurring on March 22 and another occurring on March 24 into 25. Isolated convection occurred on March 23, 24, and 26. During the March 26 flight, the Norte and isolated convection again caused a decrease in the number concentration and a significant decrease in volume concentration when compared to the previous flight on March 22. The values were similar to what was measured on March 16. Interestingly, though no widespread nucleation was observed on the March 28 research flight, widespread nucleation appears to have been occurring on March 29. The delay in new particle formation may be a result of the isolated convection occurring in the MCMA area from March 26 until the end of the campaign, which subsequently decreased the amount of incoming solar radiation.

The average number and volume concentration for all flights within this domain are plotted in Figure 10. The measured number and volume concentration were placed into a 0.5° grid space. The values within each grid were averaged. The averages were then interpolated across the grids to create Figure 10. What is readily apparent is that Tula has on average a very high aerosol number concentration exceeding 20,000 cm^{-3}. Another feature is the plume of aerosols being advected towards the north and northeast away from Tula. To better illustrate this advection, the ratio of the measured to background concentrations are shown in Figure 10. The method used to calculate the

background aerosol concentration is discussed in the next section. Mexico City also exerts a strong influence on the area within 150 km of the city center, as number concentration in this region is on average greater than 10,000 cm^{-3} and the ratio of measured to background concentration exceeds one. High volume concentrations can be seen on the northern side of Mexico City. This is the location of the exposed ancient lake bed of Lake Texcoco and is where the aerosol from the MCMA is being advected out of the basin. Higher volume concentrations were also measured to the east of the basin near Puebla, Mexico, and over the Gulf of Mexico.

The TDMA measured a total of 405 growth distributions at dry diameters of 0.025, 0.05, 0.1, 0.2, and 0.3 μm within the 300 km domain. Table 7 shows the number of growth distributions measured for each dry diameter. A TDMA scan through all sizes was completed every 12 to 15 minutes depending on the concentration of particles.

All measured κ values within the defined domain are plotted in Figure 11. The aerosol within the Aitkin mode is mostly monomodal, and κ approaches values close to pure ammonium sulfate beyond 150 km from Mexico City. Values near the city are barely soluble and are mostly composed of organics. Aerosol with a dry diameter of 0.100 μm has growth distributions that are at times bimodal. This aerosol at this diameter is less soluble than the other dry diameters measured. The aerosol within accumulation mode has growth distributions that are almost exclusively bimodal. Often this aerosol has a soluble and less soluble mode. Both modes are plotted within Figure 11.

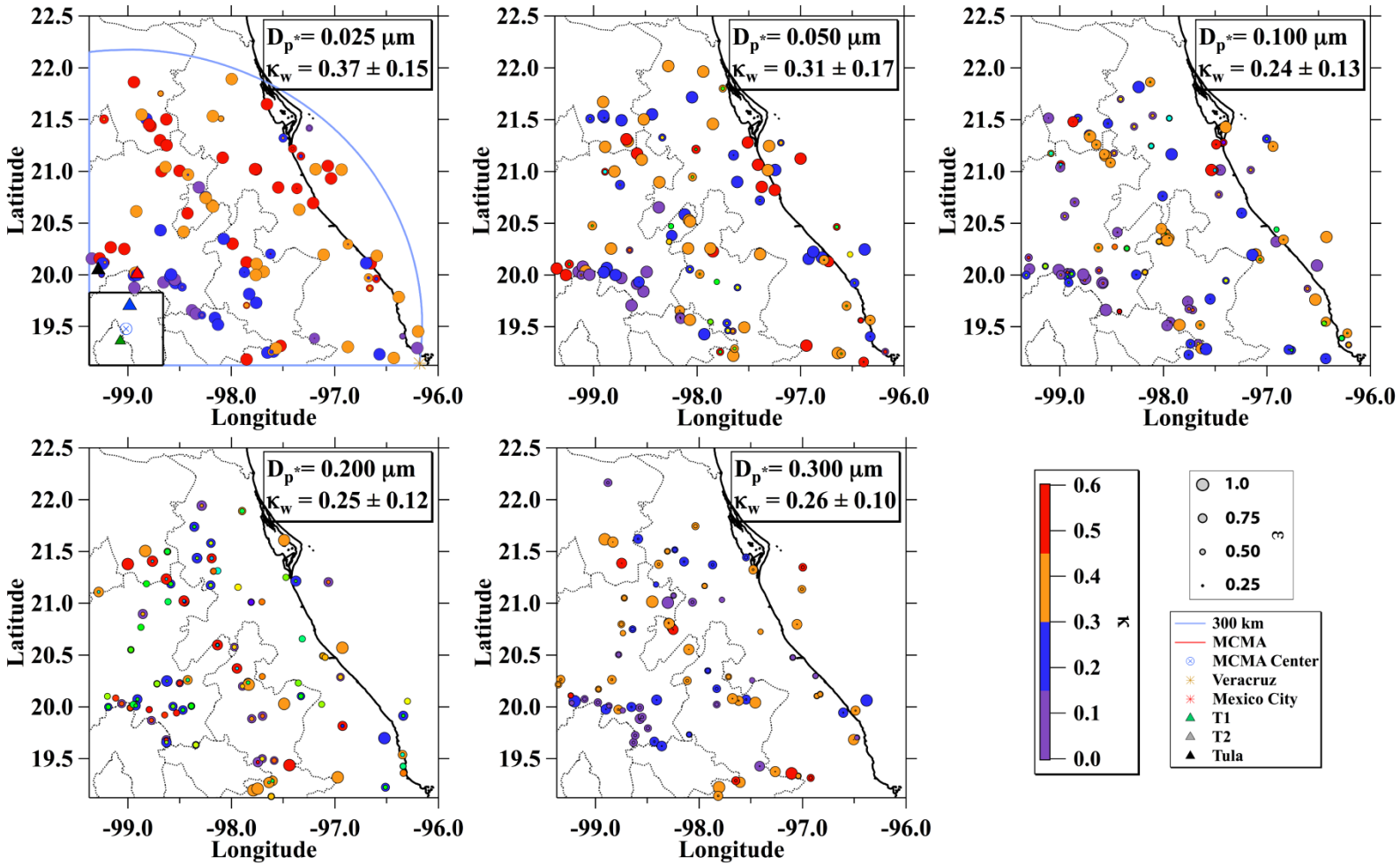

Figure 11. κ values northeast of the MCMA within the 300 km domain. The color of the marker indicates the κ value, and the sizea of the marker indicates its overall contribution to the measured growth distribution. The annotation indicates the dry diameter and the average κ_w.

As discussed above, the solubility of the aerosol increases as the distance away from the MCMA increases. To test this hypothesis, a linear regression analysis (κ_w=m*[distance] + b) was run for each dry diameter. The analysis included the distance from Mexico City versus the measured κ_w within the 300 km domain and the MCMA. Table 7 includes the results from the linear regression analysis. The κ_w value increases by roughly 0.08 to 0.10 per every 100 km across the domain. Although the correlation of the data is low, the trend is fairly strong. The aerosol is clearly undergoing modification through oxidization, condensation of gas phase species onto the aerosol surface, and/or coagulation.

Table 7. Average κ_w for each dry diameter within the basin and the 300 km domain to the northeast of Mexico City. The coefficients from a linear regression analysis of κ_w versus distance from Mexico City are also included.

D_p* (μm)	κ_w (Basin)	σ	N	κ_w (Domain)	σ	N	m (per 100km)	Intercept (b)	r^2
0.025	0.21	0.12	20	0.37	0.16	97	0.09	0.21	0.18
0.050	0.13	0.09	19	0.31	0.17	80	0.06	0.19	0.09
0.100	0.09	0.06	20	0.22	0.12	83	0.00	0.22	0.00
0.200	0.13	0.06	18	0.25	0.12	74	0.05	0.15	0.11
0.300	0.17	0.04	18	0.26	0.10	71	0.05	0.17	0.16

2.5.4 Evolution of the Mexico City plume

The one caveat in the analysis of κ and aerosol concentration in the previous section is that it only considered the spatial variability and did not explicitly analyze the temporal variability of the aerosol as it is advected out of Mexico City. The analysis also did not differentiate between MCMA and background aerosol. To narrow down the aerosol source, the origin of the measured aerosol was determined using the seven-day

kinematic back trajectories calculated by the Fuelberg research group at Florida State University. Any back trajectory passing through the previously defined MCMA was tagged as being influenced by Mexico City. The time in transport was defined as the time since the aerosol had been advected outside of the MCMA. All back trajectories that passed within 15 km of Tula or Veracruz were excluded.

The first analysis is to determine if there is a significant difference between the physical properties of the aerosol within the Mexico City plume (MCMA) when compared to outside of the plume (background). The average values for CO concentration, number concentration, and volume concentration for all flights are shown in Table 8. The MCMA plume is significantly different (α=0.05) from the background aerosol, with number concentration almost tripling and volume concentration almost doubling. CO concentration was included to demonstrate that an urban plume was being measured. The CO concentration within the plume was significantly different (α=0.05) than the background concentration.

Table 8. The average CO, number, and volume concentration for aerosol within and outside of the Mexico City plume.

	CO (ppb)	σ	N	Number Conc. (cm^{-3})	σ	N	Volume Conc. ($\mu m^3/cm^3$)	σ	N
Background	129	47	353	3800	3775	588	4.2	3.7	588
MCMA	207	127	405	9927	8790	443	7.9	6.0	443

The most probable size distributions within the plume and for the background aerosol are shown in Figure 12. The number size distribution within the plume appears urban, with a dominant Aitken mode that merges into a size distribution that resembles

aged continental aerosol. Outside of the plume there are hints of a Nucleation/Aitken mode; however, the most probable size distribution is dominated by aged continental aerosol. To investigate the occurrence of the Nucleation/Aitken mode, a ratio of the integrated concentration from 0.012 to 0.050 μm to the total integrated concentration was calculated. If the ratio was greater than 60%, it was determined that a strong Aitken mode was present. This occurred 44% of the time in the plume compared to 27% of the time in the background. The average integrated concentration from 0.012 to 0.050 μm within the plume was 13909 +/- 10225 cm^{-3}, which is significantly greater (α=0.05) than the number concentration of 6060 +/- 4210 cm^{-3} measured outside the plume. The amplitude of the volume size distribution within the plume was almost double the amplitude of the volume distribution outside of the plume. The aerosol size distributions measured within the Mexico City plume are significantly different from the background aerosol.

The concentration of particles within the Mexico City plume should theoretically decrease over time as a result of dispersion and deposition. A power law distribution was fitted to model the decrease in the measured number and volume concentration with respect to length of time in transport (Figure 13). The fit for number concentration did not include data from six hours in transport. These data were outliers that were biased from the widespread nucleation occurring on March 18. The scaling exponent (B) in the fit is similar, with the number concentration at -0.422 +/- 0.049 and the volume concentration at -0.476 +/- 0.029. This implies that the process controlling the decrease in volume and number concentration is similar. The slightly higher scaling exponent for

the volume concentration may be a result of the larger particles being more susceptible to loss from dry and wet deposition. Overall, the majority of the decrease occurs with the first 12 hours of transport.

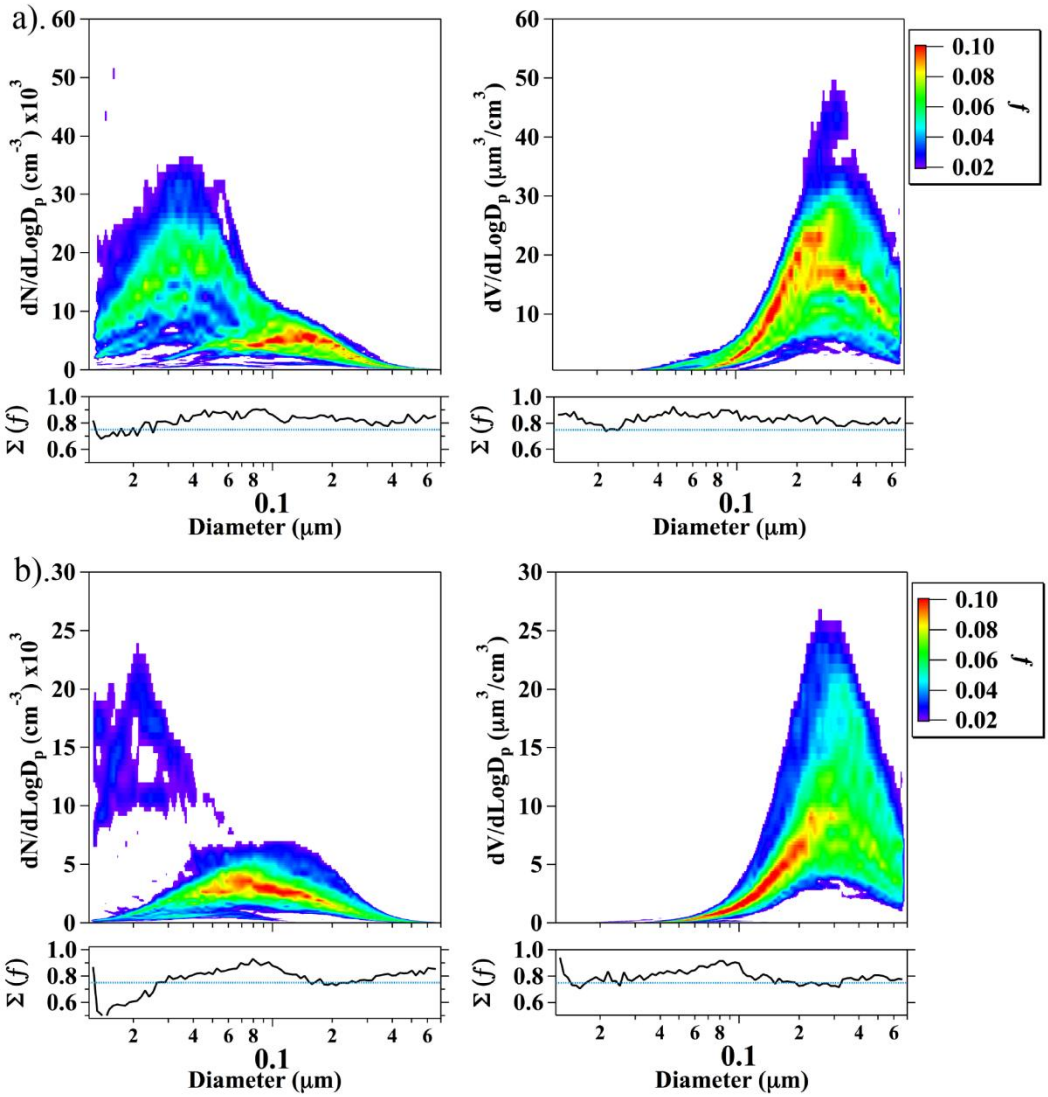

Figure 12. The most probable size distribution for aerosols within (a) and outside of the plume (b). Aerosol outside of the plume is considering background aerosol. The most probable number distribution is plotted on the left, and the most probable volume distribution is plotted on the right. The strip chart below each size distribution indicates the percentage of all probable values that is displayed in the corresponding size distribution. Note the maximum of the y axis in (a) is double the maximum in (b).

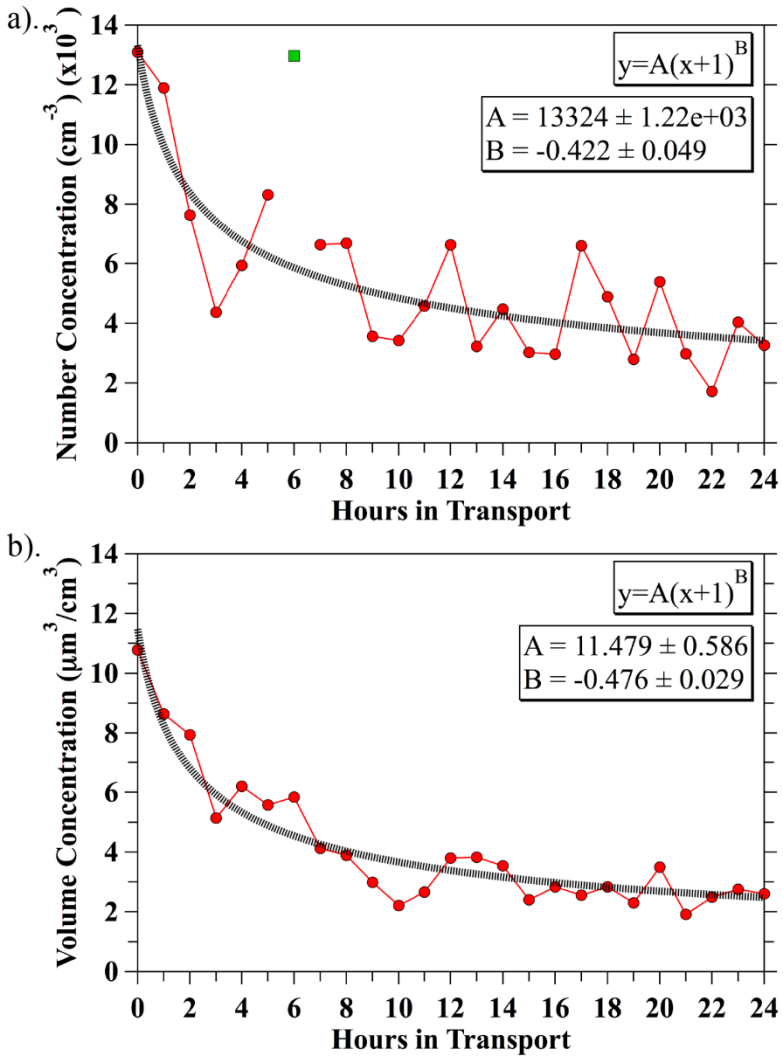

Figure 13. Number (a) and volume (b) concentration plotted versus hours in transport. The power law distribution fit is shown as a dashed line, and the coefficients for the fit are annotated.

TDMA measurements of κ_w within the plume and outside of the plume are shown in Table 9. For all measured values of κ_w, the background aerosol is more soluble than the aerosol within the plume. However, the only significant difference is for a 0.100 μm dry diameter aerosol. The difference for 0.050 and 0.200 μm dry diameter aerosol is just barely not significant (α=0.10). Looking at how the measured κ_w changes

spatially, the aerosol is becoming more soluble as it is transported further away from Mexico City. At 100 km, the difference between the 0.100, 0.200, and 0.300 μm dry diameter aerosol within the plume and outside of the plume is significant. The difference for 0.050 μm dry diameter aerosol is significant at α=0.10. However, at distances greater than 200 km the difference is no longer significant. Also, the background aerosol is less soluble the closer it is Mexico City, which indicates the city has a strong influence on the area local region. The increase in solubility could be partially attributable to the oxidation of the organic aerosols. An increase in oxygenated organic aerosol was observed by the ATOFMS [*DeCarlo et al.*, 2008] and through the analysis of samples collected on Teflon filters [*Gilardoni et al.*, 2009] aboard the C-130. In addition, an AMS aboard the DOE ARM Aerial Facility G-1 aircraft noted an increase in oxygenated organic mass with increasing aerosol age [*Kleinman et al.*, 2008]The analysis above has shown that the aerosol is undergoing chemical changes as it is being advected away from Mexico City. The remaining question is how fast the aerosol is being chemically modified. Using the back trajectory model, each measurement of κ was assigned a time since advection from the MCMA. The hours of transport, measured κ, and the ε was used to create the cumulative histograms in Figure 14. The TDMA measurements were broken in to 5 separate time ranges: less than 3 hours, from 3 hours to 6 hours, from 6 hours to 12 hours, from 12 to 24 hours, and from 24 to 48 hours since being advected from the MCMA. For each dry diameter and time frame, a histogram of κ_w was created. Each bin in the histogram has a width of 0.05 κ_w, and the bins range from 0.00 to 0.60 κ_w. Instead of using 1 for the occurrence of a κ value, the ε for that κ

value was used. This prevented κ values with low ε from biasing the histogram. From each histogram a cumulative histogram was calculated.

Table 9. Average k_w for each dry diameter within the 300 km domain, within 100 km of Mexico City, and greater than 200 km from Mexico City. MCMA indicates data measured within the plume, and non-MCMA is background aerosol measured outside of the plume.

Background	All			< 100km			> 200km		
Dp (μm)	Avg. κ_w	σ	N	Avg. κ_w	σ	N	Avg. κ_w	σ	N
0.025	0.38	0.15	68	0.29	0.14	13	0.44	0.16	33
0.05	0.34	0.16	66	0.25	0.16	15	0.37	0.17	33
0.1	0.25	0.12	70	0.17	0.07	12	0.29	0.13	35
0.2	0.26	0.12	59	0.20	0.06	8	0.28	0.13	29
0.3	0.28	0.10	55	0.22	0.07	14	0.31	0.10	23
MCMA									
0.025	0.35	0.16	29	0.20	0.14	9	0.46	0.11	10
0.05	0.29	0.14	35	0.12	0.11	8	0.33	0.07	12
0.1	0.20	0.12	30	0.10	0.07	9	0.25	0.10	9
0.2	0.22	0.12	31	0.14	0.06	14	0.24	0.09	6
0.3	0.25	0.11	31	0.16	0.06	9	0.28	0.09	8

For almost all diameter sizes, the change in solubility terminates after 6 to 12 hours since advection. The Aitken mode aerosol still undergoes some chemical changes out to 24 hours; however, a majority of the transformation occurs in less than 12 hours. The 0.100 μm and accumulation mode aerosol have no noticeable change in solubility after six hours. This very rapid transformation explains the results from the previous analysis that showed a change of κ_w of roughly 0.06 to 0.1 per 100 km. That κ_w within 100 km of the MCMA is significantly different within the plume compared to the background; however, this is not true at distances greater than 200 km.

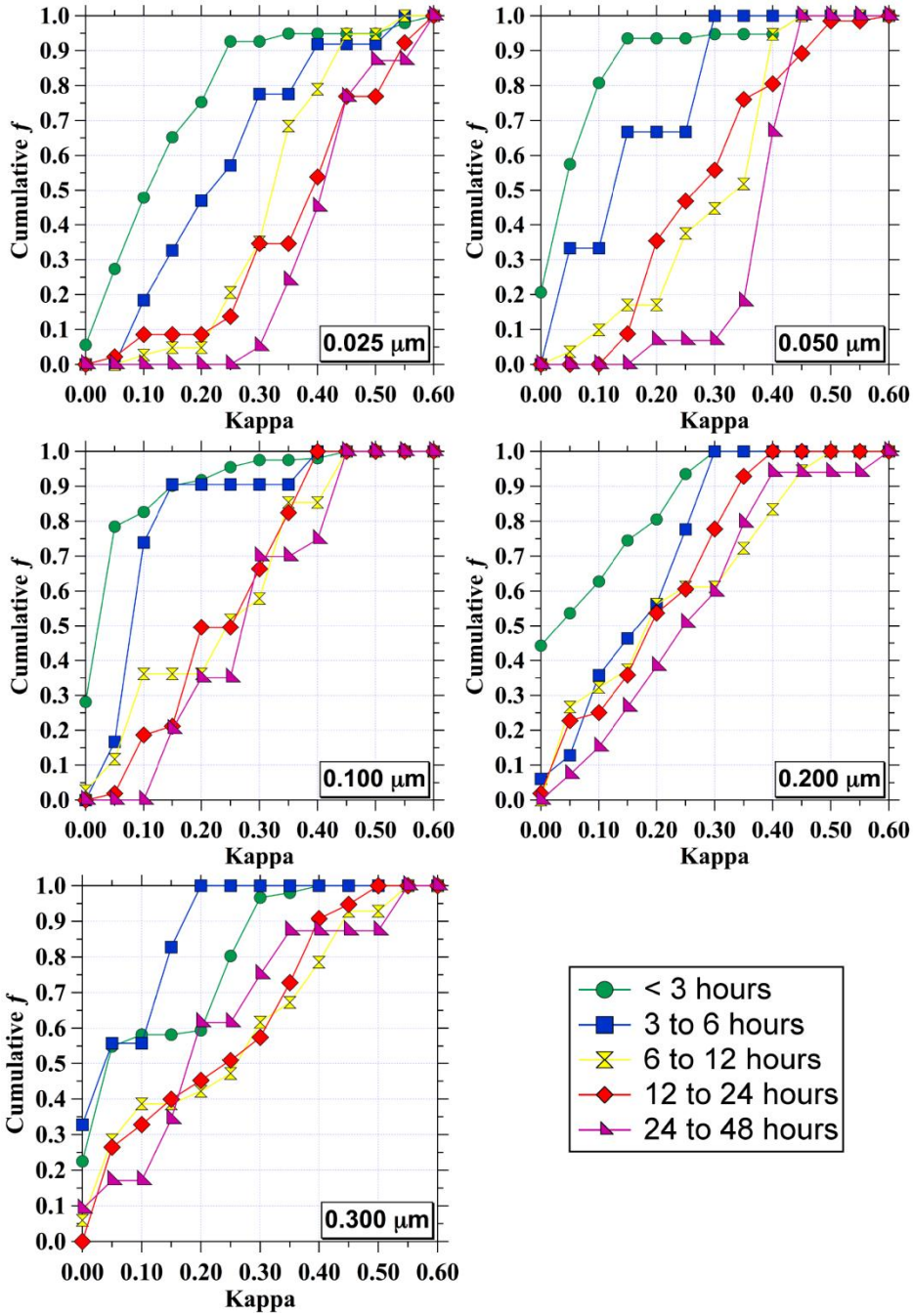

Figure 14. Cumulative histograms of κ for each dry diameter. Each histogram contains 5 time ranges; less than 3 hours, 3 to 6 hours, 6 to 12 hours, 12 to 24 hours, and 24 to 48 hours. The dry diameter is annotated on each plot.

As discussed above, some of the increase in hygroscopicity over time appears to be attributable to the formation of secondary organic aerosol through the oxidation of the primary organic aerosol. In a recent Science paper [*Andreae,* 2009; *Jimenez et al.,* 2009], an increase in the measure κ_{org} (organic) within the Mexico City plume was shown to correlate strongly with an increase in the ratio of oxygen to carbon mass (O/C). Higher values of O/C indicate higher values of oxidation. In addition, the measurements made during MILAGRO correlate well with laboratory measurements of the increase in hygroscopicity of α-pinene with increasing oxidation. This result underscores the importance that oxidation of organic aerosol plays in aerosol solubility within urban environments. However, the current SOA models have difficulty replicating the observed SOA yields during MILAGRO [*Dzepina et al.*, 2009]. The failure of the SOA models has prompted the recent development of a 2D volatility basis set modeling framework using organic aerosol volatility and oxidation state [*Jimenez et al.*, 2009]. This model has demonstrated the ability to predict reasonable SOA mass yields and the O/C ratio, which is important in determining the hygroscopicity of the organic aerosol.

To corroborate the rapid increase in κ_w measured by the TDMA, the mass of sulfate, ammonium, and organics measured by the AMS was analyzed. The AMS measurements of particle mass were tagged with a backtrajectory that yielded the hours the particles had been in transport from the MCMA. The SO_4 mass increased by a factor of 5, and NH_4 increased by a factor of 2 over a period of 8 to 12 hours as shown in Figure 15. Over the same time frame the organic mass increased by factor of 2; however, before the increase, the mass decreased by a factor of 5. Throughout the transport of the

aerosol, the sum of the SO_4 and NH_4 organic mass constitutes 84.5 ± 4.7 % of the total aerosol mass. Near the MCMA, organic mass contributes a little more than 65%, and SO_4 and NH_4 contribute 15% to the overall mass. However, after 8 to 12 hours, SO_4 and NH_4 contribute roughly 37% to the overall mass and organics now contribute roughly 46% to the overall mass. The fraction of NH_4 mass in the aerosol phase changes very little during transport, increasing from roughly 10% to 15% to the overall mass. The timeframe for the increase in SO_4 matches the measured increase in hygroscopicity discussed above and indicates that the condensation of sulfate into the particle phase and/or coagulational growth is occurring. The mass of SO_4 increased from 0.49 ± 0 .64 to 2.69 ± 0.75 μg/m^3 over the 10-hour transport period.

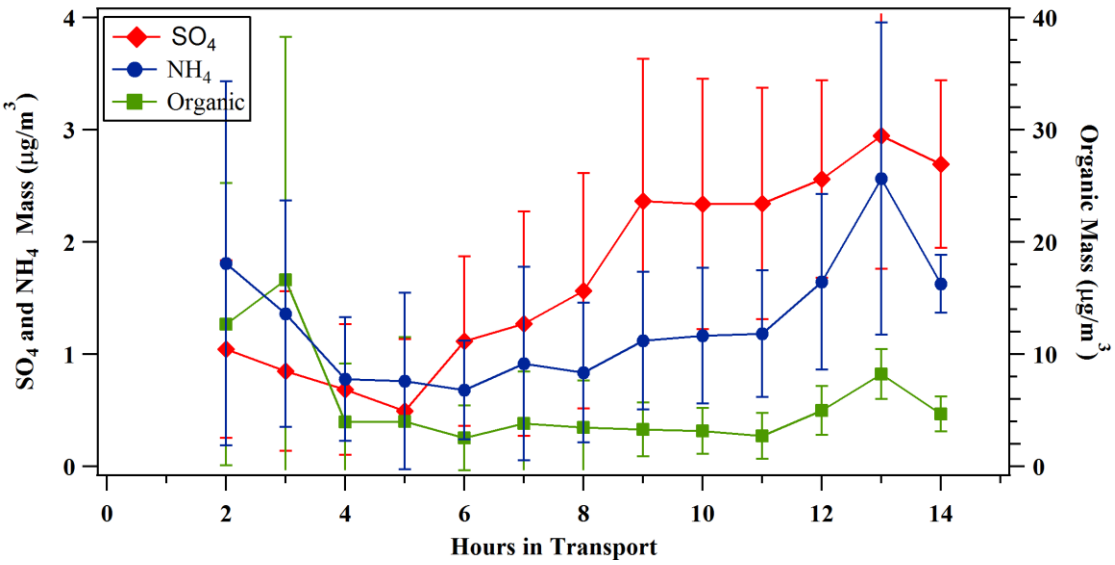

Figure 15. The measured mass of SO_4, NH_4, and organics in the particle phase versus hours in transport. The y-axis scale for organic mass is located on the right-hand side of the figure and is an order of magnitude greater than the y-axis scale for SO_4 and NH_4 mass. Both the SO_4 and NH_4 mass increase as the hours in transport increase.

Gas phase SO_2 was also measured aboard the NCAR C-130. A plot of SO_2 versus hours in transport is shown in Figure 16. No to little change in the concentration of SO2 is observed during transport. This indicates that there is a large regional source of SO_2 found to the northeast of Mexico City. This source is contributing to the increase in the aerosol hygroscopicity through gas phase condensation.

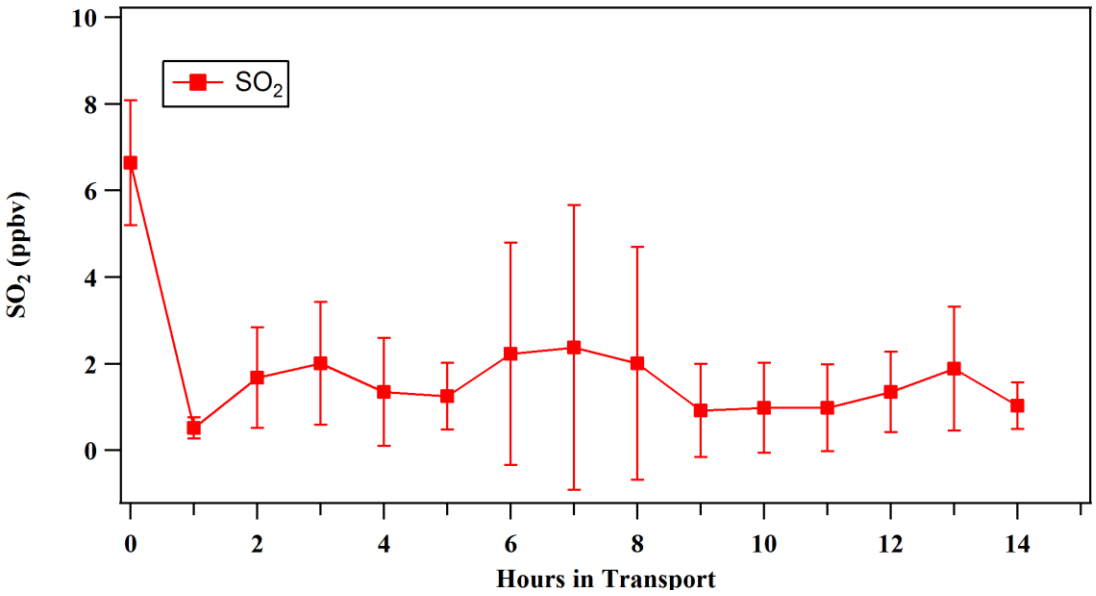

Figure 16. The concentration of gas phase SO_2 versus hours in transport.

If condensational growth was occurring, the geometric mean diameter of the accumulation mode should be shifting to larger sizes during the transport of the aerosol away from the MCMA. The DMA distributions were fitted with lognormal distributions using the same manner described for the TDMA growth distributions. Any geometric mean diameter greater than 0.09 μm was considered part of the accumulation mode. If more than one mode was present, each mode's contribution to the overall distribution was normalized to each other to derive their overall contributions to the accumulation

mode. The contribution to the accumulation mode was then used to calculate a weighted average for the geometric mean diameter of the accumulation mode. A linear regression analysis indicates that the geometric mean diameter of the accumulation mode increases by about 0.002 μm for every 1 hour of transport (Figure 17). After 12 hours of transport, the diameter has increased from 0.144 ± 0.036 μm to 0.166 ± 0.045 μm. This difference is significant and indicates that some condensational growth is occurring.

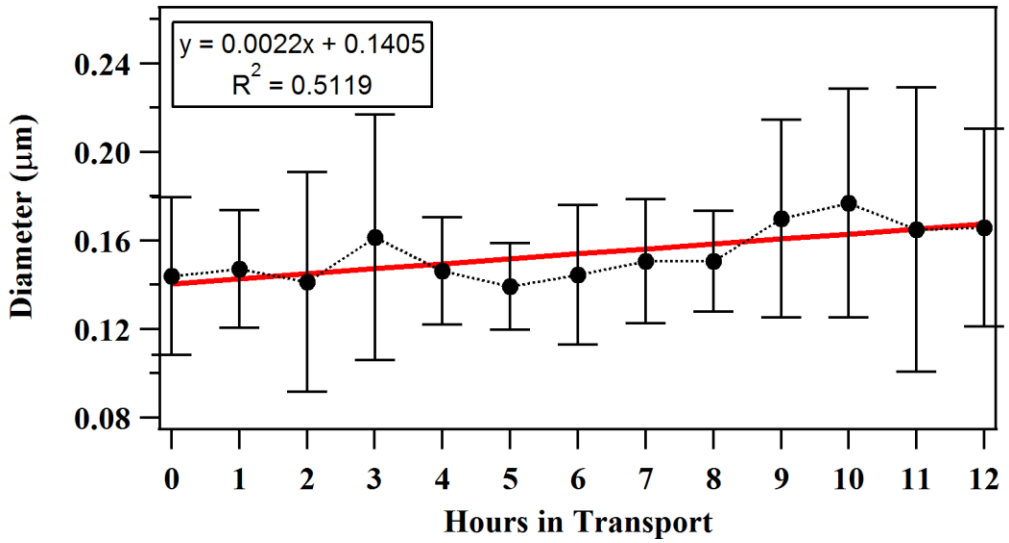

Figure 17. The geometric mean diameter of the accumulation mode versus hours in transport. The red line represents the fit from the linear regression.

One remaining question is whether the observed increase in the aerosol hygroscopicity can be solely explained by the increase in sulfate in the particle phase. The most probable size distribution indicated in Figure 12a was used to represent the most probable size distribution in the Mexico City plume from 0.1 to 0.67 μm. The average TDMA measurement of κ after 6 to 12 hours of transport is used in conjunction with the Kohler equation to estimate the soluble and insoluble mass at 0.1, 0.2, and 0.3 μm. Interpolating the calculated mass values across the distribution and multiplying the resulting mass within each bin by the number concentration of particles in the bin yields an estimate of the total soluble and insoluble mass for each bin. Total soluble and insoluble mass at the end of 12 hours is 6.6 $\mu g/m^3$ soluble and 4.8 $\mu g/m^3$ insoluble totaling 11.3 $\mu g/m^3$. This is in agreement with the AMS estimated total mass after 12 hours of transport of 10.8 $\mu g/m^3$. However, the AMS only measured 4.2 $\mu g/m^3$ of soluble mass after 12 hours of transport. This indicates that there is a little over 2 $\mu g/m^3$ of soluble material that needs to be accounted for to explain the increase in hygroscopicity. This missing material may be explained by the oxidation of organics, which has been shown to increase the hygroscopicity of the organics in the aerosol phase [*Jimenez et al.*, 2009]

2.5.5 Aerosol and cloud interactions

The aerosol from Mexico City undergoes rapid chemical transformation as it is advected towards the northeast. One of the goals of MILAGRO was to investigate how the physicochemical properties of the aerosol could affect both the local and regional

environment. This is especially important when it comes to the effect on clouds. The aerosol could cause a decrease in precipitation through the first indirect effect and an increase in the clouds' lifetime and reflectivity through the second indirect effect.

To investigate this potential influence, an extended Kohler theory was used to predict the critical supersaturation of the aerosol for a given dry diameter and κ (GF). The equations were discussed within the methodology. In this instance, the aerosol was assumed to be composed of the soluble inorganic ammonium sulfate and an insoluble organic aerosol.

The calculated critical supersaturation values are shown in Table 10. The 0.100 μm transitions from a high S_c to a S_c that would be common in a cumulus cloud or potentially stratus cloud over a period of 12 hours. The κ_w for the 0.100 μm aerosol at less than 3 hours was 0.0874 +/- 0.0601 and for a 0.200 μm aerosol was 0.131 +/-.118. Assuming a supersaturation of 0.30 %, the activation diameter is located between 0.100 and 0.200 μm. Assuming a linear relationship in κ_w, the activation diameter was iteratively solved to be approximately 0.115 μm at less than 3 hours of transport. Repeating this calculation for a transport time of 6 to 12 hours, the activation diameter is approximately at 0.075 μm.

The decrease in the activation diameter will lead to an increase in the number of aerosols that are activating to become cloud condensation nuclei within the clouds to the northeast of Mexico City. The increase in the concentration of CCN should increase the lifetime of the cloud, first indirect effect, and decrease the precipitation, second indirect effect. However, with more particles activating, more particles will be removed by wet

deposition if sufficient water vapor is present. This could in effect reduce the range of the Mexico City aerosol effect. The exact interplay between the Mexico City aerosol plume and the clouds needs to be studied in a regional model to work out the magnitude of the effect and over what distances it occurs.

Table 10. The predicted critical supersaturation for a 0.050, 0.100, and 0.200 μm dry diameter aerosol. .The average κ_w at each time range is used in the prediction.

Diameter (μm)	Less than 3 S (%)	3 to 6 S (%)	6 to 12 S (%)
0.050	0.80	0.70	0.49
0.100	0.41	0.34	0.22
0.200	0.10	0.08	0.07

3. RESULTS FROM THE INTEX-B FIELD CAMPAIGN

3.1 Overview of the Transport of Asian Pollution

Over the past decade, eastern Asia has seen a rapid increase in industrialization and as a result, a rapid increase in the emission of atmospheric pollutants. This rapid rise is evident by the difficulties scientists have had in estimating Asian pollution. In 2000, estimates of the present and future emissions of China were published by *Streets and Waldhoff [2000]*. Sulfur dioxide emissions were projected to increase from 25.2 Tg/yr in 1995 to 30.6 Tg/yr in 2020, provided emission controls are implemented on major power plants; if this does not happen, emissions could increase to as much as 60.7 Tg/yr by 2020. Emissions of nitrogen oxides are projected to increase from 12.0 Tg/yr in 1995 to somewhere in the range of 26.6–29.7 Tg/yr by 2020, with little in the way of pollution controls or other emission reduction measures in place. Emissions of carbon monoxide are projected to decline from 115 Tg/yr in 1995 to 96.8 Tg/yr in 2020, due to more efficient combustion techniques, especially in the transportation sector; if these measures are not realized, carbon monoxide emissions could increase to 130 Tg/yr by 2020.

The above estimations were modified in 2003 following atmospheric modeling and analysis of observations taken during the Transport and Chemical Evolution over the Pacific experiment (TRACE-P) and the Aerosol Characterization Experiment-Asia (ACE-Asia) [*Streets et al.*, 2003] In 2006, the concentration of carbon monoxide emitted from China was further modified from 116 Tg/yr to 157 Tg/yr, which is well

beyond the values estimated in 2000. The revised emission rate was a result of further modeling with TRACE-P data, which indicated that the emission of CO from the industrial sector was being underestimated. The emissions from the residential sector may still be underestimated due to the difficulty of approximating biomass burning [*Streets et al.*, 2006]. The estimated levels of anthropogenic emissions for 2001 are listed in Table 11.

Table 11. Current estimates of the yearly emission rates for China, Japan, South Korea, and North Korea. Rates are provided for SO_2, NO_x, CO_2, CO, CH_4, nonmethane volatile organic compounds (NMVOC), submicron black carbon aerosol (BC), submicron organic carbon aerosol (OC), andNH_3 [*Streets et al.*, 2006; *Streets et al.*, 2003].

	Emissions (Tg/yr)								
Country	SO_2	NO_x	CO_2	CO	CH_4	NMVOC	BC	OC	NH_3
China	20.39	11.35	3817	157	38.36	17.43	1.05	3.39	13.57
Japan	0.8	2.2	1203	6.81	1.14	1.92	0.05	0.07	0.35
Korea, Rep. of	0.83	1.32	411	2.82	1.43	1.16	0.02	0.03	0.17
Korea, DPR	0.23	0.27	120	3.56	1.35	0.23	0.02	0.11	0.1
Total	22.24	15.14	5551	170.19	42.28	20.75	1.15	3.59	14.19

In 2009, a new inventory for Asian emissions was generated for the Intercontinental Chemical Transport Experiment-Phase B (INTEX-B) [*Zhang et al.*, 2009]. Total Asian anthropogenic emissions in the year 2006 were estimated as follows: 47.1 $TgSO_2$, 36.7 $TgNO_x$, 298.2 TgCO, 54.6 TgNMVOC, 29.2 $TgPM_{10}$, 22.2 $TgPM_{2.5}$, 2.97 TgBC, and 6.57 TgOC. China's anthropogenic emissions in the year 2006 were estimated as follows: 31.0 $TgSO_2$, 20.8 $TgNO_x$, 166.9 TgCO, 23.2 TgNMVOC, 18.2 $TgPM_{10}$, 13.3$TgPM_{2.5}$, 1.8 TgBC, and 3.2 TgOC. Compared to the 2001 emission estimates for China listed above in Table 11, there is a 36% increase for SO_2, 55% for NO_x, 18% for CO, 29% for VOC, 13% for PM_{10}, 14% for $PM_{2.5}$, BC, and OC. Remarkably, China has already exceeded the 2020 estimation of 30.6 Tg/yr for $SO_2$and

157 Tg/yr of CO. This sharp and dramatic increase in the emissions from Asia and China underscore the importance in understanding the transport of the Asian pollution across the Pacific Ocean.

Transport of the East Asian pollution is most frequent in the spring when the development of low pressure baroclinic systems over Asia vent the boundary layer and loft the pollution into the free troposphere where it can be carried rapidly across the North Pacific [*Yienger et al.*, 2000]. The export of the aerosols and gas phase pollutants from Asia occurs either through the wet processes of convective lifting and transport on warm conveyer belts [*Bethan et al.*, 1998; *Browning and Roberts*, 1994; *Cooper et al.*, 2002; *Liu et al.*, 2003] or through dust events where lifting occurs through dry processes [*Husar et al.*, 2001; *McKendry et al.*, 2001; *Vaughan et al.*, 2001]. Measurements off the coast of China were made by aircraft during the Aerosol Characterization Experiment-Asia (ACE-Asia) during the spring of 2001. An Aerosol Mass Spectrometer aboard the Center for Interdisciplinary Remotely Piloted Aircraft Studies (CIRPAS) Twin Otter measured the aerosol composition from the boundary layer up to 3700 m. The aerosols consisted of sulfates, organics, and some ammonium [*Bahreini et al.*, 2003]. Elevated levels of sulfate were also observed aboard the NCAR/NSF C-130 during ACE-Asia [*Kline et al.*, 2004]. These measurements showed that the particles are composed of large amounts of sulfate that is hygroscopic. This will make the aerosol population prone to precipitation scavenging and reduce the concentration transported to North America.

The transport of Asian anthropogenic aerosols was first observed at the surface in the 1980s from island sites during dust events with a spring maximum [*Arimoto et al.*, 1996; *Huebert et al.*, 2001; *Prospero et al.*, 2003; *Prospero et al.*, 1985; *Zieman et al.*, 1995]. Recent studies have begun to investigate the impact of the Asian pollution plume on North America [*Jaffe et al.*, 1999] . Over the past eighteen years, the springtime background O_3 mixing ratios have increased by approximately 10 ppbv, i.e., 30% along the U.S. west coast [*Jaffe et al.*, 2003]. Samples of Asian PM-2.5 aerosol from sites in the western cordillera of North America have indicated a constituent fraction of ~30% mineral, 28% organic compounds, 4% elemental carbon, 10% sulfate, <5% nitrate, and <1% sea salt [*VanCuren*, 2003]).

In 2002 at Trinidad Head, California, the National Oceanographic and Atmospheric Administration Intercontinental Transport and Chemical Transformation 2002 (ITCT 2K2) experiment was conducted to make in situ measurements of the Asian pollution off the west coast of the United States. An Aerodyne AMS measured the composition of the accumulation mode to be composed principally of sulfate, ammonium, and organic chemicals. The organic component bore a mass spectral signature that indicated a high degree of chemical oxidation [*Allan et al.*, 2004]. GEOS-CHEM and MOZART model simulations during ITCT 2k2 suggested that on average 10% of observed ozone (4 +/- 1 ppb), along with 33% of observed CO was transported to Trinidad Head from Asia [*Goldstein et al.*, 2004]. The calculated lifetimes were between 3 to 7 days for nitrate, sulfate, aerosol organics, and ammonium. The aerosol number density lifetime was calculated at 9.8 days [*Millet et al.*, 2004].

Model studies with GEOS-CHEM have determined the main component of Asian pollution to be sulfate [*Heald et al.*, 2006; *Park et al.*, 2004]. This is a result of the relatively efficient escape of SO_2 from the continental boundary layer observed during ACE-Asia and ITCT 2K2. As the aerosols are transported across the Pacific, removal of the sulfate aerosols occurs through precipitation scavenging as they pass through warm conveyor belts [*Cooper et al.*, 2004], and this is followed by particle production through the condensation of gas phase SO_2 into the aerosol phase during transport across the Pacific [*Brock et al.*, 2004; *Peltier et al.*, 2008]. The baseline concentration of sulfate in the western U.S. is 1.52 $\mu g/m^3$, of which 0.13 $\mu g/m^3$ to 0.16 $\mu g/m^3$ is from Asia with 24-hour maxima concentrations averaging 0.60 $\mu g/m^3$ and values up to 1.5 $\mu g/m^3$ in Washington State [*Heald et al.*, 2006; *Park et al.*, 2004]. In comparison, the EPA Regional Haze Rule mandates the achievement of "natural visibility conditions," which would require a sulfate concentration of 0.09 $\mu g/m^3$ by 2064 [*Park et al.*, 2004].

To fully ascertain the effects the aerosol emitted from Asia will have on the United States, further in situ measurements must be made to determine the size distribution and hygroscopic properties of the aerosol. In addition, the mixing state of the aerosol population and the effects of dry deposition and precipitation scavenging on the aerosol population need to be examined in greater detail. The information obtained from these types of measurements can determine the effect the transported aerosol will have on air quality, visibility, and clouds along the western coast of the United States.

3.2 INTEX-B Overview

The National Aeronautics and Space Administration (NASA) sponsored the Intercontinental Chemical Transport Experiment – Phase B (INTEX-B), and its primary goals were to measure the intercontinental transport of the Asian pollution plume as it was advected across the Pacific Ocean and to measure the long-range transport of the Mexico City pollution plume during MILAGRO. More information about the campaign can be found in *Singh et al.* [2009]. The NCAR C-130 participated in the second half of INTEX-B and flew a total of 94 hours over 12 research flights with operations based at Paine Field in Everett, Washington, to the north of Seattle. During the first half of INTEX-B, the DC-8 was based in Houston, and during the second half it was deployed further upstream from Seattle with flight operations being conducted out of Honolulu, Hawaii, from April 17 to 30, 2006, and Anchorage, Alaska, from May 1 to May 15, 2006. During the second half, several research flights were coordinated in an attempt to try to measure a more complete picture of the evolution of the physicochemical properties of the plume. Throughout the following discussion, INTEX-B will refer to the second half of the campaign.

In addition to the DC-8, a Cessna 207 operated by Environment Canada was also deployed in western Canada during INTEX-B and conducted measurements near the Whistler Peak Station (50.1^{o}N, 122.9^{o}W). The aircraft measured aerosol size, number density, and composition along with measurements of CO and O_3. The University of Washington Beechcraft Duchess 76 was operated out of Paine Field and made local measurements of CO, O_3, Hg, and aerosols.

The NCAR/NSF C-130 conducted flight operations from April 15 to May 15, 2006. The flights at the beginning and end of the field campaign were considered research flights, as most instruments were operating while the aircraft transited from and back to the Rocky Mountain Metropolitan Airport near Boulder, Colorado. The research flight on April 26, 2006, was a local flight around Seattle, and the research flight on May 3, 2006, was through the California Central Valley. An overview map of all the research flights is shown in Figure 18.

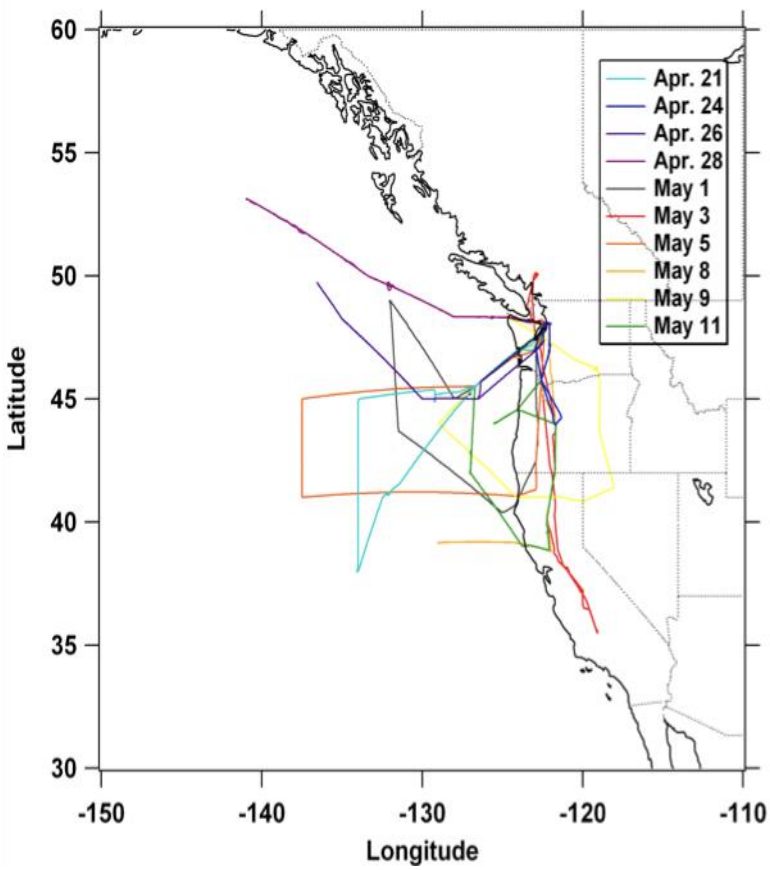

Figure 18. The NCAR C-130 flight paths during INTEX-B.

The primary goal of the research flights was to intercept the layers of the Asian pollution plume over the Pacific Ocean and the west coast of the United States. April and May of 2006 had a typical spring weather pattern with very strong lows passing through Asia, lofting aerosol and dust into the atmosphere. This pollution was subsequently advected across the Pacific by a strong jet stream. All research flights, except for the transit flights, intercepted pollution from Asia. The aircraft sampling during INTEX-B was fairly representative of the larger scale region, but with a slight bias towards higher influence from Asian contributions [*Pfister et al.*, 2010]. On average, the plume had been transported anywhere from 10 days to as short as 3 days at the measurement location. This variability has created the opportunity to analyze the physiochemical properties of the aerosol over various time scales of evolution.

3.3 Instrumentation

The aerosol sampled by the TAMU DMA/TDMA instrument was pulled into the aircraft through the same passive solid diffuser inlet mounted on the starboard side of the NCAR C-130 that was used during MIRAGE. The DMA/TDMA status and the number of size and growth distributions measured are shown in Table 12. The DMA had an unknown failure on April 21, and data were not collected for most of the flight. Otherwise, the instrument performed nominally. The TDMA experienced no problems and performed nominally.

Table 12. The number of DMA and TDMA measurements during the INTEX-B research flights.

	Julian Day	Flight Hours	DMA	TDMA				
				0.025 μm	0.050 μm	0.100 μm	0.300 μm	0.600 μm
04/17/06	**107**	8.83	189	12	13	13	11	
04/21/06	**111**	7.73	19		18	18	13	4
04/24/06	**114**	5.27	146	20	19	20	20	
04/26/06	**116**	7.50	159	18	17	19	12	
04/28/06	**118**	7.95	184	20	21	21	17	
05/01/06	**121**	8.65	149	20	21	21	19	
05/03/06	**123**	8.50	264	31	31	31	26	
05/05/06	**125**	8.45	280	27	29	29	24	
05/08/06	**128**	8.22	214	18	19	19	17	3
05/09/06	**129**	7.55	207	25	29	29	28	
05/11/06	**131**	7.75	198	27	28	28	25	
05/15/06	**135**	7.50	139	22	22	22	14	
TOTAL		**93.9**	**2148**	**240**	**267**	**270**	**226**	**7**

The aerosol drawn into the DMA/TDMA instrument was dried by passing the sample flow through a Nafion tube maintained at 2.3 +/- 2.2 % RH throughout the INTEX-B campaign. On average, the DMA measured one size distribution from 0.012 to 0.70 μm every 90 sec for a total of 2148 size distributions throughout the campaign. The TDMA cycled through the dry diameters of 0.025, 0.050, 0.100, and 0.300 μm roughly every 15 minutes and measured 240, 267, 270, and 226 growth distributions respectively. On two research flights, a high concentration of dust was forecasted, and an attempt was made to measure the solubility of 0.600 μm aerosols. On the April 21 flight, the 0.025 μm aerosol was not measured to enable the measurement of the 0.600 μm aerosol. The TDMA relative humidity was set to 85% and on average was maintained at 84.7 +/- 3.0 % throughout the campaign.

The Cloud Condensation Nuclei (CCN) concentration was measured by a Droplet Measurement Technology continuous-flow stream-wise thermal-gradient CCN counter (CCNc) [*Lance et al.*, 2006; *Roberts and Nenes*, 2005]. A stream-wise temperature gradient establishes a supersaturation within the column. An optical particle counter at the base of the column detects activated particles.

3.4 Back Trajectory Model

The analysis of the origin of the measured aerosol was determined using 10-day kinematic back trajectories calculated by the Fuelberg research group at Florida State University (http://fuelberg.met.fsu.edu/research/intexb). The back trajectories were modeled at 1-second intervals along the C-130 flight path. Every DMA distribution and TDMA growth distribution was tagged with the back trajectory calculated nearest to the midpoint time of the measurement.

Four domain areas were set up over East Asia (Figure 19) to track the source of the aerosol. The northern, middle, and southern domain areas within China contain the cities of Beijing, Shanghai, and Guangzhou. The fourth domain area is over Japan and contains the city of Tokyo. A back trajectory intercepting one of the domains was tagged as having been influenced by that domain.

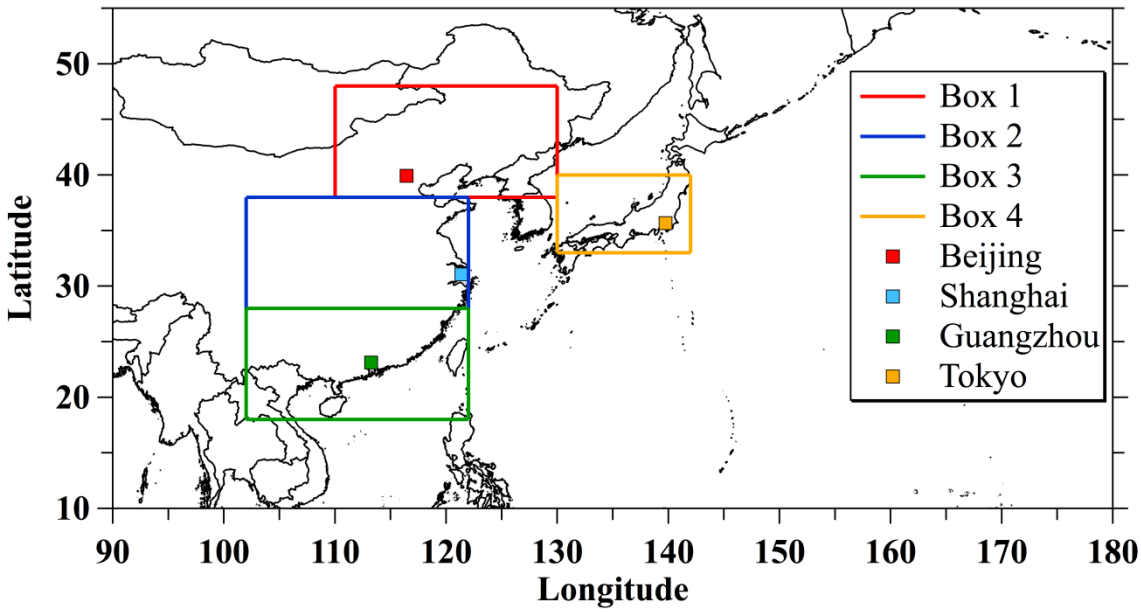

Figure 19. Five domain areas are defined as source regions in East Asia. The location of the major city in each source region is also indicated.

3.5 Data Discussion

The discussion below will first analyze the background physicochemical properties over the Pacific Ocean and contrast the background with the physicochemical properties of the plume. The second section will examine the transformation of the aerosol that occurs as it is being advected across the Pacific Ocean. The third section will conclude the discussion by investigating the aerosol and cloud interactions.

3.5.1 Sampling overview

The C-130 conducted eight flights with a large fraction of the flight path over the Pacific Ocean. Most of the following analyses will use data collected over the Pacific

Ocean within the free troposphere unless specified. The free troposphere has been defined as an altitude greater than 2.25 km ASL or AGL depending on the location of the aircraft. An overview of these flights along with the respective back trajectories is shown in Figure 20.

As shown in Figure 20, all the research flights were remarkably successful in intercepting the Asian plume. For flights on April 21, May 8, May 9, May 11, and portions of the May 1 flight, the meteorological setup established the transport of the pollution plume with little divergence. Table 13 gives an overview of the transport times for each day from each region. On May 8, rapid transport occurred with the aerosol in transit for only 4.3 +/- 0.4 days from North China and 3.5 days from Japan. At the beginning of the May 1 flight, aerosol was sampled that had been in transport for 3.5 days from North China and less than 3 days from Japan. Another rapid transport day was April 21, with aerosol sampled after 4.6 +/- 1.5 days of transport from North China, 4.0 +/- 0.3 days from Central China, and 3. 9 +/- 1.0 days from Japan. The flight days with the longest transport time were April 26 and May 11. The plume was in transport for 8 to 9 days from China and 7 days from Japan on April 26 and May 11.

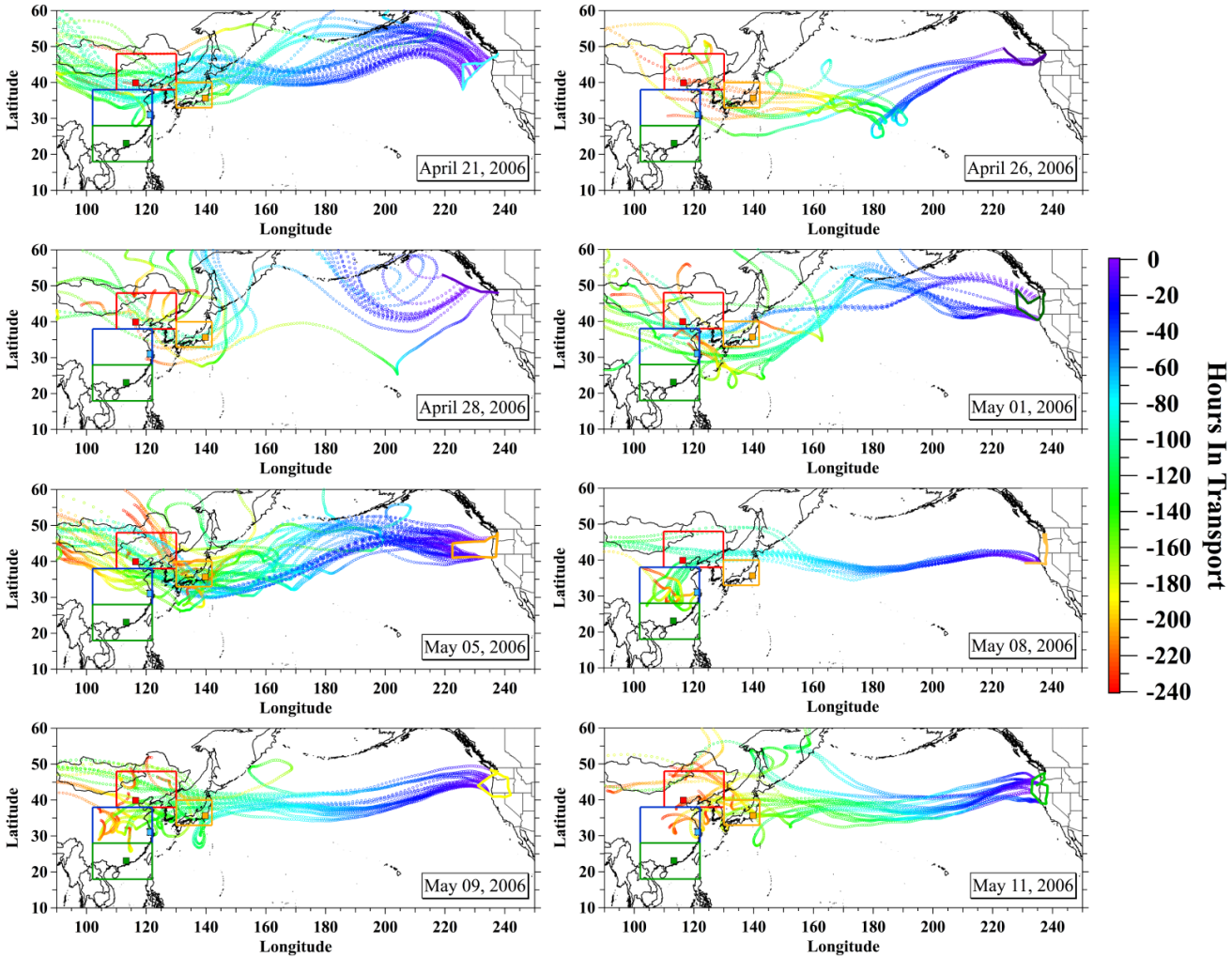

Figure 20. An overview of the back trajectories from the INTEX-B flights over the Pacific Ocean. The duration of the hours in transport is indicated by the color.

Table 13. Average hours in transport at the time of sampling for each research flight. Also indicated is the average, maximum, and minimum for all research flights.

	Average All Regions	σ	North China	σ	Central China	σ	South China	σ	Japan	σ
4/21/2006	-4.3	1.2	-4.6	1.5	-4.0	0.3	-5.3		-3.9	1.0
4/26/2006	-7.7	1.8	-7.6	1.7	-9.0	1.2	-9.7		-6.9	1.6
4/28/2006	-6.1	1.9	-6.4	1.9	-6.8	1.9			-5.3	1.9
5/1/2006	-5.3	2.3	-5.6	2.1	-5.8	2.3			-4.2	2.4
5/5/2006	-5.5	2.0	-5.8	2.3	-6.1	1.4			-5.0	2.0
5/8/2006	-5.0	1.3	-4.3	0.4	-5.6	0.8	-6.9	1.6	-3.5	
5/9/2006	-5.9	1.7	-6.0	1.4	-7.8	1.5	-7.3		-4.5	0.4
5/11/2006	-7.9	1.0	-8.1	1.0	-9.1	0.8			-7.1	0.4
Average	-5.7	2.0	-5.5	2.0	-5.3	2.0	-5.2	2.0	-5.8	2.6
Min	-4.3		-4.3		-4.0		-5.3		-3.5	
Max	-7.9		-8.1		-9.1		-9.7		-7.1	

For 3% of the overall measurements, the C-130 intercepted the plume after 2 to 3 days of transport. On average, the most common transport duration was between 3 to 4 days with this occurring for 21% of the measured aerosol. Overall, roughly 70% of the aerosol was sampled after 3 to 7 days of transport. Average transport for all data from all regions was 5.6 +/- 2.a days. The most common source for the aerosol was north China with 44%, followed by Japan with 32%, then central China with 22%, and finally south China with 2% of the back trajectories intercepting the respective region. Japan is strongly influenced by emissions from China, with 93% of the Japan back trajectories passing through or originating in China.

3.5.2 DMA size distributions

The number concentrations measured by the DMA from near the surface up to eight km above sea level are shown in Figure 21 for all research flights over the Pacific Ocean. During INTEX-B, the o-ring only failed after the DMA was exposed to large pressure drops over extended periods. Therefore, the measured size distributions from

the DMA were often valid for the first 5 to 10 minutes at high altitudes. To filter out the leak-contaminated distributions, the DMA size distributions were compared to the measured size distributions from University of Hawaii's Scanning Mobility Particle Sizer. Any DMA distribution not in agreement was discarded from the analysis.

Within the plume, an elevated layer of aerosol with number concentrations exceeding 2000 cm^{-3} and volume concentrations exceeding 2.0 $\mu m^3/cm^3$ was measured at 6 km on May 01. The elevated number concentration measured by the DMA was corroborated by the NCAR condensation particle counter (CPC) aboard the C-130 on May 1. Both instruments measured number concentrations in excess of 1,800 cm^{-3}. The size distributions within the plume were narrow and monomodal with a mean geometric diameter of approximately 0.100 μm. On the April 21, the DMA failed shortly after takeoff; however, several measurements within another elevated Asian plume were collected. The number concentration was in excess of 800 cm^{-3} however no increase in volume concentration was observed. The NCAR CPC also measured number concentration in excess of 800 cm^{-3} during the same time period. The April 21 concentrations were not as elevated as on May 1. This is most likely a result of slower transport, which enabled more aging of the aerosol. A case study of the May 1 will be presented in the following section.

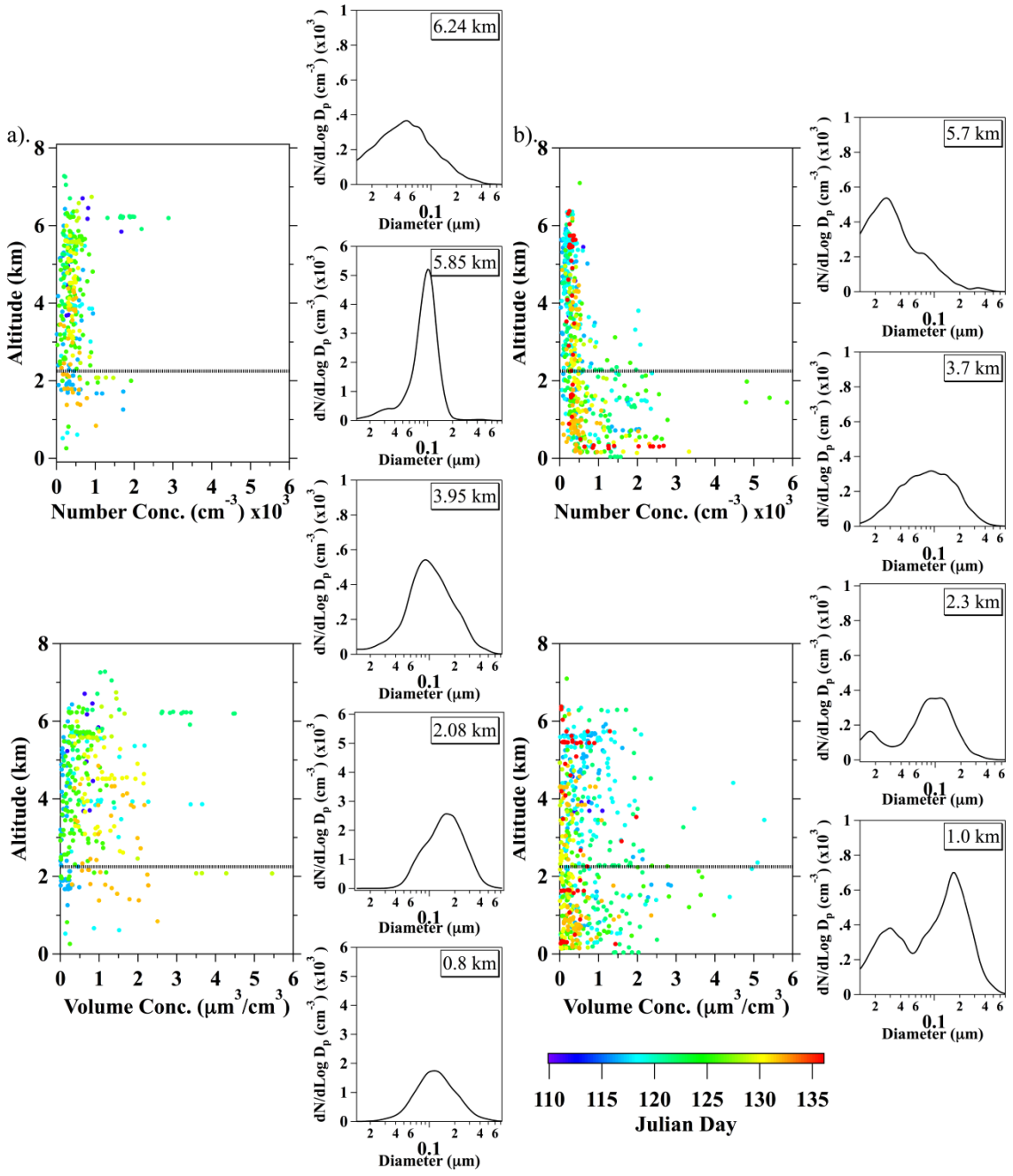

Figure 21. Number and volume concentration by altitude measured within (a) and outside (b) of the Asian plume. The marker color indicates the date of the measurement. Example number distributions plotted from higher to lower altitudes are included**.**

For the Asian plume, the geometric mean diameter of the number size distributions increase from approximately 0.050 μm to approximately 0.180 μm as the altitude decrease within the free troposphere. This shift is a result of the large particles in the atmosphere settling out through deposition. The lifetime of most aerosols within the atmosphere is about 3 to 10 days [*Andreae and Rosenfeld*, 2008; *Andreae et al.*, 1995], and a majority of the aerosols were sampled after 3 to 7 days of transport. The number size distributions within the marine boundary layer (MBL) do not exhibit the expected bimodal distributions [*Berg et al.*, 1998; *Dusek et al.*, 2003; *Massling et al.*, 2007; *Massling et al.*, 2003; *Swietlicki et al.*, 2000; *Swietlicki et al.*, 2008; *Tomlinson et al.*, 2007; *Vakeva et al.*, 2002a; *Vakeva et al.*, 2002b; *Zhou et al.*, 2001], and the geometric mean diameter shifts back towards smaller diameters around 0.100 μm. An increase in aerosol number and volume concentration is observed below the top of the MBL. This is a residual layer of Asian aerosol that is undergoing cloud processing and has not been removed through deposition processes.

The background aerosol does not exhibit the elevated concentration in the upper levels; however, it does have elevated number and volume concentrations in the mid-levels of the atmosphere. This aerosol could have been entrained into the free troposphere from the marine boundary layer (MBL) below through a warm conveyer belt, and an analysis of the hygroscopicity of the aerosol presented in the next section will help to validate this hypothesis. Throughout the MBL, elevated number and volume concentrations are observed resulting from cloud processing, local emissions from the Pacific Ocean, and mixing within the marine boundary layer. Similar to the Asian

aerosol, there is an increase in aerosol number and volume concentration at the top of the MBL as a result of cloud processing.

The size distributions of the background aerosol in the upper levels (6km) and mid levels (4km) of the atmosphere are similar to the size distributions observed within the Asian plume. However, at the top of and within the MBL, a bimodal size distribution is often measured. The distribution at the top of the MBL is mostly dominated by a mode with a geometric mean diameter of 0.100 μm and a small secondary mode centered on 0.020 μm. Within the MBL, a bimodal distribution is observed with an accumulation mode centered around 0.200 μm and a secondary Aitken mode centered on 0.030 μm. The minimum in the distribution is around 0.060 to 0.070 μm.

In Table 14, the highest measured number and volume concentration originated in north China and from multiple sources. A multiple source is defined as any back trajectory that intercepted more than one region. North China has an average number concentration of 480 +/- 172 cm^{-3}, and the concentration is significantly higher (α=0.10) than the average number concentration from a source region of central China, southern China, or Japan. North China also has the highest volume concentration of 0.9 +/- 0.6 $\mu m^3/cm^3$; however, this is only significantly higher (α=0.10) than the average volume concentration of aerosol from central China. Illustrating the influence that north China has on the Asian plume, there is no significant difference in the number and volume concentration in the aerosol from north China when compared to multiple sources. On average, the Asian plume has a number concentration of 456 +/- 364 cm^{-3} and a volume

concentration of 0.8 +/- 0.8 $\mu m^3/cm^3$, which is significantly higher (α=0.10) than the background number concentration of 308 +/- 249 and a volume concentration of 0.5 +/- 0.6 $\mu m^3/cm^3$.

The most probable number and volume distributions within the free troposphere are displayed in Figure 22. The top row is aerosol within the Asian plume, and the bottom row is background aerosol. The Asian number distribution is a broad monomodal distribution with a geometric mean diameter between 0.080 and 0.100 μm. The shape is typically of an aged aerosol. Below 0.020 μm, the most probable distribution only accounts for 60% of all possible distributions. This is indicative that a nucleation mode is occasionally observed within the Asian plume. The volume distribution is centered on a geometric mean diameter between 0.300 and 0.400 μm.

Table 14. Average CO, number, and volume concentration from each source region. For comparison, the average concentration within the background is included.

	Altitude (km)	CO Conc. (ppbv)	σ	Number Conc. (cm^{-3})	σ	Volume Conc. ($\mu m^3/cm^3$)	σ
All Asia	4.75	132	40	456	364	0.8	0.8
North China Only	4.35	131	21	480	172	0.9	0.6
Central China	4.87	125	19	267	134	0.4	0.3
South China	5.93			262	64	0.3	0.0
Japan	4.52	118	26	368	173	0.8	0.6
Multiple Source	4.89	134	47	479	436	0.8	0.9
Background	4.50	121	27	308	249	0.5	0.6

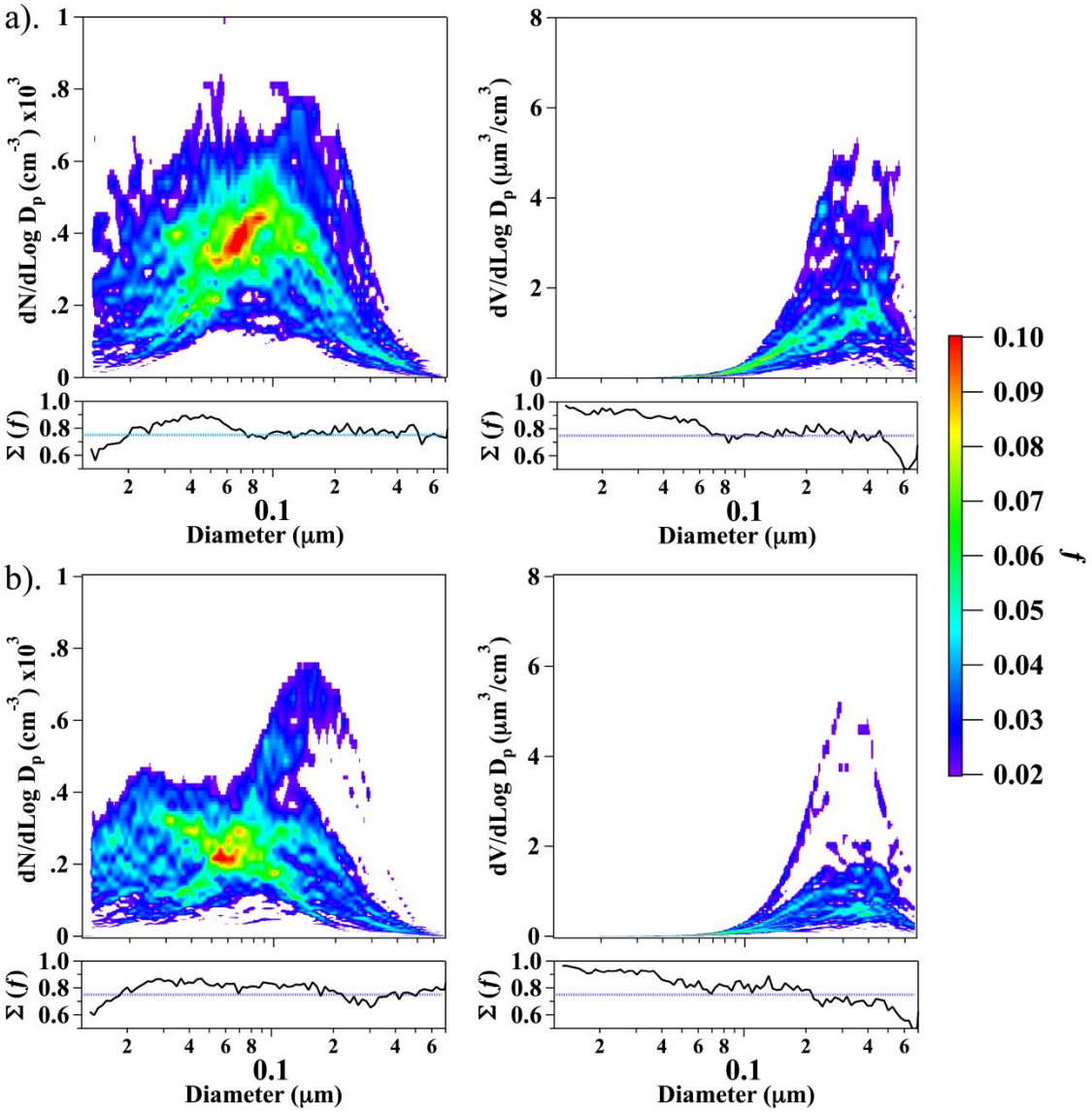

Figure 22. The most probable size distribution within (a) and outside (b) of the Asian plume. The number distribution is on the left, and volume distribution is on the right. The strip chart below each size distribution indicates the percentage of all probable values that is displayed in the corresponding size distribution.

The number distribution of the background aerosol is variable. However, most of the time an aged aerosol number distribution centered on 0.070 μm is observed. Occasionally, an accumulation mode is observed with a geometric mean diameter around 0.180 μm, and there is a Nucleation/Aitken mode that is highly variable. The distribution for the background aerosol is roughly half the magnitude of the number distribution for the Asian aerosol. The background volume distribution has roughly the same geometric mean diameter as the Asian volume distribution. However, the magnitude of the volume distribution is roughly half the magnitude of distribution measured for the Asian aerosol.

3.5.3 TDMA growth distributions

The TDMA operated throughout all research flights conducting measurements of the aerosol hygroscopicity from near the surface up to 7.5 km over the Pacific Ocean. The measured growth factor is subsequently converted to κ in post processing. The backtrajectory closest to the midpoint time for each TDMA measurement is used to determine if the aerosol was influenced or originated in Asia or is background aerosol that originated in another location. A plot of all the TDMA measurements throughout INTEX-B is shown in Figure 23. The marker shape gives the origin of the aerosol, the color of the marker indicates the flight day, and the size of the marker indicates the contribution the mode had to the overall growth distribution.

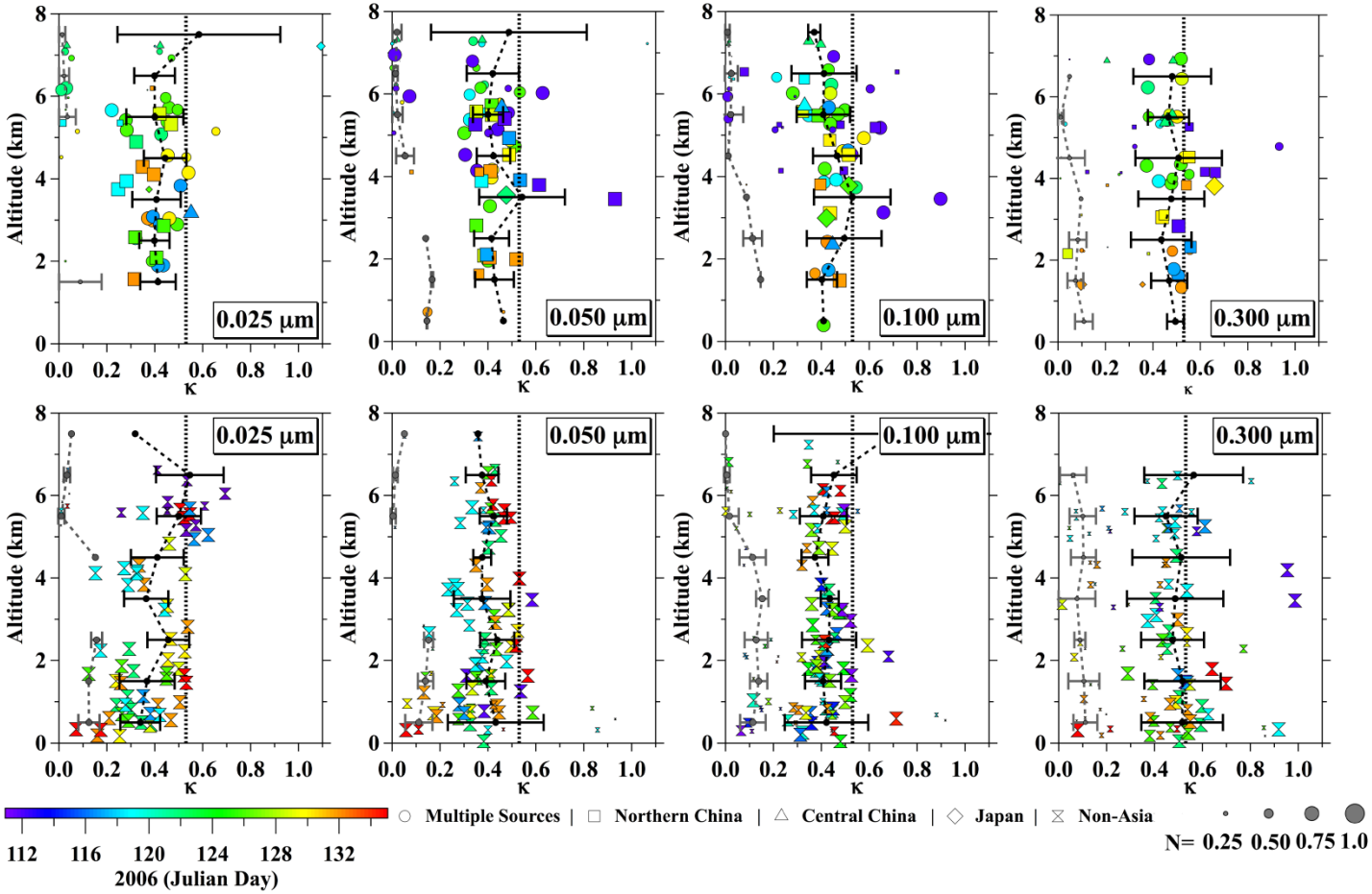

Figure 23. κ values by altitude for each dry diameter. The top row is within the Asian plume, and the bottom row is outside of the plume. The color of the marker indicates the date of the measurement, the size of the marker indicates its contribution to the overall growth distribution, and the shape of the marker indicates the source. Also plotted is the average κ of the more soluble and less soluble modes in 1km intervals. The theoretical κ for ammonium sulfate is plotted as a dashed line.

The top row of plots is from aerosol from Asia, and the bottom row is background aerosol. The Asian aerosol has two distinct modes that have been separated into soluble ($\kappa \geq 0.20$) and low solubility ($\kappa < 0.20$). The average κ value for the soluble and low soluble aerosol is plotted above with 1 σ error bars at 1-km intervals. The average values are shown in Table 15. On average, the κ value oscillates between 0.40 and 0.53 for all dry diameters of the soluble Asian aerosol within the free troposphere. This is surprisingly consistent and indicates that the aerosol has undergone cloud processing or that the condensation of gas phase sulfate has coated the aerosol. The process that is occurring is consistent at all levels and therefore should be reproducible in atmospheric chemistry models. The aerosol exhibits the highest κ for dry diameters equal to and greater than 0.050 μm at altitudes 3 to 4.5 km ASL. The aerosol at these altitudes is most likely almost pure ammonium sulfate and has the lowest occurrence of an insoluble mode. However between 4.5 and 7.5 km, the aerosol at all dry diameters exhibits the lowest values of κ, and has a growth distribution with a persistent secondary mode dominated by low soluble aerosols.

Table 15. Average κ by altitude for the Asian (a) and the background (b) aerosol for each dry diameter. The averages for the more soluble aerosols are on the left, and the less soluble aerosols are on the right.

a).

Altitude	0.025 μm			0.050 μm			0.100 μm			0.300 μm			Altitude	0.025 μm			0.050 μm			0.100 μm			0.300 μm		
(km)	κ	σ	N	κ	σ	N	κ	σ	N	κ	σ	N	(km)	κ	σ	N	κ	σ	N	κ	σ	N	κ	σ	N
0.5				0.46	NaN	1	0.41	NaN	1	0.50	0.04	2	**0.5**	0.11	NaN	1	0.15	0.00	2				0.11	0.04	2
1.5	0.41	0.07	5	0.43	0.08	3	0.40	0.06	4	0.47	0.08	4	**1.5**	0.09	0.09	2	0.17	0.00	2	0.15	0.00	2	0.07	0.03	2
2.5	0.40	0.06	7	0.42	0.07	5	0.50	0.16	6	0.44	0.13	7	**2.5**	0.13	NaN	1	0.14	NaN	1	0.11	0.04	2	0.08	0.04	3
3.5	0.41	0.10	9	0.54	0.18	8	0.53	0.16	9	0.48	0.14	8	**3.5**	0.19	NaN	1				0.09	NaN	1	0.10	NaN	1
4.5	0.44	0.09	7	0.42	0.07	10	0.47	0.10	9	0.51	0.18	13	**4.5**	0.01	NaN	1	0.05	0.04	2	0.01	NaN	1	0.05	0.07	3
5.5	0.40	0.12	16	0.40	0.06	20	0.41	0.11	24	0.47	0.09	12	**5.5**	0.04	0.04	6	0.02	0.02	10	0.02	0.05	7	0.01	0.01	5
6.5	0.40	0.09	9	0.42	0.11	13	0.41	0.14	14	0.48	0.16	8	**6.5**	0.03	0.02	6	0.01	0.01	9	0.02	0.03	7	0.05	NaN	1
7.5	0.58	0.34	4	0.49	0.33	5	0.37	0.03	3				**7.5**	0.02	0.01	3	0.02	0.02	4	0.01	0.01	3			

b).

Altitude	0.025 μm			0.050 μm			0.100 μm			0.300 μm			Altitude	0.025 μm			0.050 μm			0.100 μm			0.300 μm		
(km)	κ	σ	N	κ	σ	N	κ	σ	N	κ	σ	N	(km)	κ	σ	N	κ	σ	N	κ	σ	N	κ	σ	N
0.5	0.34	0.08	17	0.43	0.20	22	0.42	0.17	26	0.52	0.17	26	**0.5**	0.13	0.04	7	0.11	0.06	9	0.11	0.05	13	0.11	0.05	11
1.5	0.37	0.12	12	0.39	0.08	15	0.41	0.08	15	0.52	0.16	13	**1.5**	0.12	NaN	1	0.14	0.03	5	0.14	0.04	3	0.11	0.07	5
2.5	0.46	0.09	6	0.44	0.07	10	0.43	0.11	14	0.48	0.13	10	**2.5**	0.16	0.02	2	0.15	0.02	3	0.13	0.05	5	0.09	0.02	3
3.5	0.36	0.09	6	0.38	0.12	14	0.44	0.04	11	0.49	0.20	11	**3.5**							0.15	0.03	3	0.08	0.08	4
4.5	0.41	0.11	10	0.38	0.04	2	0.37	0.06	4	0.51	0.20	7	**4.5**	0.15	NaN	1				0.11	0.06	3	0.10	0.05	4
5.5	0.50	0.09	16	0.42	0.06	16	0.41	0.10	16	0.45	0.13	14	**5.5**	0.01	0.01	7	0.00	0.01	9	0.02	0.04	8	0.10	0.06	5
6.5	0.55	0.14	3	0.38	0.07	5	0.45	0.10	7	0.56	0.21	6	**6.5**	0.03	0.01	3	0.01	0.01	5	0.01	0.01	6	0.06	0.06	3
7.5	0.32	NaN	1	0.36	NaN	1	0.70	0.50	2				**7.5**	0.05	NaN	1	0.05	NaN	1	0.00	NaN	1			

Aerosol with a κ value less than 0.20 is considered in this study to have low solubility. For 0.100 μm aerosol and less, there is very little low soluble aerosol until 4.5 km and higher. The aerosol growth distributions at this altitude and higher exhibit bimodality 55% of the time for aerosol with dry diameters of 0.025, 0.050, and 0.300 μm within the Asian plume. Aerosols with a dry diameter of 0.100 mm demonstrate bimodality slight less often at 49%. The secondary mode contributes 20–33% to the overall growth distribution and on average has a κ value of 0.179 +/ 0.172, 0.027+/- 0.058, 0.052 +/- 0.096, and 0.142 +/- 0.139 for dry diameters of 0.025, 0.050, 0.100, and 0.300 μm, respectively. The secondary mode is less soluble than the primary mode 86.2% of the time for all dry diameters. Occasionally, a monomodal growth distribution with a κ value less than 0.10 is observed at dry diameter less than 0.050 μm. At these low levels of κ, the aerosol is considered insoluble and is most likely elemental carbon (soot) or possibly organics. Aged soot has been observed to be internally mixed [*Hasegawa and Ohta*, 2002] with sulfate, and in remote areas up to 45% of the sulfate particles contain soot [*Posfai et al.*, 1999]. Recent laboratory studies by *Zhang et al.* [2008] have demonstrated that the soot particles acquire a large mass fraction of sulfuric acid during atmospheric aging, thus increasing their solubility. However, the 0.050 and 0.100 μm particles contained a sizeable fraction of particles where it appears little or no condensation of gas phase sulfate has occurred. This could have resulted from a limited concentration of gas phase sulfate, or there is possibly still an incomplete understanding of this process. For the larger aerosol diameter (> 0.200 μm), the coagulation and condensation processes has most likely slightly increased the solubility of the less

soluble particles. However, it is still lower than expected, and approximately 55% of the measured growth distributions have a secondary mode that contributes 33% +/- 9.1% to the overall growth distribution with a κ of 0.142 +/- 0.139. With rapid enough transport, insoluble aerosol at all diameters can be transported across the Pacific Ocean. Not accounting for the transport of this low soluble aerosol in atmospheric models could cause errors in the estimation of the radiative transfer and cloud processes.

Within the free troposphere, the κ value of the background aerosol is less consistent in the vertical dimension compared to the Asian aerosol, with the κ value varying between 0.32 and 0.56. For dry diameters of 0.025 and 0.050 μm, the solubility is highest in the lower levels of the free troposphere at the top of the marine boundary layer, and the insoluble mode is almost nonexistent at 3–4.5 km. The insoluble mode is observed for altitudes above 4.5 km. Aerosols with dry diameters of 0.100 μm and 0.300 μm aerosol exhibit a fairly consistent value of κ for both the soluble and insoluble mode throughout the marine boundary layer and free troposphere. However, above 5 km, there is a marked decrease in the κ value of the insoluble mode for the 0.100 μm aerosol. This observation of a consistent hygroscopicity of the aerosol throughout the boundary layer up to 2 km above the boundary layer for aerosol with diameters greater than and equal to 0.100 μm indicates that the marine boundary layer and free troposphere may be more connected than previously assumed. This observation is in concert with observed consistent value of number and volume concentration between the aurface and 4 km for the background aerosol. This is possibly a result of the entrainment of aerosol from the

marine boundary layer into the free troposphere by warm conveyer belts where stronger upward velocities occur.

At altitudes of 4.5 km to 7.5 km, the aerosol exhibits a bimodal growth distribution at all dry diameters except for 0.025 μm more often than the Asian aerosols. On average, the aerosol growth distributions exhibit bimodality 50%, 68%, 73%, and 80% of the time for dry diameters of 0.025, 0.050, 0.100 and 0.300 μm, respectively. In the same order of dry diameters, the secondary mode contributes 0.234 +/- 0.129, 0.180 +/- 0.116, 0.225 +/- 0.117, and 0.332 +/- 0.091 with κ values of 0.061 +/- 0.131, 0.010 +/- 0.016, 0.086 +/- 0.171, and 0.142 +/- 0.146. The secondary mode is less soluble than primary mode 92.6% of the time for all dry diameters. The data set used for this analysis did not discount aerosol transported from Europe or Russia and instead treated it as background. Low soluble and insoluble aerosols were present throughout INTEX-B at altitudes above 4.5 km regardless of the source. This result is surprising and indicates the aerosol within the mid to upper levels of the atmosphere can travel long distances potentially globally and survive over a week within the atmosphere and influence the United States.

3.5.4 May 01, 2006, case study

An overview of the data collected during the May 1, 2006 research flight is shown in Figure 24 (additional data from other research flights is presented in Appendix A). The C-130 departed Paine Field at approximately 18:30 UTC (11:30 AM PDT) and headed towards the southwest while gaining altitude up to 6 km. The flight path and profile for this flight are shown in the Figure 24. The aircraft conducted six level legs in

the mid to upper levels of the troposphere. Each level leg was followed by a profile of the atmosphere. From 20:21 to 21:02 UTC, extended sampling within the MBL was conducted. During one profile around 22:00 UTC, the aircraft sampled the entrainment layer at the top of the MBL.

The aerosol within the marine boundary layer exhibits a bimodal size distribution with a primary Aitken mode centered between 0.030 to 0.040 μm and a minor secondary accumulation mode centered on 0.150 μm. The minimum in the distribution occurs around 0.080 μm. The measured κ values are 0.31 +/- 0.02, 0.38 +/- 0.02, 0.50 +/- 0.03 and 0.56 +/- 0.05 for 0.025, 0.050, 0.100, and 0.300 μm particles, respectively. The growth distributions were monomodal for all particles, except for one bimodal distribution observed for a 0.050 μm particle. The κ values exhibit the typical cloud processing signature within the MBL where the aerosol hygroscopicity increases with increasing diameter [*Swietlicki et al.*, 2000; *Swietlicki et al.*, 2008; *Tomlinson et al.*, 2007]. No Asian aerosol was observed within the marine boundary layer.

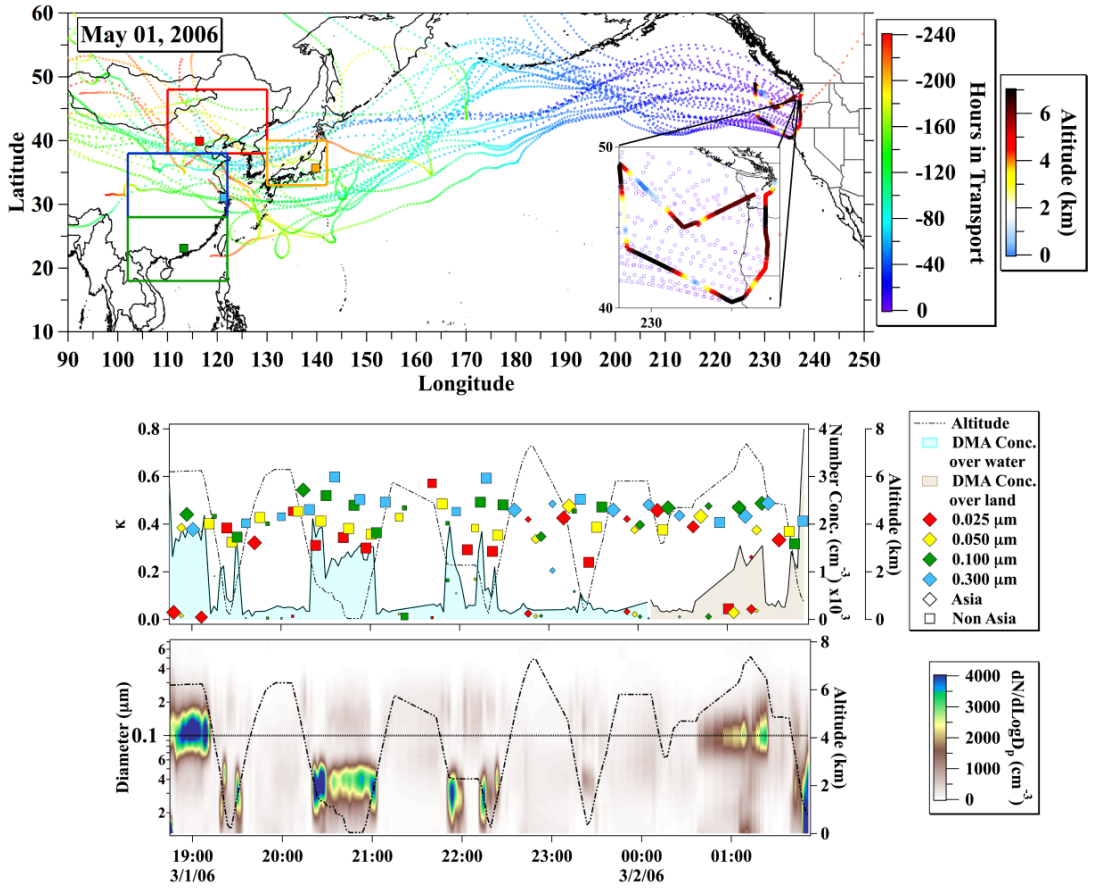

Figure 24. An overview of the DMA/TDMA data from the May 1, 2006, research flight. In figure (a), the color of the flight path indicates the aircraft altitude, and the backtrajectory marker color indicates the hours in transport for the aerosol. In figure (b), the altitude is indicated by the dashed line, the marker color indicates the dry diameter size, the marker shape indicates the source, and the integrated concentration is indicated by the blue, measured over water, and brown shading, measured over land. The measurement time is indicated in (c). In figure (c), altitude is again noted by the dashed line, the diameter of the aerosol is indicated on the y-axis, and the color of the shading indicates the magnitude of the concentration.

Shortly after takeoff, the C-130 intercepted a young plume of Asian aerosol and leveled off. The average altitude of this plume was 6.20 km, and the average transport time was 3.2 +/ 0.5 days. The average CO concentration was 289 +/- 17 ppb, the average ultrafine concentration (> 0.003 μm) measured by a ultrafine condensation particle counter (UCPC) was 2654 +/- 229 cm^{-3}, the average number concentration (> 0.012 μm) measured by a condensation particle counter (CPC) was 1797 +/- 158 cm^{-3}, and the average number concentration measured by the DMA was 1897 +/- 384 cm^{-3}. The average volume concentration was 3.2 +/- 0.6 $\mu m^3/cm^3$. There was no significant difference between the number concentration measured by the DMA and the CPC, illustrating the validity of the technique used to remove the leak-contaminated distributions. These measured number and volume concentrations were the highest observed in the middle to upper level levels of the troposphere during INTEX-B. The geometric mean diameter of the monomodal number distribution was slightly greater than 0.100 μm. The aerosol at 0.025 μm was insoluble, while a fraction of the aerosol at 0.050 μm was insoluble. The aerosol at 0.100 and 0.300 μm was fairly soluble with κ values around 0.40.

The C-130 again intercepted this plume shortly before landing around 01:00 UTC. The plume had now been in transport for 5.0 +/- 1.0 days, 1.5 days longer than what was measured earlier in the flight. All measured concentrations were significantly lower (α=0.05). The CO concentration was 246 +/- 44 ppb, ultrafine number concentration was 1633 +/- 432 cm^{-3}, the CPC number concentration was 1256 +/- 432 cm^{-3}, the DMA number concentration was 1313 +/- 236 cm^{-3}, and the DMA volume

concentration was 2.1 +/- 0.7 $\mu m^3/cm^3$. Even though these numbers are lower, they are still considerably higher than the background aerosol concentrations at this altitude.

An aged Asian plume in the mid levels of the atmosphere that had been in transport for 6.5 +/- 1.6 days was intercepted at 5.0 +/- 1.0 km. The transport time for the aerosol within the aged layer was highly variable, with times between 6 to 10 days. However, the measured concentration did not exhibit much variability, and on average, the number concentration was 247 +/- 95 cm^{-3} and the volume concentration was 0.6 +/- 0.4 $\mu m^3/cm^3$. The average CO concentration had also decreased to 137 +/- 10.0 ppb. These concentration values make the plume indistinguishable from the background aerosol.

Within the young plume, the κ values for the 0.100 and 0.300 μm aerosols approached the expected values for aerosol composed mostly of ammonium sulfate. During the first intercept, the growth distribution was monomodal with κ values of 0.44 and 0.38 for a 0.100 and 0.300 μm particle, respectively. During the second intercept, the growth distributions were still monomodal, with κ values of 0.48 +/- 0.01 and 0.45 +/- 0.02. Within the aged plume located in the mid levels, the growth distributions have become bimodal, with the more soluble mode having a k value of 0.45 +/- 0.08 and 0.47 +/- 0.02 for a 0.100 and 0.300 μm particle, respectively. For the 0.100 μm particles, a bimodal distribution that contributed 35 +/- 9 % to the overall distribution with an average k value of 0.01 +/- 0.0 was measured 60% of the time. For a 0.300 μm particle, a bimodal distribution that contributed 28 +/- 13% to the overall growth distribution with an average k value of 0.07 +/- 0.11 was measured 50% of the time.

These observations indicate that gas phase SO_2 is still condensing on the 0.100 and 0.300 μm particles and increasing the hygroscopicity. As the SO_2 condenses, the larger particles in this plume become composed mostly of sulfate in the form of either ammonium bisulfate or ammonium sulfate, and the κ values are approaching the expected value for pure ammonium sulfate of 0.53. An Aerosol Mass Spectrometer aboard the C-130 determined the composition of this young plume during the May 1 flight to be mostly ammonium bisulfate [*Dunlea et al.*, 2009], which is in agreement with TDMA observations. The same study also measured the ratio of aerosol sulfate to total sulfur to be 0.5, indicating that a large fraction of sulfur still existed in the gas phase. Within the aged plume discussed above that ratio had increased to 0.9, indicating a large fraction of gas phase SO_2 had been converted to aerosol phase. This is a strong indication that condensational growth was indeed still occurring, and this supports the TDMA observation of the increase in κ as the plume age increases.

However, the AMS cutoff is around 0.100 μm, and the growth distributions indicate that the particles smaller than this diameter are not composed purely of ammonium bisulfate. During the first plume intercept, insoluble particles dominate the 0.025 μm and 0.050 μm growth distribution. For a 0.025 μm particle, the first measurement indicated a monomodal distribution with a κ value of 0.03, and the second measurement indicated a bimodal distribution with the primary mode (87%) having a κ value of 0.01 and the secondary mode (13%) having a κ value of 0.37. For a 0.050 μm particle, the first measurement indicated a monomodal distribution with a κ value of 0.045, and the second measurement indicated a bimodal distribution, with the primary

mode (68%) having a k value of 0.04 and the secondary mode (32%) having a k value of 0.26.

During the second intercept of the young plume, insoluble particles again dominated the growth distribution for 0.025 μm particles. The first measurement is monomodal with a κ value of 0.05, and the second measurement indicated a bimodal distribution with the primary mode (68%) having a κ value of 0.04 and the secondary mode (32%) having a κ value of 0.26. The measurement of 0.050 μm particles indicates bimodal distributions. The first distribution has a primary mode (83%) with a κ value of 0.03 and a secondary mode (17%) with a κ value of 0.48. The second distribution has a primary mode (71%) with a κ value of 0.38 and a secondary mode (29%) with a κ a value of 0.04.

Within the aged older layer in the mid levels, the more soluble species begin to dominate the 0.025 and 0.050 μm growth distributions. The more soluble 0.025 μm particles have an average κ value of 0.40 +/- 0.05, and the less soluble species have a κ value of 0.03 +/- 0.1. Bimodal growth distributions occur 43% of the time, and the less soluble species in the bimodal distributions contribute 38 +/- 23 % to the overall distribution. The more soluble 0.050 μm particles have an average κ value of 0.38 +/- 0.05, and the less soluble species have a κ value of 0.02 +/- 0.01. Bimodal growth distributions occurred 66% of the time, and the less soluble species in the distribution contribute 37 +/- 6% to the overall distribution.

As the above discussion illustrates, even the smaller particles are still undergoing compositional changes three to seven days after being emitted from China. This is not surprising considering the amount of gas phase SO_2 still available after three days of transport. However, even as a fraction of the particles are become more soluble, a sizable fraction maintain their insolubility. The hypothesis that the gas phase sulfate condenses on the aerosol surface needs to be investigated further. The next section will take a more in-depth look at the evolution of the Asian plume.

3.5.5 Evolution of the Asian plume

The analysis above has shown that the aerosol is undergoing chemical changes as it is being advected away from Asia even after three to seven days in transport. The remaining question is whether this transformation occurs in all Asian plumes, or whether the May 1 case is a more isolated example. Using the back trajectory model, each measurement of κ was assigned a time since advection from Asia. This information in conjunction with the measured κ and the ε was used to create the cumulative histograms in Figure 25. The TDMA measurements were broken into days since being advected from Asia starting at 2 to 3 days and ending at 9 to 10 days. For each dry diameter and time frame, a histogram of κ_w was created. Each bin in the histogram has a width of 0.05, and the bins range from 0.00 to 0.80. Instead of using one for the occurrence of a κ value in a specific bin, the ε for that value was used. This prevented κ values with low ε from biasing the histogram. From each histogram, a cumulative histogram was calculated.

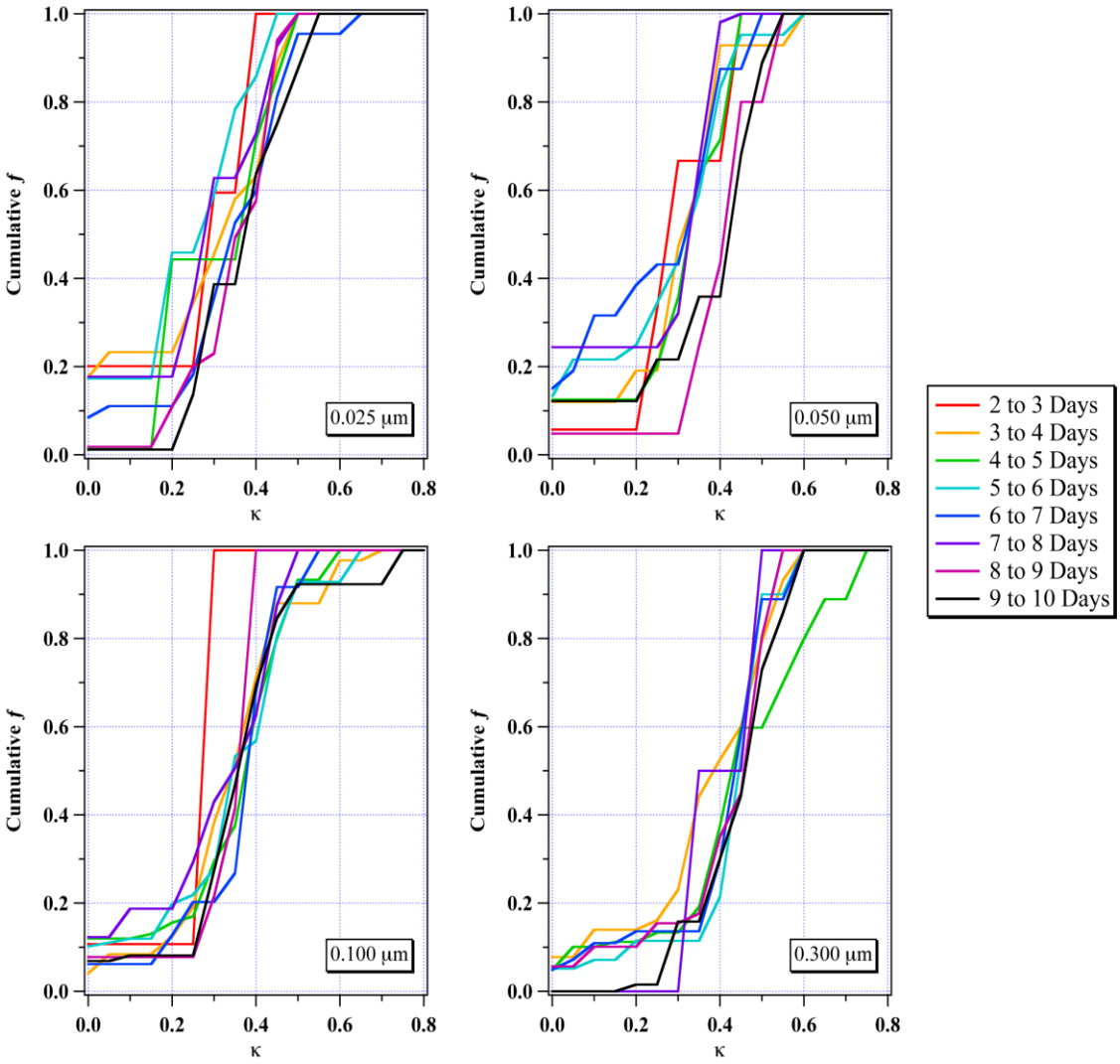

Figure 25. Cumulative histograms of κ split into increments of days in transport for each dry diameter

For the cumulative histograms in Figure 25, the 2 to 3 days and 3 to 4 days curves are to the left of the 8 to 9 days and 9 to 10 days curves. This is indicative that gas phase sulfate is still condensing onto the surface of the aerosol. However, the change is not as dramatic when compared to the Mexico City plume. The cumulative histogram for the 0.025 µm particles does not show a consistent pattern. Looking at the

50% point of the curve, the particles exhibit a steady increase in κ_w between 2 to 3 days and 4 to 5 days. However, after 4 to 5 days, the κ_w decreases back to values observed at the 2 to 3 day timeframe. The highest κ_w are observed at 9 to 10 days of transport. The 0.050 μm have the least solubility at 2 to 3 days of transport and the highest solubility at 9 to 10 days. These particles exhibit a noticeably higher solubility at the 8 to 10 day timeframe than the 2 to 8 day timeframe. The 0.100 μm and 0.300 μm particles exhibit very little change over the timeframe shown here. The least soluble particles at both diameters are found in the 2 to 3 day timeframe; however, as the length of transport increases there is a very small increase in the aerosol solubility. For 0.100 μm particles, the 9 to 10 day timeframe has the highest probability (10%) of having particles with a κ_w equal to and greater than the solubility for ammonium sulfate and the lowest probability for having aerosols with low solubility. For 0.300 μm particles, the 9 to 10 day timeframe has the lowest probability for low soluble aerosols; however, the 4 to 5 day timeframe has the highest probability for particles with high solubility. This illustrates that beyond several days of emission, the chemical transformation becomes complex and is more dependent on what processes the aerosol are exposed to during transport. The one lone exception to this is the 0.50 μm aerosols, which exhibited a significant gain in solubility.

A similar cumulative histogram (Figure 26) was created to analyze the changes in the number and volume concentrations within the plume as the aerosol is advected

from Asia. The data were split into the same timeframes used for the analysis of κ_w. The bins for the histogram are logarithmically spaced.

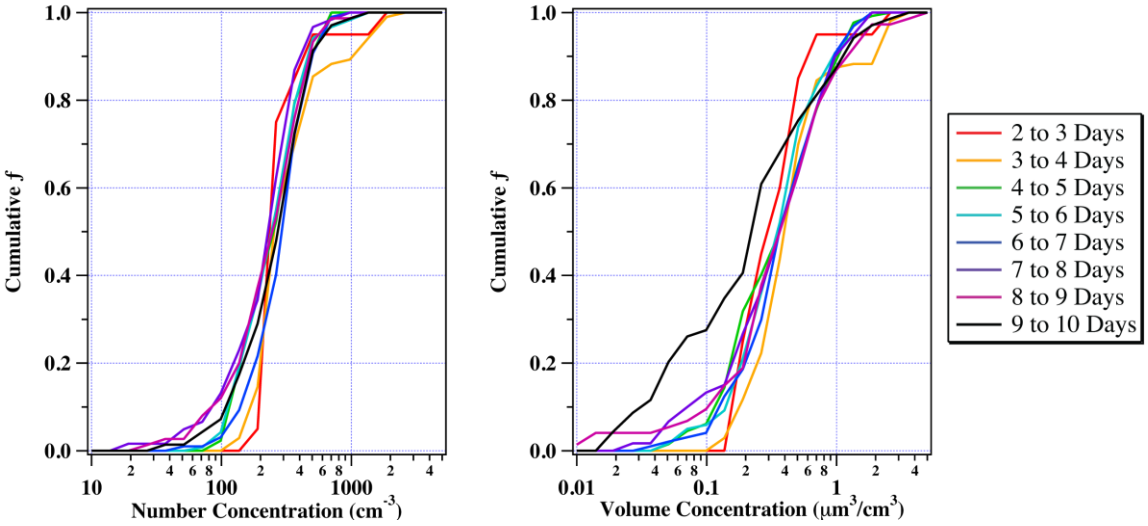

Figure 26. Cumulative histograms of number and volume concentration split into increments of days in transport

The number concentration within the plume undergoes very little change during the transport from Asia. One noticeable characteristic is that only in the 2 to 3 day and 3 to 4 day timeframe are high number concentrations observed. Over this timeframe there is 0% probability of measuring number concentration less than 100 cm^{-3}. The occurrence of low number concentrations increases with increase in transport time. However, at the 50% point within the cumulative histogram there is very little difference between the different transport times. On average across all transport times, the particle concentration is 255 +/- 20 cm^{-3}.

The volume concentration has more variability. The highest probability for high volume concentration (> 1 $\mu m^3/cm^3$) is in the 3 to 4 day timeframe, and surprisingly, the lower probability is in the 2 to 3 day timeframe. This lower probability may result from the condensational growth of the particles still occurring as discussed in the previous section. The 2 to 3 day and 3 to 4 day timeframes have 0% probability of low volume concentration (< 0.1 $\mu m^3/cm^3$). Between 3 to 4 days and 8 to 9 days there is little change in the volume concentration at the 50% with an average value of 0.4 +/- 0.02 $\mu m^3/cm^3$ for the 3 to 9 day timeframe. The lowest volume concentration observed were for the 9 to 10 day timeframe with almost 30% percent of the measure concentrations being low. At the 50% point the volume concentration was 0.2 $\mu m^3/cm^3$.

Although the number concentration shows little change, the volume concentration undergoes a noticeable change as the duration in transport increases. The observations of low volume concentration increase, and after 9 to 10 days the observed particles have the lowest volume concentration. This was likely caused by removal from the atmosphere through wet and dry deposition.

The removal of the aerosol through wet deposition is partially controlled by the solubility and size of the particles, which determine the supersaturation at which the particles will activate and become cloud condensation nuclei. The next section will examine the activation properties of the aerosol measured during INTEX-B.

3.5.6 Aerosol cloud interaction

The magnitude of the first and second indirect effect is dependent on the number of atmospheric aerosols that activate to become cloud condensation nuclei (CCN) at the

supersaturations present within a cloud. Upon activation, the CCN can grow into cloud droplets. The concentration of CCN (N_{CCN}) within a cloud is dependent on the chemical composition and size distribution of the aerosol and the supersaturation and the amount of liquid water available within the cloud. The N_{CCN} for a measured size distribution can be estimated by assuming the aerosol is composed purely of a soluble inorganic, normally ammonium sulfate, and using Kohler theory [*Kohler*, 1936] to estimate the activation diameter for a specified supersaturation. However, within the atmosphere, this is overly simplistic at times. The aerosol is often composed of a mixture of insoluble or slightly soluble organics along with a soluble inorganic. To estimate the effects of organics on the N_{CCN}, an extended Kohler theory [*Seinfeld and Pandis*, 2006] is used. The derivation of the extended Kohler theory was discussed in the Methodology section of the dissertation. The extended Kohler theory is used in conjunction with the physicochemical measurements of the aerosol to attempt a CCN closure study. A successful closure study is when the ratio of the measured to predicted N_{CCN} is close to unity or within the range of error for the measured N_{CCN}. This indicates that the chemical composition of the aerosol and the processes that lead to the formation of CCN are reasonably understood.

Measurements of N_{CCN} within the atmosphere were first conducted over 40 years ago [*Radke and Hobbs*, 1969; *Twomey and Wojciechowski.T. A.*, 1969; *Twomey and Davidson*, 1970] using cloud chambers. The first attempts at predicting N_{CCN} [*Bigg*, 1986; *Quinn et al.*, 1993] assumed the aerosol was composed of pure ammonium sulfate aerosol, which caused an overprediction in the N_{CCN} and failed to reach closure. *Martin*

et al. [1994] also assumed pure ammonium sulfate and obtained closure for a maritime air mass, but not for continental air masses. The pure ammonium sulfate assumption obtained closure for 10 out of 12 data sets measured at Chebugue Point, Nova Scotia, during the North Atlantic Regional Experiment (NARE) campaign in a maritime air mass [*Liu et al.*, 1996].

CCN closure studies in the late 1990s began to use a TSI Scanning Mobility Particle Sizer (SMPS) or Differential Mobility Analyzer (DMA) to measure the size distributions. The earlier studies often utilized a PCASP for measurements of size distributions, which can only measure particles with diameters greater than 0.100 μm. These new instruments pushed the size distribution well below the 0.100 μm threshold and into the Aitken mode. In addition, the chemical composition was sometimes inferred through a hygroscopic growth factor measured by a hygroscopic tandem differential mobility analyzer (TDMA) [*Covert et al.*, 1998; *Zhou et al.*, 2001]. However, even with these improvements the N_{CCN} was often over-predicted [*Chuang et al.*, 2000; *Covert et al.*, 1998; *Dusek et al.*, 2003; *Snider and Brenguier*, 2000; *Wood et al.*, 2000; *Zhou et al.*, 2001].

During the Indian Ocean experiment, an aerosol time of flight mass spectrometer was utilized to measure the size-resolved chemical composition of the aerosol [*Cantrell et al.*, 2001]. A TSI scanning mobility particle sizer was used to measure the size distribution. Closure was obtained for 8 out of the 10 data sets. When closure was not obtained, a high organic fraction was observed and the N_{CCN} was over-predicted. Closure was also obtained for marine stratocumulus clouds by refining the Kohler

equation [*Snider et al.*, 2003]. *Roberts et al.* [2002] achieved closure in the Amazon even though the air mass was dominated by organic material (80% by mass). *Gasparini et al.* [2006] achieved closure of predicted N_{CCN} for supersaturations between 0.06 and 0.70% during the May 2003 Atmospheric Radiation Measurement Program (ARM) Aerosol Intensive Operational Period.

Ground-based closure studies have recently begun to utilize the DMT continuous-flow streamwise thermal-gradient CCN counter, which can measure N_{CCN} at 1 HZ [*Lance et al.*, 2006; *Roberts and Nenes*, 2005]. Some recent studies utilizing this instrument have obtained CCN closure [*Bougiatioti et al.*, 2009; *Gunthe et al.*, 2009; *Medina et al.*, 2007]. Other studies have failed to obtain closure [*Stroud et al.*, 2007]. During the International Consortium for Atmospheric Research on Transport and Transformation (ICARTT) field experiment at Chebogue Point (2004), *Ervens et al.* [2007] had mixed success. At high supersaturation, the mean error was 5%, while at low supersaturation, the predicted N_{CCN} was off by a factor of 2.4. Even with the improvement in instrumentation, the previous studies all over-predicted the N_{CCN}. Closure studies utilizing the University of Toronto thermal gradient diffusion chamber (TGDC) have had success at achieving closure. *Broekhuizen et al.* [2006] achieved closure utilizing the TGDC in downtown Toronto and by assuming insoluble organics. *Chang et al.* [2007] predicted CCN concentrations within 15% at a semi-rural site near Egbert, Ontario, using the TGDC and attained closure.

Early closure studies aboard aircraft proved to be very difficult and failed to reach closure [*Chuang et al.*, 2000; *Snider and Brenguier*, 2000; *Wood et al.*, 2000]. The

first aircraft-based study with any measured success was during the Cirrus Regional Study of Tropical Anvils and Cirrus Layers-Florida Area Cirrus Experiment (CRYSTAL-FACE) field campaign [*VanReken et al.*, 2003]. This study assumed a composition of pure ammonium sulfate at a supersaturation of 0.2% and achieved a ratio for $N_{predicted}/N_{observed} = 1.047$. *Rissman et al.* [2006] performed an inverse closure during the 2003 Atmospheric Radiation Measurement (ARM) Aerosol Intensive Observational Period (IOP) at the ARM Southern Great Plains site near Ponca City, Oklahoma. This study achieved closure when the population of the aerosol was treated as an external mixture of particles with the insoluble material preferentially disturbed in particles less than 50nm diameter. Recently, aircraft studies have begun to use the DMT continuous-flow streamwise thermal-gradient CCN counter (CCNc). This instrumented has enabled recent aircraft-based studies to achieve closure when assuming a binary aerosol composition [*Lance et al.*, 2009; *Wang et al.*, 2008] or come within 25% of the measured N_{CCN} [*Rissler et al.*, 2004]. However, *Roberts et al*. [2006] failed to obtain closure over the Eastern Pacific Ocean while testing a prototype of the DMT CCNc. The aerosol was composed mostly of anthropogenic Asian aerosol and dust, which was hypothesized to have caused the failure in the closure experiment.

Many of the above studies achieved closure by assuming a binary aerosol composed of a soluble inorganic mixed with an insoluble organic [*Bougiatioti et al.*, 2009; *Broekhuizen et al.*, 2006; *Cantrell et al.*, 2001; *Gasparini et al.*, 2006; *Lance et al.*, 2009; *Liu et al.*, 1996; *Medina et al.*, 2007; *Roberts et al.*, 2002; *VanReken et al.*, 2003; *Wang et al.*, 2008]. Others using the insolubility assumption exhibited substantial

differences between the predicted and measured N_{CCN} [*Chuang et al.*, 2000; *Rissman et al.*, 2006; *Stroud et al.*, 2007]. In general, anthropogenic aerosols with large organic fractions or insufficient sampling resolution of the instrumentation often influenced the failed closure studies. However, one may notice that the more recent experiments even within the urban environments have had much higher success rates than the earlier experiments, as a result of improved instrumentation. This indicates that extended Kohler theory should be sufficient to predict the N_{CCN} so long as the chemical composition and size distribution of the aerosol are measured accurately and at a high sampling rate.

Throughout the MILAGRO and INTEX-B field campaigns, scientists from Scripps Research Institute operated a Droplet Measurement Technologies Cloud Condensation Nuclei counter (CCNc) [*Lance et al.*, 2006; *Roberts and Nenes*, 2005; *Rose et al.*, 2008]. The instrument was located on the same inlet as the TAMU DMA/TDMA. The CCNc was set to a constant supersaturation of 0.2% for both field campaigns and maintained at a supersaturation of 0.24 +/- 0.06% for INTEX-B. Only data from level legs were used in the subsequent analysis.

During INTEX-B, a size distribution was measured every 90 sec, and a complete set of hygroscopic growth distribution across 4 dry diameters required roughly 720 sec; however, the aircraft was traveling at 100 m/s through plumes of aerosol. For a successful closure, the aerosol composition and size distribution need to be fairly homogenous across a broad swath of the atmosphere. For this reason, a closure study of the Mexico City aerosol was not attempted. However, the Asian aerosol had been in

transport for over three days, allowing for mixing and diffusion processes to take hold and spread the plume across a wide area. The CCN closure study below estimates the number of particles that activate to become cloud condensation nuclei at a specified supersaturation using Kohler theory with the assumption that the aerosol is composed of a mixture of soluble inorganic and an insoluble organic species. A brief description of the methodology will be provided; however, more details can be found in the *Gasparini et al.* [2006] paper.

A DMA distribution and the TDMA growth distributions are interpolated to the time when the CCN counter measured the concentration of activated aerosol at a prescribed supersaturation. Only DMA distributions measured with 180 sec and TDMA measurements within 720 sec of the CCN measurement were used. If a complete set of measurements including growth distributions at four different dry diameters was not available, the prediction of the number of CCN was not attempted. Throughout the discussion of this section, the solubility of the aerosol will be described using the growth factor G(85). This measurement facilitates the direct measurement of the volume of the soluble material within the aerosol.

For each DMA size bin, the TDMA G(85) distributions provide a measurement of the solubility of the aerosol. The first step in the prediction is to interpolate these measurements into a matrix of values of number concentration, $\Delta N_{Dp^*,G(85)}$, as shown in Figure 27. This matrix yields the number of particles that have a specified dry diameter and G(85) value. Figure 27 demonstrates an example from the research flights on May 8, 2006. Four growth distributions were measured at 0.025, 0.050, 0.100, and 0.300 μm

across the size distribution. The TDMA growth distributions are then interpolated across the size distribution to yield the matrix of $\Delta N_{Dp^*,G(85)}$ shown in the Figure 27.

The next step is to then predict the concentration of CCN that would activate for a specified supersaturation. An array of supersaturation values are calculated for a specified range of D_p^* and G(85) values. The soluble material is assumed to be ammonium bisulfate, and the assumption is based on AMS measurements aboard the C130 [*Dunlea et al.*, 2009]. For each D_p^* and G(85) value, equations (6) through (12) are used to solve for the mass of the solute as described in the methodology. The mass of the solute is then used to solve equation (14) for the supersaturation. This is repeated for all the possible combinations of D_p^* and G(85) and creates an array of activation curves for a specified solute. In Figure 27c, a black dashed line demonstrates a predicted activation curve for the supersaturation of 0.225% overlaid onto the array of $\Delta N_{Dp^*,G(85)}$ values. The predicted concentration of particles that will activate to become CCN is calculated by summing up all $\Delta N_{Dp^*,G(85)}$ values on and to the right of the activation curve.

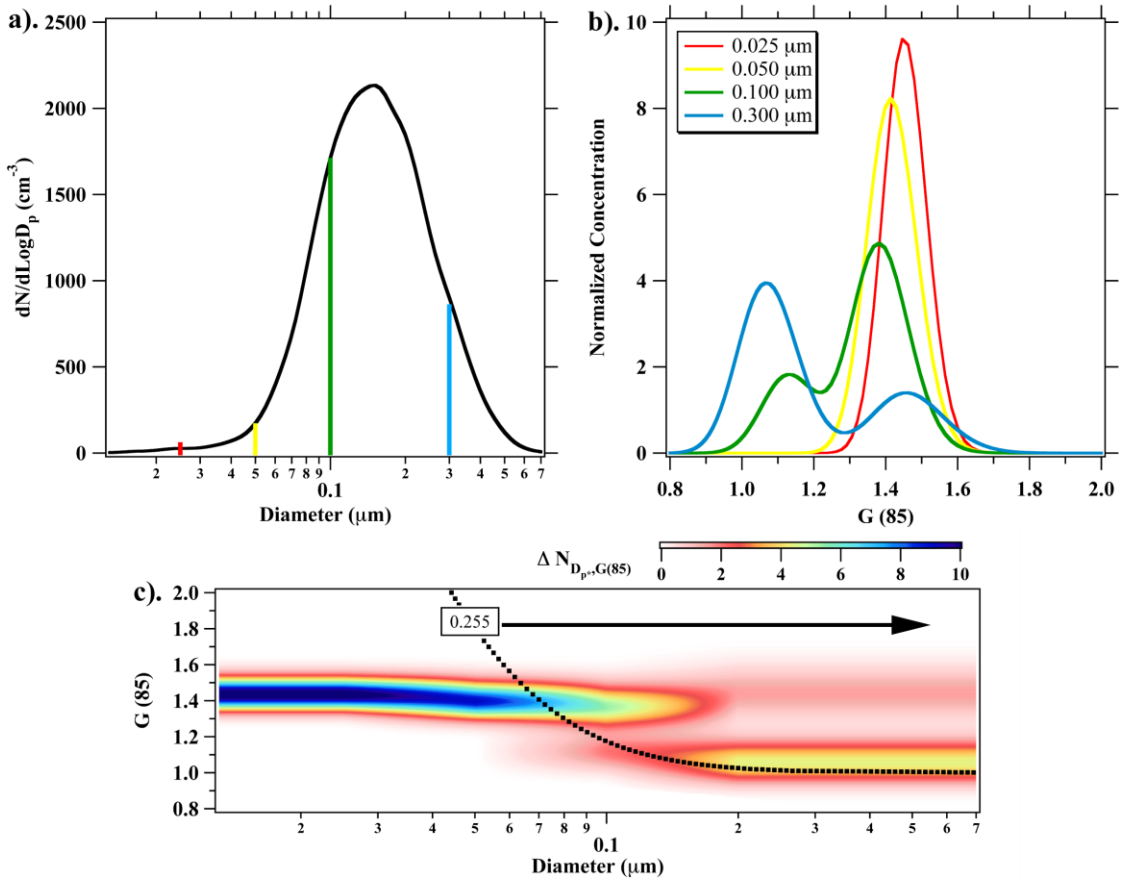

Figure 27. The interpolation of the DMA/TDMA measurements into a matrix of values of number concentration. An example number distribution is shown in figure (a) with the location of the TDMA measurements indicated. The corresponding TDMA measurements are shown in (b). These measurements are interpolated into the matrix of $\Delta N_{Dp^*,G(85)}$ values shown in (c). The $\Delta N_{Dp^*,G(85)}$ concentrations are indicated by the color scale in figure (c). The activation curve for an aerosol composed of ammonium bisulfate at a supersaturation of 0.255% is indicated by the dashed line in figure (c).

The method described above was used to attempt CCN closure with the measured CCN concentrations during the research flights on April 24, 26, and 28, and May 03, 08, 09, and 11. The CCN was operated without a constant pressure inlet, and the supersaturation has been corrected for changes in atmospheric pressure [*Roberts and*

Nenes, 2005; *Rose et al.*, 2008], which results in the supersaturation varying from ~0.3% near the surface to ~0.15% at higher altitudes. In the closure study presented here, two assumptions were tested. The first assumption was an aerosol composed purely of the soluble inorganic ammonium bisulfate and will be referred to as the pure NH_4HSO_4 assumption. The second assumption is of an aerosol composed of a mixture of NH_4HSO_4 and an insoluble organic aerosol. The mass of solute, ammonium bisulfate, present within an aerosol of a specific dry diameter and measured growth factor is determined by iteratively solving for equations (8) and (10) until both equations are satisfied. This method will be referred to as the GF assumption.

The first closure attempt used all data collected. This included measurements from the Seattle area and the California Central Valley. In Figure 28, the predicted CCN concentration is plotted on the y-axis, and the measured CCN concentration is plotted on the x-axis. The scatter plot on the left demonstrates the predictive capability of the pure NH_4HSO_4 assumption. A linear regression analysis determined $CCN_{predicted} = 1.84*CCN_{measured}$ with an r^2 of 0.84. The y-intercept of the fit has been forced to 0. In comparison, the scatter plot of predicted versus measured CCN concentration using the GF assumption is shown on the right. A linear regression analysis determined $CCN_{predicted} = 0.90 * CCN_{measured}$ with an r^2 of 0.86. The y-intercept of this fit has also been forced to 0.

The plots in Figure 28 illustrate the failure of the pure ammonium bisulfate assumption for the polluted urban and continental areas of the United Sates. The aerosols within these regions are often composed of significant quantities of either

slightly soluble or insoluble species. However, with the GF assumption, closure was obtained. On average, the GF assumption slightly under-predicts the CCN concentration measured by the CCN counter. This prediction, though, is within the standard deviation of the CCN counter, which is on average 25% of the measured values. Also, there is no strong bias exhibited by the prediction. For the above reasons, this was an excellent result for an aircraft-based closure study. The slight under-prediction is most likely caused by the insoluble organic species being slightly hydrophillic. This would theoretically slightly decrease the critical supersaturation for the aerosol.

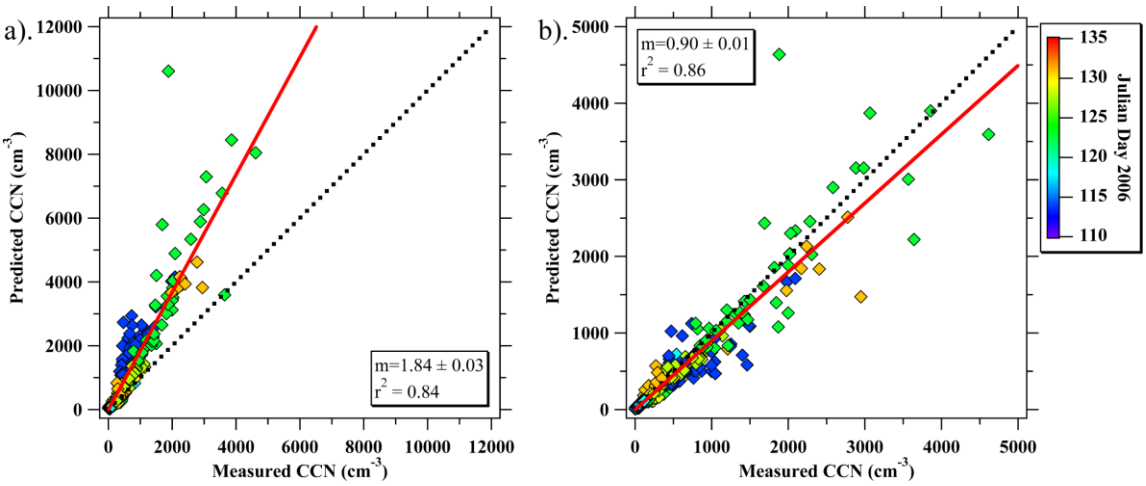

Figure 28. Scatter plots of predicted versus measured CCN concentration for pure ammonium bisulfate (a) and a bimodal composition of ammonium bisulfate and an insoluble organic (b) for all data. The coefficients of the linear regression are annotated on the figure. The red line represents the linear fit, and the dashed line is the 1:1 line. The color of the marker indicates the date of the research flight.

Another CCN closure study was conducted using only the data collected over the Pacific Ocean. This effectively removed all the local emission from the Continental United States. The scatter plots in Figure 29 illustrate this closure study. Like the

previous figure, the pure NH_4HSO_4 assumption is plotted on the left, and the GF assumption is potted on the right. A linear regression analysis for the NH_4HSO_4 assumption determined $CCN_{predicted}$ =1.13* $CCN_{measured}$ with an r^2 of 0.87. The linear regression for the GF assumption determined $CCN_{predicted}$ = 0.88*$CCN_{measured}$ with an r^2 of 0.89. Both y intercepts have been forced to 0.

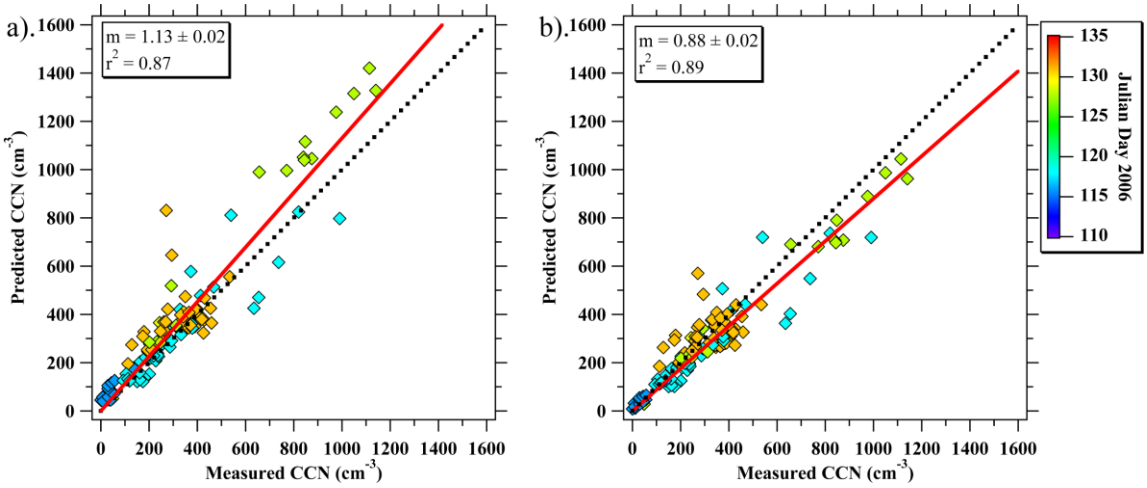

Figure 29 Scatter plots of predicted versus measured CCN concentration for pure ammonium bisulfate (a) and a bimodal composition of ammonium bisulfate and an insoluble organic (b) for all data measured over the Pacific Ocean. The coefficients of the linear regression are annotated on the figure. The red line represents the linear fit, and the dashed line is the 1:1 line. The color of the marker indicates the date of the research flight.

The calculated slopes indicate that both assumptions have achieved closure, and the results give us further insight into the aerosol activation properties. The pure NH_4HSO_4 assumption over-predicts the CCN concentration, indicating that the aerosol is not composed purely of NH_4HSO_4. The GF assumption under-predicts the CCN concentration, indicating that the assumption that the organic material is insoluble is not

totally valid, and some of the organic species are hydrophilic. The organic aerosol was observed by the AMS to be undergoing oxidation during the INTEX-B campaign [*DeCarlo et al.*, 2008]. Results from the MILAGRO campaign discussed within this dissertation and *Jimenez et al.* [2009] have indicated that the oxidation of organics increases their hygroscopicity. Even with the slight disagreement in predicted CCN concentrations, at supersaturations of less than 0.25% both assumptions are valid and achieve closure. However, there is a caveat here. At supersaturations greater than 0.25%, particles with smaller dry diameters have a potential for activation. As the discussion above has indicated, the smaller diameter particles have a greater fraction of insoluble material in comparison to the larger diameter particles. Therefore, it is very likely that the magnitude of over-prediction by the pure ammonium bisulfate assumption will increase as the supersaturation increases. At some point, this assumption will fail to meet closure and should be used in atmospheric modeling with caution.

4. SUMMARY

The primary goal of the MILAGRO and INTEX-B field campaigns were to understand the transport and transformation of aerosols and to assess their impact on air quality and climate. MILAGRO was focused on studying this on a local to regional scale, whereas INTEX-B was focused on the on the intercontinental scale. To achieve this goal, Texas A&M operated a DMA/TDMA system to measure aerosol size distributions and hygroscopicity aboard the NCAR/NSF C-130.

During MILAGRO, the system was operated during 72 out of 86 hours of research flights, measuring over 2450 size distributions and between 216 to 236 TDMA growth distributions for dry diameters of 0.025, 0.050, 0.100, 0.200, and 0.300 μm. Measurements were made from Mexico City to the Gulf of Mexico, and one flight was even conducted over biomass burning in the Yucatan. However, the majority of measurements were made within Mexico City and within the plume to the northeast of Mexico City. All of the flights intercepted the Mexico City plume at a variety of times over a period of emission to two days in transportation.

During INTEX-B, the system was operated during all 94 hours of research flying, collecting over 2100 size distributions and between 240 to 270 TDMA growth distributions for dry diameters of 0.025, 0.050, 0.100, and 0.300 μm. The measurements were made in a variety of locations throughout the West Coast of the United States; however, the predominant location was over the northeastern Pacific Ocean. All research flights intercepted the Asian plume at a variety of different durations in

transport time since emission from Asia. This has generated a data set for studying aerosol that had been in transport for 2 to 10 days.

One of the primary goals of MILAGRO was to examine the physicochemical properties of the MCMA aerosol and plume evolution to predict the effect it has on the local, regional, and global environment. The previous sections have described the physicochemical properties of the Mexico City aerosol. Within the basin, the aerosol has number concentrations on average of 13,659 +/ 7998 cm^{-3} and a volume concentration of 11.2 ± 7.0 $\mu m^3/cm^3$. The most probable size distribution had a distinct Aitken mode and occasionally widespread nucleation occurred. The passage of fronts and occurrence of convection removes large particles through wet deposition, which enables new particle formation through nucleation to occur. The most soluble aerosols are the primary emissions that make up the Aitken mode, and the least soluble aerosol is at 0.100 μm. The aerosol in the accumulation mode is more soluble and typically bimodal.

The plume advected from Mexico City to the northeast has significantly higher number and volume concentration of aerosol in comparison to the background aerosol. The size distribution within the plume routinely has a pronounced Aitken mode. The plume over time decreases by the way of a power law distribution. After 12 hours, there is little change in the number and volume concentration.

The most profound discovery from this data was this change in solubility of aerosols composed mostly of organics. During 12 hours of transport, the mostly organic aerosol undergoes a rapid transformation that causes rapid increase in solubility. The

most pronounced change occurs over 6 hours for 0.100 μm particles with κ_w increasing from 0.09 ± 0.06 within the MCMA to 0.305 _± 0.090 after 12 hours of transport. This increase in hygroscopicity correlated well with an increase in O/C measured by the HRTOFAMS [*DeCarlo et al.*, 2008; *Jimenez et al.*, 2009]. The change in κ_w corresponds to the critical supersaturation decreasing from 0.408 to 0.223 %. This decrease would allow for the 0.100 μm aerosol to activate in cumulus clouds and possibly in stratus clouds if the updraft velocity was strong enough. With all particle sizes becoming more soluble, the activation diameter for a supersaturation of 0.30 % shifts from 0.115 μm to 0.075 μm during the 12 hours of transport. This would result in an increase in the percentage of the number size distribution that can activate to become cloud condensation nuclei (CCN) within the cloud as long as there is sufficient water vapor available. The increase in the number of CCN should have a pronounced effect on clouds to the northeast of MCMA. However, as more particles are capable of activating, more particles can be removed by wet deposition. With much of the aerosol being removed, the MCMA plume would have a limited effect on clouds on the global scale and only be a regional effect.

Measurements during INTEX-B were remarkably successful intercepting the Asian plume. The most common transport time for the aerosol was 3 to 4 days, and the most common source region was Northern China. Occasionally, rapid transport was observed with the aerosol that was measured 2 to 3 days after emission. The number concentration within the rapid transport plumes was elevated with concentrations exceeding 2000 cm^{-3} with a pronounced narrow peak in the size distribution centered on

0.100 μm. The volume concentration was also elevated, with measured values exceeding 2 $\mu m^3/cm^3$. Within the Asian plume, the geometric mean diameter size distribution shifts to the right as the altitude decreases within the free troposphere. Within the background aerosol, these high of values of concentration in the mid to upper levels of the troposphere were never measured. However, on occasion there were concentration measurements of this magnitude in the lower levels of the atmosphere at three km and below. The size distribution is monomodal in the free troposphere and exhibits bimodality within the marine boundary layer.

On average, the κ value oscillates between 0.40 and 0.53 for all dry diameters of the soluble Asian aerosol within the free troposphere. This is surprisingly consistent and indicates that the aerosol has undergone cloud processing or gas phase condensation has coated the aerosol with sulfate. Aerosol with a κ value less than 0.20 was considered in this study to have low solubility. For 0.100 μm aerosol and less, there was very little low-soluble aerosol until 4.5 km and higher. The aerosol growth distributions at this altitude and higher exhibit bimodality roughly 50% of the time. The secondary mode contributes 20 to 33% to the overall growth distribution and on average has a κ value of 0.179 ± 0.172, 0.027±0.058, 0.052 ± 0.096, and 0.142 ± 0.139 for dry diameters of 0.025, 0.050, 0.100, and 0.300 μm, respectively.

Within the free troposphere, the κ value of the background aerosol is less consistent in the vertical dimension compared to the Asian aerosol with the κ value varying between 0.32 and 0.56. At altitudes of 4.5 km to 7.5 km, the aerosol exhibits bimodal growth distribution at all dry diameters except for 0.025 μm more often than the

Asian aerosols. On average, the aerosol growth distributions exhibit bimodality 50%, 68%, 73%, and 80% of the time for dry diameters of 0.025, 0.050, 0.100 and 0.300 μm, respectively. In the same order of dry diameters, the secondary mode contributes 0.234 ± 0.129, 0.180 ± 0.116, 0.225 ± 0.117, and 0.332 ± 0.091 with κ values of 0.061 ± 0.131, 0.010 ± 0.016, 0.086 ± 0.171, and 0.142 ± 0.146. This is a surprising result and indicates the presence of elemental carbon (soot) or slightly soluble organic aerosol throughout the mid to upper levels of the free troposphere.

The evolution of the Asian aerosol during transport was investigated through the creation of cumulative histograms. The 0.050 μm diameter particles have the lowest solubility after 2 to 3 days of transport and the highest solubility at 9 to 10 days. These particles exhibit a noticeably higher solubility at the 8 to 10 day timeframe than the 2 to 8 day timeframe. The 0.100 μm and 0.300 exhibit very little change over the timeframe studied. Therefore, overall the chemical composition is only slightly changing, and a majority of the transformation has occurred shortly after being emitted from Asia. However, there are always exceptions, as the May 1 case studied demonstrated. During rapid transport, elevated levels of gas phase SO_2 could still be present. This will condense on the particles with diameters greater than 100 μm, increasing their hygroscopicity over time until the gas phase SO_2 has been totally condensed into the aerosol phase.

The evolution of the Asian aerosol concentration during transport was also studied. However, on average, the number concentration within the plume undergoes very little change during the transport from Asia. Again, as the May 1 case

demonstrates, there are exceptions to this observation. During rapid transport of 3 to 4 days compared to 5 days there was a noticeable change in number concentration. The volume concentration has more variability. The highest probability for high volume concentration (> 1 $\mu m^3/cm^3$) is in the 3 to 4 day timeframe, and surprisingly the lower probability is in the 2 to 3 day timeframe. This lower probability may result from the condensational growth of the particles still occurring as shown in the May 1 case study. The lowest volume concentrations observed were for the 9 to 10 day timeframe as a result of deposition processes.

A closure study was conducted to investigate the capabilities of the data to predict the number of Cloud Condensation Nuclei activity at a specified supersaturation. The supersaturation was defined by a DMT CCN counter that measured the number of CCN active. The model used a modified Kohler equation and two different assumptions to predict the number of CCN. The first assumption is that the particle is pure NH_4HSO_4, and the second assumption is that the aerosol is composed of a mixture of NH_4HSO_4 and an insoluble organic aerosol. Overall, the later assumption achieved closure over both the continental United States and the Pacific Ocean, whereas the NH_4HSO_4 assumption only achieved closure over the Pacific Ocean. This successful closure using the NH_4HSO_4 assumption indicates for diameters greater than and equal to 100 μm the aerosol should readily activate in most clouds over the Pacific Ocean. For clouds with lower supersaturation (< 0.25%), modelers should be able to readily predict the number of CCN by using the assumption of pure ammonium sulfate. However,

another result of this study was the observation that the roughly 25% of the aerosol at 0.050 and 0.025 contains fairly insoluble species of particles.

This dissertation has used 166 hours of airborne measurement to characterize the physicochemical properties of the aerosol over Mexico City, to the northeast of Mexico City, over the Western United States, and over the northeastern Pacific Ocean. The size of the data set provided a truly unique opportunity to statistically study the transport and evolution of aerosols from primary emissions all the way to being in transport within the atmosphere for up to 10 days. The study of the evolution of the aerosol has yielded insights into how the aerosol could interact with clouds and affect the radiative budget of the Earth through the first and second indirect effect.

REFERENCES

Ackerman, A. S., O. B. Toon, D. E. Stevens, A. J. Heymsfield, V. Ramanathan, et al. (2000), Reduction of tropical cloudiness by soot, *Science*, *288*(5468), 1042-1047.

Aiken, A. C., D. Salcedo, M. J. Cubison, J. A. Huffman, P. F. DeCarlo, et al. (2009), Mexico City aerosol analysis during MILAGRO using high resolution aerosol mass spectrometry at the urban supersite (T0) - Part 1: Fine particle composition and organic source apportionment, *Atmospheric Chemistry and Physics*, *9*(17), 6633-6653.

Albrecht, B. A. (1989), Aerosols, cloud microphysics, and fractional cloudiness, *Science*, *245*(4923), 1227-1230.

Allan, J. D., K. N. Bower, H. Coe, H. Boudries, J. T. Jayne, et al. (2004), Submicron aerosol composition at Trinidad Head, California, during ITCT 2K2: Its relationship with gas phase volatile organic carbon and assessment of instrument performance, *Journal of Geophysical Research-Atmospheres*, *109*(D23S24), doi:10.1029/2003JD004208.

Andreae, M. O. (2009), A new look at aging aerosols, *Science*, *326*(5959), 1493-1494.

Andreae, M. O., and P. Merlet (2001), Emission of trace gases and aerosols from biomass burning, *Global Biogeochemical Cycles*, *15*(4), 955-966.

Andreae, M. O., and D. Rosenfeld (2008), Aerosol-cloud-precipitation interactions. Part 1: The nature and sources of cloud-active aerosols, *Earth-Science Reviews*, *89*(1-2), 13-41.

Andreae, M. O., W. Elbert, and S. J. Demora (1995), Biogenic sulfur emissions and aerosols over the Tropical South-Atlantic: 3. Atmospheric dimethylsulfide, aerosols and cloud condensation nuclei, *Journal of Geophysical Research-Atmospheres*, *100*(D6), 11335-11356.

Arimoto, R., R. A. Duce, D. L. Savoie, J. M. Prospero, R. Talbot, et al. (1996), Relationships among aerosol constituents from Asia and the North Pacific during PEM-West A, *Journal of Geophysical Research-Atmospheres*, *101*(D1), 2011-2023.

Bahreini, R., J. L. Jimenez, J. Wang, R. C. Flagan, J. H. Seinfeld, et al. (2003), Aircraft-based aerosol size and composition measurements during ACE-Asia using an

Aerodyne aerosol mass spectrometer, *Journal of Geophysical Research-Atmospheres, 108*(D23), doi:10.1029/2002jd003226.

Baumgardner, D., G. B. Raga, and A. Muhlia (2004), Evidence for the formation of CCN by photochemical processes in Mexico City, *Atmospheric Environment*, *38*(3), 357-367.

Baumgardner, D., M. Grutter, J. Allan, C. Ochoa, B. Rappenglueck, et al. (2009), Physical and chemical properties of the regional mixed layer of Mexico's Megapolis, *Atmospheric Chemistry and Physics, 9*(15), 5711-5727.

Berg, O. H., E. Swietlicki, and R. Krejci (1998), Hygroscopic growth of aerosol particles in the marine boundary layer over the Pacific and Southern Oceans during the First Aerosol Characterization Experiment (ACE 1), *Journal of Geophysical Research-Atmospheres, 103*(D13), 16535-16545.

Bethan, S., G. Vaughan, C. Gerbig, A. Volz-Thomas, H. Richer, et al. (1998), Chemical air mass differences near fronts, *Journal of Geophysical Research-Atmospheres*, *103*(D11), 13413-13434.

Bigg, E. K. (1986), Discrepancy between observation and prediction of concentrations of cloud condensation nuclei, *Atmospheric Research*, *20*(1), 81-86.

Bougiatioti, A., C. Fountoukis, N. Kalivitis, S. N. Pandis, A. Nenes, et al. (2009), Cloud condensation nuclei measurements in the marine boundary layer of the eastern Mediterranean: CCN closure and droplet growth kinetics, *Atmospheric Chemistry and Physics, 9*(18), 7053-7066.

Bravo, H. A. (1960), Variation of different pollutants in the atmosphere of Mexico City, *Journal of the Air Pollution Control Association*, *10*(6), 447-449.

Brock, C. A., P. K. Hudson, E. R. Lovejoy, A. Sullivan, J. B. Nowak, et al. (2004), Particle characteristics following cloud-modified transport from Asia to North America, *J. Geophys. Res.*, *109*(D23S26), doi:10.1029/2003jd004198.

Broekhuizen, K., R. Y. W. Chang, W. R. Leaitch, S. M. Li, and J. P. D. Abbatt (2006), Closure between measured and modeled cloud condensation nuclei (CCN) using size-resolved aerosol compositions in downtown Toronto, *Atmospheric Chemistry and Physics, 6*(9), 2513-2524.

Browning, K. A., and N. M. Roberts (1994), Structure of a frontal cyclone, *Quarterly Journal of the Royal Meteorological Society*, *120*(520), 1535-1557.

Canagaratna, M. R., J. T. Jayne, J. L. Jimenez, J. D. Allan, M. R. Alfarra, et al. (2007), Chemical and microphysical characterization of ambient aerosols with the Aerodyne aerosol mass spectrometer, *Mass Spectrometry Reviews*, *26*(2), 185-222.

Cantrell, W., G. Shaw, G. R. Cass, Z. Chowdhury, L. S. Hughes, et al. (2001), Closure between aerosol particles and cloud condensation nuclei at Kaashidhoo Climate Observatory, *Journal of Geophysical Research-Atmospheres*, *106*(D22), 28711-28718.

Chang, R. Y. W., P. S. K. Liu, W. R. Leaitch, and J. P. D. Abbatt (2007), Comparison between measured and predicted CCN concentrations at Egbert, Ontario: Focus on the organic aerosol fraction at a semi-rural site, *Atmospheric Environment*, *41*(37), 8172-8182.

Charlson, R. J., S. E. Schwartz, J. M. Hales, R. D. Cess, J. A. Coakley, et al. (1992), Climate forcing by anthropogenic aerosols, *Science*, *255*(5043), 423-430.

Chuang, P. Y., D. R. Collins, H. Pawlowska, J. R. Snider, H. H. Jonsson, et al. (2000), CCN measurements during ACE-2 and their relationship to cloud microphysical properties, *Tellus Series B-Chemical and Physical Meteorology*, *52*(2), 843-867.

Coakley, J. A., R. L. Bernstein, and P. A. Durkee (1987), Effect of ship-stack effluents on cloud reflectivity, *Science*, *237*(4818), 1020-1022.

Collins, D. R., R. C. Flagan, and J. H. Seinfeld (2002), Improved inversion of scanning DMA data, *Aerosol Science and Technology*, *36*(1), 1-9.

Collins, D. R., D. R. Cocker, R. C. Flagan, and J. H. Seinfeld (2004), The scanning DMA transfer function, *Aerosol Science and Technology*, *38*(8), 833-850.

Cook, J., and E. J. Highwood (2004), Climate response to tropospheric absorbing aerosols in an intermediate general-circulation model, *Quarterly Journal of the Royal Meteorological Society*, *130*(596), 175-191.

Cooper, O. R., J. L. Moody, D. D. Parrish, M. Trainer, T. B. Ryerson, et al. (2002), Trace gas composition of midlatitude cyclones over the western North Atlantic Ocean: A conceptual model, *Journal of Geophysical Research-Atmospheres*, *107*(D7-8), doi:10.1029/2001jd000901.

Cooper, O. R., C. Forster, D. Parrish, M. Trainer, E. Dunlea, et al. (2004), A case study of transpacific warm conveyor belt transport: Influence of merging airstreams on trace gas import to North America, *Journal of Geophysical Research-Atmospheres*, *109*(D23S08), doi:10.1029/2003jd003624.

Covert, D. S., J. L. Gras, A. Wiedensohler, and F. Stratmann (1998), Comparison of directly measured CCN with CCN modeled from the number-size distribution in the marine boundary layer during ACE 1 at Cape Grim, Tasmania, *Journal of Geophysical Research-Atmospheres*, *103*(D13), 16597-16608.

de Foy, B., J. D. Fast, S. J. Paech, D. Phillips, J. T. Walters, et al. (2008), Basin-scale wind transport during the MILAGRO field campaign and comparison to climatology using cluster analysis, *Atmospheric Chemistry and Physics*, *8*(5), 1209-1224.

DeCarlo, P. F., J. R. Kimmel, A. Trimborn, M. J. Northway, J. T. Jayne, et al. (2006), Field-deployable, high-resolution, time-of-flight aerosol mass spectrometer, *Analytical Chemistry*, *78*(24), 8281-8289.

DeCarlo, P. F., E. J. Dunlea, J. R. Kimmel, A. C. Aiken, D. Sueper, et al. (2008), Fast airborne aerosol size and chemistry measurements above Mexico City and central Mexico during the MILAGRO campaign, *Atmospheric Chemistry and Physics*, *8*(14), 4027-4048.

Delgado-Granados, H., L. C. Gonzalez, and N. P. Sanchez (2001), Sulfur dioxide emissions from Popocatepetl volcano (Mexico): case study of a high-emission rate, passively degassing erupting volcano, *Journal of Volcanology and Geothermal Research*, *108*(1-4), 107-120.

Drewnick, F., S. S. Hings, P. DeCarlo, J. T. Jayne, M. Gonin, et al. (2005), A new time-of-flight aerosol mass spectrometer (TOF-AMS) - Instrument description and first field deployment, *Aerosol Science and Technology*, *39*(7), 637-658.

Dunlea, E. J., P. F. DeCarlo, A. C. Aiken, J. R. Kimmel, R. E. Peltier, et al. (2009), Evolution of Asian aerosols during transpacific transport in INTEX-B, *Atmospheric Chemistry and Physics*, *9*(19), 7257-7287.

Dunn, M. J., J. L. Jimenez, D. Baumgardner, T. Castro, P. H. McMurry, et al. (2004), Measurements of Mexico City nanoparticle size distributions: Observations of new particle formation and growth, *Geophysical Research Letters*, *31*(10), doi:10.1029/2004GL019483.

Duplissy, J., M. Gysel, M. R. Alfarra, J. Dommen, A. Metzger, et al. (2008), Cloud forming potential of secondary organic aerosol under near atmospheric conditions, *Geophysical Research Letters*, *35*(3), doi:10.1029/2007gl031075.

Dusek, U., D. S. Covert, A. Wiedensohler, C. Neususs, D. Weise, et al. (2003), Cloud condensation nuclei spectra derived from size distributions and hygroscopic properties of the aerosol in coastal south-west Portugal during ACE-2, *Tellus Series B-Chemical and Physical Meteorology*, *55*(1), 35-53.

Dusek, U., G. P. Frank, L. Hildebrandt, J. Curtius, J. Schneider, et al. (2006), Size matters more than chemistry for cloud-nucleating ability of aerosol particles, *Science*, *312*(5778), 1375-1378.

Dzepina, K., R. M. Volkamer, S. Madronich, P. Tulet, I. M. Ulbrich, et al. (2009), Evaluation of recently-proposed secondary organic aerosol models for a case study in Mexico City, *Atmospheric Chemistry and Physics*, *9*(15), 5681-5709.

Ervens, B., M. Cubison, E. Andrews, G. Feingold, J. A. Ogren, et al. (2007), Prediction of cloud condensation nucleus number concentration using measurements of aerosol size distributions and composition and light scattering enhancement due to humidity, *Journal of Geophysical Research-Atmospheres*, *112*(D10S32), doi:10.1029/2006jd007426.

Facchini, M. C., M. Mircea, S. Fuzzi, and R. J. Charlson (1999), Cloud albedo enhancement by surface-active organic solutes in growing droplets, *Nature*, *401*(6750), 257-259.

Facchini, M. C., S. Decesari, M. Mircea, S. Fuzzi, and G. Loglio (2000), Surface tension of atmospheric wet aerosol and cloud/fog droplets in relation to their organic carbon content and chemical composition, *Atmospheric Environment*, *34*(28), 4853-4857.

Fast, J. D., and S. Y. Zhong (1998), Meteorological factors associated with inhomogeneous ozone concentrations within the Mexico City basin, *Journal of Geophysical Research-Atmospheres*, *103*(D15), 18927-18946.

Fast, J. D., B. de Foy, F. A. Rosas, E. Caetano, G. Carmichael, et al. (2007), A meteorological overview of the MILAGRO field campaigns, *Atmospheric Chemistry and Physics*, *7*(9), 2233-2257.

Feingold, G., and P. Y. Chuang (2002), Analysis of the influence of film-forming compounds on droplet growth: Implications for cloud microphysical processes and climate, *Journal of the Atmospheric Sciences*, *59*(12), 2006-2018.

Feingold, G., W. L. Eberhard, D. E. Veron, and M. Previdi (2003), First measurements of the Twomey indirect effect using ground-based remote sensors, *Geophysical Research Letters*, *30*(6), doi:10.1029/2002gl016633.

Foster, P., V. Ramaswamy, P. Artaxo, T. Berntsen, R. Betts, et al. (2007), Changes in atmospheric constituents and in radiative forcing, in *Climate Change 2007: The Physical Science Basis. Contribution of Working Group I to the Fourth Assessment Report of the Intergovernmental Panel on Climate Change*, edited by S. Solomon, D. Qin, M. Manning, Z. Chen, M. Marquis, K. B. Averyt, M. Tignor and H. L. Miller, pp. 129-234, Cambridge University Press, Cambridge, UK.

Gasparini, R., D. R. Collins, E. Andrews, P. J. Sheridan, J. A. Ogren, et al. (2006), Coupling aerosol size distributions and size-resolved hygroscopicity to predict humidity-dependent optical properties and cloud condensation nuclei spectra, *Journal of Geophysical Research-Atmospheres*, *111*(D5S13), doi:10.1029/2005jd006092.

Gilardoni, S., S. Liu, S. Takahama, L. M. Russell, J. D. Allan, et al. (2009), Characterization of organic ambient aerosol during MIRAGE 2006 on three platforms, *Atmospheric Chemistry and Physics*, *9*(15), 5417-5432.

Goldstein, A. H., D. B. Millet, M. McKay, L. Jaegle, L. Horowitz, et al. (2004), Impact of Asian emissions on observations at Trinidad Head, California, during ITCT 2K2, *Journal of Geophysical Research-Atmospheres*, *109*(D23S17), doi:1029/2003JD004406.

Gunthe, S. S., S. M. King, D. Rose, Q. Chen, P. Roldin, et al. (2009), Cloud condensation nuclei in pristine tropical rainforest air of Amazonia: size-resolved measurements and modeling of atmospheric aerosol composition and CCN activity, *Atmospheric Chemistry and Physics*, *9*(19), 7551-7575.

Hallquist, M., J. C. Wenger, U. Baltensperger, Y. Rudich, D. Simpson, et al. (2009), The formation, properties and impact of secondary organic aerosol: current and emerging issues, *Atmospheric Chemistry and Physics*, *9*(14), 5155-5236.

Hansen, J., M. Sato, and R. Ruedy (1997), Radiative forcing and climate response, *Journal of Geophysical Research-Atmospheres*, *102*(D6), 6831-6864.

Hasegawa, S., and S. Ohta (2002), Some measurements of the mixing state of soot-containing particles at urban and non-urban sites, *Atmospheric Environment*, *36*(24), 3899-3908.

Heald, C. L., D. J. Jacob, R. J. Park, B. Alexander, T. D. Fairlie, et al. (2006), Transpacific transport of Asian anthropogenic aerosols and its impact on surface air quality in the United States, *Journal of Geophysical Research-Atmospheres*, *111*(D14), doi:10.1029/2005JD006847.

Herrera, J. R., and J. J. Castro (1988), Production of cloud condensation nuclei in Mexico-City, *Journal of Applied Meteorology*, *27*(10), 1189-1192.

Huang, Y., W. L. Chameides, and R. E. Dickinson (2007), Direct and indirect effects of anthropogenic aerosols on regional precipitation over east Asia, *Journal of Geophysical Research-Atmospheres*, *112*(D3), doi:10.1029/2006jd007114.

Huebert, B. J., C. A. Phillips, L. Zhuang, E. Kjellstrom, H. Rodhe, et al. (2001), Long-term measurements of free-tropospheric sulfate at Mauna Loa: Comparison with global model simulations, *Journal of Geophysical Research-Atmospheres*, *106*(D6), 5479-5492.

Husar, R. B., D. M. Tratt, B. A. Schichtel, S. R. Falke, F. Li, et al. (2001), Asian dust events of April 1998, *Journal of Geophysical Research-Atmospheres*, *106*(D16), 18317-18330.

Iida, K., M. R. Stolzenburg, P. H. McMurry, and J. N. Smith (2008), Estimating nanoparticle growth rates from size-dependent charged fractions: Analysis of new particle formation events in Mexico City, *Journal of Geophysical Research-Atmospheres*, *113*(D5), doi:10.1029/2007jd009260.

Jacobson, M. Z. (2002), Control of fossil-fuel particulate black carbon and organic matter, possibly the most effective method of slowing global warming, *Journal of Geophysical Research-Atmospheres*, *107*(D19), doi:10.1029/2001jd001376.

Jaffe, D., H. Price, D. Parrish, A. Goldstein, and J. Harris (2003), Increasing background ozone during spring on the west coast of North America, *Geophysical Research Letters*, *30*(12), doi:10.1029/2003GL017024.

Jaffe, D., T. Anderson, D. Covert, R. Kotchenruther, B. Trost, et al. (1999), Transport of Asian air pollution to North America, *Geophysical Research Letters*, *26*(6), 711-714.

Jayne, J. T., D. C. Leard, X. F. Zhang, P. Davidovits, K. A. Smith, et al. (2000), Development of an aerosol mass spectrometer for size and composition analysis of submicron particles, *Aerosol Science and Technology*, *33*(1-2), 49-70.

Jimenez, J. L., M. R. Canagaratna, N. M. Donahue, A. S. H. Prevot, Q. Zhang, et al. (2009), Evolution of organic aerosols in the atmosphere, *Science*, *326*(5959), 1525-1529.

Johnson, B. T., K. P. Shine, and P. M. Forster (2004), The semi-direct aerosol effect: Impact of absorbing aerosols on marine stratocumulus, *Quarterly Journal of the Royal Meteorological Society*, *130*(599), 1407-1422.

Kim, B. G., S. E. Schwartz, M. A. Miller, and Q. L. Min (2003), Effective radius of cloud droplets by ground-based remote sensing: Relationship to aerosol, *Journal of Geophysical Research-Atmospheres*, *108*(D23), doi:10.1029/2003jd003721.

Kleinman, L. I., S. R. Springston, P. H. Daum, Y. N. Lee, L. J. Nunnermacker, et al. (2008), The time evolution of aerosol composition over the Mexico City plateau, *Atmospheric Chemistry and Physics*, *8*(6), 1559-1575.

Kline, J., B. Huebert, S. Howell, B. Blomquist, J. Zhuang, et al. (2004), Aerosol composition and size versus altitude measured from the C-130 during ACE-Asia, *Journal of Geophysical Research-Atmospheres*, *109*(D19S08), doi:10.1029/2004jd004540.

Kohler, H. (1936), The nucleus in and the growth of hygroscopic droplets, *Transactions of the Faraday Society*, *32*(2), 1152-1161.

Kulmala, M., H. Vehkamaki, T. Petaja, M. Dal Maso, A. Lauri, et al. (2004), Formation and growth rates of ultrafine atmospheric particles: A review of observations, *Journal of Aerosol Science*, *35*(2), 143-176.

Lance, S., J. Medina, J. N. Smith, and A. Nenes (2006), Mapping the operation of the DMT continuous flow CCN counter, *Aerosol Science and Technology*, *40*(4), 242-254.

Lance, S., A. Nenes, C. Mazzoleni, M. K. Dubey, H. Gates, et al. (2009), Cloud condensation nuclei activity, closure, and droplet growth kinetics of Houston aerosol during the Gulf of Mexico Atmospheric Composition and Climate Study (GoMACCS), *Journal of Geophysical Research-Atmospheres*, *114*(D00F15), doi:10.1029/2008jd011699.

Liu, H. Y., D. J. Jacob, I. Bey, R. M. Yantosca, B. N. Duncan, et al. (2003), Transport pathways for Asian pollution outflow over the Pacific: Interannual and seasonal variations, *Journal of Geophysical Research-Atmospheres*, *108*(D20), doi:10.1029/2002JD003102.

Liu, P. S. K., W. R. Leaitch, C. M. Banic, S. M. Li, D. Ngo, et al. (1996), Aerosol observations at Chebogue Point during the 1993 North Atlantic Regional Experiment: Relationships among cloud condensation nuclei, size distribution, and chemistry, *Journal of Geophysical Research-Atmospheres*, *101*(D22), 28971-28990.

Lohmann, U., and J. Feichter (2005), Global indirect aerosol effects: A review, *Atmospheric Chemistry and Physics*, *5*(3), 715-737.

Martin, G. M., D. W. Johnson, and A. Spice (1994), The measurement and parameterization of effective radius of droplets in warm stratocumulus clouds, *Journal of the Atmospheric Sciences*, *51*(13), 1823-1842.

Massling, A., S. Leinert, A. Wiedensohler, and D. Covert (2007), Hygroscopic growth of sub-micrometer and one-micrometer aerosol particles measured during ACE-Asia, *Atmospheric Chemistry and Physics*, *7*(12), 3249-3259.

Massling, A., A. Wiedensohler, B. Busch, C. Neususs, P. Quinn, et al. (2003), Hygroscopic properties of different aerosol types over the Atlantic and Indian Oceans, *Atmospheric Chemistry and Physics*, *3*(5), 1377-1397.

McFiggans, G., P. Artaxo, U. Baltensperger, H. Coe, M. C. Facchini, et al. (2006), The effect of physical and chemical aerosol properties on warm cloud droplet activation, *Atmospheric Chemistry and Physics*, *6*(9), 2593-2649.

McKendry, I. G., J. P. Hacker, R. Stull, S. Sakiyama, D. Mignacca, et al. (2001), Long-range transport of Asian dust to the lower Fraser Valley, British Columbia, Canada, *Journal of Geophysical Research-Atmospheres*, *106*(D16), 18361-18370.

McNaughton, C. S., A. D. Clarke, S. G. Howell, M. Pinkerton, B. Anderson, et al. (2007), Results from the DC-8 Inlet Characterization Experiment (DICE): Airborne versus surface sampling of mineral dust and sea salt aerosols, *Aerosol Science and Technology*, *41*(2), 136-159.

Medina, J., A. Nenes, R. E. P. Sotiropoulou, L. D. Cottrell, L. D. Ziemba, et al. (2007), Cloud condensation nuclei closure during the International Consortium for Atmospheric Research on Transport and Transformation 2004 campaign: Effects of

size-resolved composition, *Journal of Geophysical Research-Atmospheres*, *112*(D10D31), doi:10.1029/2006jd007588.

Menon, S. (2004), Current uncertainties inassessing aerosol effects on climate, *Annual Review of Environment and Resources*, *29*, 1-30.

Menon, S., J. L. Brenguier, O. Boucher, P. Davison, A. D. Del Genio, et al. (2003), Evaluating aerosol/cloud/radiation process parameterizations with single-column models and Second Aerosol Characterization Experiment (ACE-2) cloudy column observations, *Journal of Geophysical Research-Atmospheres*, *108*(D24), doi:10.1029/2003jd003902.

Millet, D. B., A. H. Goldstein, J. D. Allan, T. S. Bates, H. Boudries, et al. (2004), Volatile organic compound measurements at Trinidad Head, California, during ITCT 2K2: Analysis of sources, atmospheric composition, and aerosol residence times, *Journal of Geophysical Research-Atmospheres*, *109*(D23S16), doi:10.1029/2003JD004026.

Ming, Y., V. Ramaswamy, P. A. Ginoux, L. W. Horowitz, and L. M. Russell (2005), Geophysical Fluid Dynamics Laboratory general circulation model investigation of the indirect radiative effects of anthropogenic sulfate aerosol, *Journal of Geophysical Research-Atmospheres*, *110*(D22), doi:10.1029/2005jd006161.

Mircea, M., M. C. Facchini, S. Decesari, F. Cavalli, L. Emblico, et al. (2005), Importance of the organic aerosol fraction for modeling aerosol hygroscopic growth and activation: a case study in the Amazon Basin, *Atmospheric Chemistry and Physics*, *5*(11), 3111-3126.

Montanez, R. A., and F. Garciagarcia (1993), Some urban and meteorological effects on the production of cloud condensation nuclei in Mexico City, *Atmosfera*, *6*(1), 39-49.

Nenes, A., R. J. Charlson, M. C. Facchini, M. Kulmala, A. Laaksonen, et al. (2002), Can chemical effects on cloud droplet number rival the first indirect effect?, *Geophysical Research Letters*, *29*(17), doi:10.1029/2002gl015295.

Park, R. J., D. J. Jacob, B. D. Field, R. M. Yantosca, and M. Chin (2004), Natural and transboundary pollution influences on sulfate-nitrate-ammonium aerosols in the United States: Implications for policy, *Journal of Geophysical Research-Atmospheres*, *109*(D15), doi:10.1029/2003JD004473.

Peltier, R. E., A. H. Hecobian, R. J. Weber, A. Stohl, E. L. Atlas, et al. (2008), Investigating the sources and atmospheric processing of fine particles from Asia and the northwestern United States measured during INTEX B, *Atmospheric Chemistry and Physics*, *8*(6), 1835-1853.

Penner, J. E., X. Q. Dong, and Y. Chen (2004), Observational evidence of a change in radiative forcing due to the indirect aerosol effect, *Nature*, *427*(6971), 231-234.

Penner, J. E., M. O. Andreae, H. Annegarn, L. Barrie, J. Feichter, et al. (2001), Aerosols, their direct and indirect effects, in *Climate Change 2001: The Scientific Basis*, edited by J. T. Houghton, Y. Ding, D. J. Griggs, M. Noguer, P. J. van der Linden, X. Dai, K. Maskell and C. A. Johnson, pp. 289-348, Cambridge University Press, New York.

Petters, M. D., and S. M. Kreidenweis (2007), A single parameter representation of hygroscopic growth and cloud condensation nucleus activity, *Atmospheric Chemistry and Physics*, *7*(8), 1961 - 1971.

Pfister, G. G., L. K. Emmons, D. P. Edwards, A. Arellano, G. Sachse, et al. (2010), Variability of springtime transpacific pollution transport during 2000-2006: The INTEX-B mission in the context of previous years, *Atmospheric Chemistry and Physics*, *10*(3), 1345-1359.

Pincus, R., and M. B. Baker (1994), Effect of precipitation on the albedo susceptibility of clouds in the marine boundary layer, *Nature*, *372*(6503), 250-252.

Posfai, M., J. R. Anderson, P. R. Buseck, and H. Sievering (1999), Soot and sulfate aerosol particles in the remote marine troposphere, *J. Geophys. Res.*, *104*(D17), 21685-21693.

Prospero, J. M., D. L. Savoie, and R. Arimoto (2003), Long-term record of nss-sulfate and nitrate in aerosols on Midway Island, 1981-2000: Evidence of increased (now decreasing?) anthropogenic emissions from Asia, *Journal of Geophysical Research-Atmospheres*, *108*(D1), doi:10.1029/2001JD001524.

Prospero, J. M., D. L. Savoie, R. T. Nees, R. A. Duce, and J. Merrill (1985), Particulate sulfate and nitrate in the boundary layer over the north Pacific Ocean, *Journal of Geophysical Research-Atmospheres*, *90*(ND6), 10586-10596.

Quinn, P. K., D. S. Covert, T. S. Bates, V. N. Kapustin, D. C. Ramseybell, et al. (1993), Dimethylsulfide cloud condensation nuclei climate system - relevant size resolved

measurements of the chemical and physical properties of atmospheric aerosol particles, *Journal of Geophysical Research-Atmospheres*, *98*(D6), 10411-10427.

Radke, L. F., and P. V. Hobbs (1969), Measurement of cloud condensation nuclei, light scattering coefficient, sodium-containing particles, and Aitken nuclei in Olympic Mountains of Washington, *Journal of the Atmospheric Sciences*, *26*(2), 281-288.

Raga, G. B., D. Baumgardner, T. Castro, A. Martinez-Arroyo, and R. Navarro-Gonzalez (2001), Mexico City air quality: A qualitative review of gas and aerosol measurements (1960-2000), *Atmospheric Environment*, *35*(23), 4041-4058.

Reid, J. S., T. F. Eck, S. A. Christopher, P. V. Hobbs, and B. Holben (1999), Use of the Angstrom exponent to estimate the variability of optical and physical properties of aging smoke particles in Brazil, *Journal of Geophysical Research-Atmospheres*, *104*(D22), 27473-27489.

Rissler, J., E. Swietlicki, J. Zhou, G. Roberts, M. O. Andreae, et al. (2004), Physical properties of the sub-micrometer aerosol over the Amazon rain forest during the wet-to-dry season transition - comparison of modeled and measured CCN concentrations, *Atmospheric Chemistry and Physics*, *4*(8), 2119-2143.

Rissman, T. A., T. M. VanReken, J. Wang, R. Gasparini, D. R. Collins, et al. (2006), Characterization of ambient aerosol from measurements of cloud condensation nuclei during the 2003 Atmospheric Radiation Measurement Aerosol Intensive Observational Period at the Southern Great Plains site in Oklahoma, *Journal of Geophysical Research-Atmospheres*, *111*(D05S11), doi:10.1029/2004jd005695.

Roberts, G., G. Mauger, O. Hadley, and V. Ramanathan (2006), North American and Asian aerosols over the eastern Pacific Ocean and their role in regulating cloud condensation nuclei, *Journal of Geophysical Research-Atmospheres*, *111*(D13), doi:10.1029/2005jd006661.

Roberts, G. C., and A. Nenes (2005), A continuous-flow streamwise thermal-gradient CCN chamber for atmospheric measurements, *Aerosol Science and Technology*, *39*(3), 206-221.

Roberts, G. C., P. Artaxo, J. C. Zhou, E. Swietlicki, and M. O. Andreae (2002), Sensitivity of CCN spectra on chemical and physical properties of aerosol: A case study from the Amazon Basin, *Journal of Geophysical Research-Atmospheres*, *107*(D20), doi:10.1029/2001jd000583.

Rose, D., S. S. Gunthe, E. Mikhailov, G. P. Frank, U. Dusek, et al. (2008), Calibration and measurement uncertainties of a continuous-flow cloud condensation nuclei counter (DMT-CCNC): CCN activation of ammonium sulfate and sodium chloride aerosol particles in theory and experiment, *Atmospheric Chemistry and Physics*, *8*(5), 1153-1179.

Ryerson, T. B., M. P. Buhr, G. J. Frost, P. D. Goldan, J. S. Holloway, et al. (1998), Emissions lifetimes and ozone formation in power plant plumes, *Journal of Geophysical Research-Atmospheres*, *103*(D17), 22569-22583.

Salcedo, D., T. B. Onasch, K. Dzepina, M. R. Canagaratna, Q. Zhang, et al. (2006), Characterization of ambient aerosols in Mexico City during the MCMA-2003 campaign with aerosol mass spectrometry: Results from the CENICA Supersite, *Atmospheric Chemistry and Physics*, *6*(4), 925-946.

Schwartz, S. E. (1996), The Whitehouse effect - shortwave radiative forcing of climate by anthropogenic aerosols: An overview, *Journal of Aerosol Science*, *27*(3), 359-382.

Seinfeld, J. H., and S. N. Pandis (2006), *Atmospheric Chemistry and Physics*, 2nd Ed., John Wiley & Sons, Inc., Hoboken, NJ.

Shantz, N. C., W. R. Leaitch, and P. F. Caffrey (2003), Effect of organics of low solubility on the growth rate of cloud droplets, *Journal of Geophysical Research-Atmospheres*, *108*(D5), doi:10.1029/2002jd002540.

Singh, H. B., W. H. Brune, J. H. Crawford, F. Flocke, and D. J. Jacob (2009), Chemistry and transport of pollution over the Gulf of Mexico and the Pacific: Spring 2006 INTEX-B campaign overview and first results, *Atmospheric Chemistry and Physics*, *9*(7), 2301-2318.

SMADF (2002), Inventario de emisiones a la atmósfera. Zona Metropolitana del Valle de Mexico, 2000, Secretaria del Medio Ambiente del Distrito Federal, Mexico.

Snider, J. R., and J. L. Brenguier (2000), Cloud condensation nuclei and cloud droplet measurements during ACE-2, *Tellus Series B-Chemical and Physical Meteorology*, *52*(2), 828-842.

Snider, J. R., S. Guibert, J. L. Brenguier, and J. P. Putaud (2003), Aerosol activation in marine stratocumulus clouds: 2. Kohler and parcel theory closure studies, *Journal of Geophysical Research-Atmospheres*, *108*(D15), doi:10.1029/2002jd002692.

Streets, D. G., and S. T. Waldhoff (2000), Present and future emissions of air pollutants in China: SO2, NOx, and CO, *Atmospheric Environment*, *34*(3), 363-374.

Streets, D. G., Q. Zhang, L. T. Wang, K. B. He, J. M. Hao, et al. (2006), Revisiting China's CO emissions after the Transport and Chemical Evolution over the Pacific (TRACE-P) mission: Synthesis of inventories, atmospheric modeling, and observations, *Journal of Geophysical Research-Atmospheres*, *111*(D14), doi:10.1029/2006JD007118.

Streets, D. G., T. C. Bond, G. R. Carmichael, S. D. Fernandes, Q. Fu, et al. (2003), An inventory of gaseous and primary aerosol emissions in Asia in the year 2000, *Journal of Geophysical Research-Atmospheres*, *108*(D21), doi:10.1029/2002JD003093.

Stroud, C. A., A. Nenes, J. L. Jimenez, P. F. DeCarlo, J. A. Huffman, et al. (2007), Cloud activating properties of aerosol observed during CELTIC, *Journal of the Atmospheric Sciences*, *64*(2), 441-459.

Swietlicki, E., J. C. Zhou, D. S. Covert, K. Hameri, B. Busch, et al. (2000), Hygroscopic properties of aerosol particles in the northeastern Atlantic during ACE-2, *Tellus Series B-Chemical and Physical Meteorology*, *52*(2), 201-227.

Swietlicki, E., H. C. Hansson, K. Hameri, B. Svenningsson, A. Massling, et al. (2008), Hygroscopic properties of submicrometer atmospheric aerosol particles measured with H-TDMA instruments in various environments - a review, *Tellus Series B-Chemical and Physical Meteorology*, *60*(3), 432-469.

Tang, I. N. (1976), Phase transformation and growth of aerosol particles composed of mixed salts, *Journal of Aerosol Science*, *7*(5), 361-371.

Tang, I. N., and H. R. Munkelwitz (1977), Aerosol growth studies- III ammonium bisulfate aerosols in a moist atmosphere, *Journal of Aerosol Science*, *8*(5), 321-330.

Tang, I. N., and H. R. Munkelwitz (1994), Water activities, densities, and refractive indexes of aqueous sulfates and sodium nitrate droplets of atmospheric importance, *Journal of Geophysical Research-Atmospheres*, *99*(D9), 18801-18808.

Tomlinson, J. M., R. Li, and D. R. Collins (2007), Physical and chemical properties of the aerosol within the southeastern Pacific marine boundary layer, *J. Geophys. Res.*, *112*(D12), doi:10.1029/2006jd007771.

Twomey, S. (1974), Pollution and planetary albedo, *Atmospheric Environment*, *8*(12), 1251-1256.

Twomey, S. (1975), Comparison of constrained linear inversion and an iterative nonlinear algorithm applied to indirect estimation of particle-size distributions, *Journal of Computational Physics*, *18*(2), 188-200.

Twomey, S. (1977), Influence of pollution on shortwave albedo of clouds, *Journal of the Atmospheric Sciences*, *34*(7), 1149-1152.

Twomey, S., and Wojciechowski.T. A. (1969), Observations of geographical variation of cloud nuclei, *Journal of the Atmospheric Sciences*, *26*(4), 684-688.

Twomey, S., and K. A. Davidson (1970), Automatic observations of cloud nucleus concentrations, *Journal of the Atmospheric Sciences*, *27*(7), 1056-1059.

Vakeva, M., K. Hameri, and P. P. Aalto (2002a), Hygroscopic properties of nucleation mode and Aitken mode particles during nucleation bursts and in background air, *Journal of Geophysical Research-Atmospheres*, *107*(D19), doi:10.1029/2000jd000176.

Vakeva, M., M. Kulmala, F. Stratmann, and K. Hameri (2002b), Field measurements of hygroscopic properties and state of mixing of nucleation mode particles, *Atmospheric Chemistry and Physics*, *2*(1), 55-66.

VanCuren, R. A. (2003), Asian aerosols in North America: Extracting the chemical composition and mass concentration of the Asian continental aerosol plume from long-term aerosol records in the western United States, *Journal of Geophysical Research-Atmospheres*, *108*(D20), doi:10.1029/2003JD003459.

VanReken, T. M., T. A. Rissman, G. C. Roberts, V. Varutbangkul, H. H. Jonsson, et al. (2003), Toward aerosol/cloud condensation nuclei (CCN) closure during CRYSTAL-FACE, *Journal of Geophysical Research-Atmospheres*, *108*(D20), doi:10.1029/2003jd003582.

Vaughan, J. K., C. Claiborn, and D. Finn (2001), April 1998 Asian dust event over the Columbia Plateau, *Journal of Geophysical Research-Atmospheres*, *106*(D16), 18381-18402.

Wang, J., Y. N. Lee, P. H. Daum, J. Jayne, and M. L. Alexander (2008), Effects of aerosol organics on cloud condensation nucleus (CCN) concentration and first indirect aerosol effect, *Atmospheric Chemistry and Physics*, *8*(21), 6325-6339.

Wood, R., D. Johnson, S. Osborne, M. O. Andreae, B. Bandy, et al. (2000), Boundary layer and aerosol evolution during the 3rd Lagrangian experiment of ACE-2, *Tellus Series B-Chemical and Physical Meteorology*, *52*(2), 401-422.

Yienger, J. J., M. Galanter, T. A. Holloway, M. J. Phadnis, S. K. Guttikunda, et al. (2000), The episodic nature of air pollution transport from Asia to North America, *Journal of Geophysical Research-Atmospheres*, *105*(D22), 26931-26945.

Zhang, Q., D. G. Streets, G. R. Carmichael, K. B. He, H. Huo, et al. (2009), Asian emissions in 2006 for the NASA INTEX-B mission, *Atmospheric Chemistry and Physics*, *9*(14), 5131-5153.

Zhang, R., A. F. Khalizov, J. Pagels, D. Zhang, H. Xue, et al. (2008), Variability in morphology, hygroscopicity, and optical properties of soot aerosols during atmospheric processing, *Proceedings of the National Academy of Sciences*, *105*(30), 10291-10296.

Zhou, J. C., E. Swietlicki, O. H. Berg, P. P. Aalto, K. Hameri, et al. (2001), Hygroscopic properties of aerosol particles over the central Arctic Ocean during summer, *Journal of Geophysical Research-Atmospheres*, *106*(D23), 32111-32123.

Zieman, J. J., J. L. Holmes, D. Connor, C. R. Jensen, W. H. Zoller, et al. (1995), Atmospheric aerosol trace element chemistry at Mauna Loa observatory .1. 1979-1985, *Journal of Geophysical Research-Atmospheres*, *100*(D12), 25979-25994.

APPENDIX A

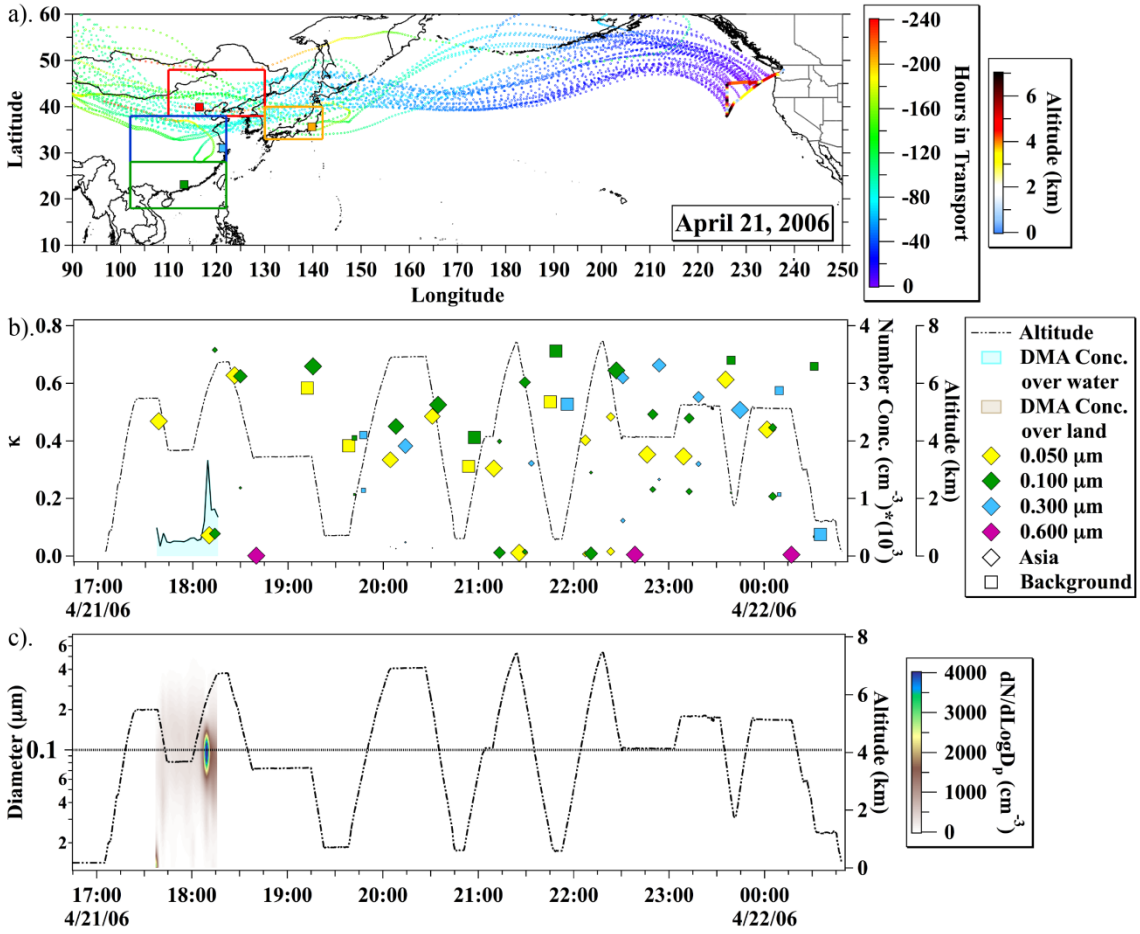

A-1. An overview of the DMA/TDMA data from the April 21, 2006, research flight. In figure (a), the color of the flight path indicates the aircraft altitude, and the backtrajectory marker color indicates the hours in transport for the aerosol. In figure (b), the altitude is indicated by the dashed line, the marker color indicates the dry diameter size, the marker shape indicates the source, and the integrated concentration is indicated by the blue, measured over water, and brown shading, measured over land. The measurement time is indicated in (c). In figure (c), altitude is again noted by the dashed line, the diameter of the aerosol is indicated on the y-axis, and the color of the shading indicates the magnitude of the concentration. The rest of the figures in Appendix A will follow this format. The C-130 flew towards the southwest, turned to the north, then east, and finally flew towards the northeast returning to Paine Field. The DMA failed shortly after takeoff on this research flight.

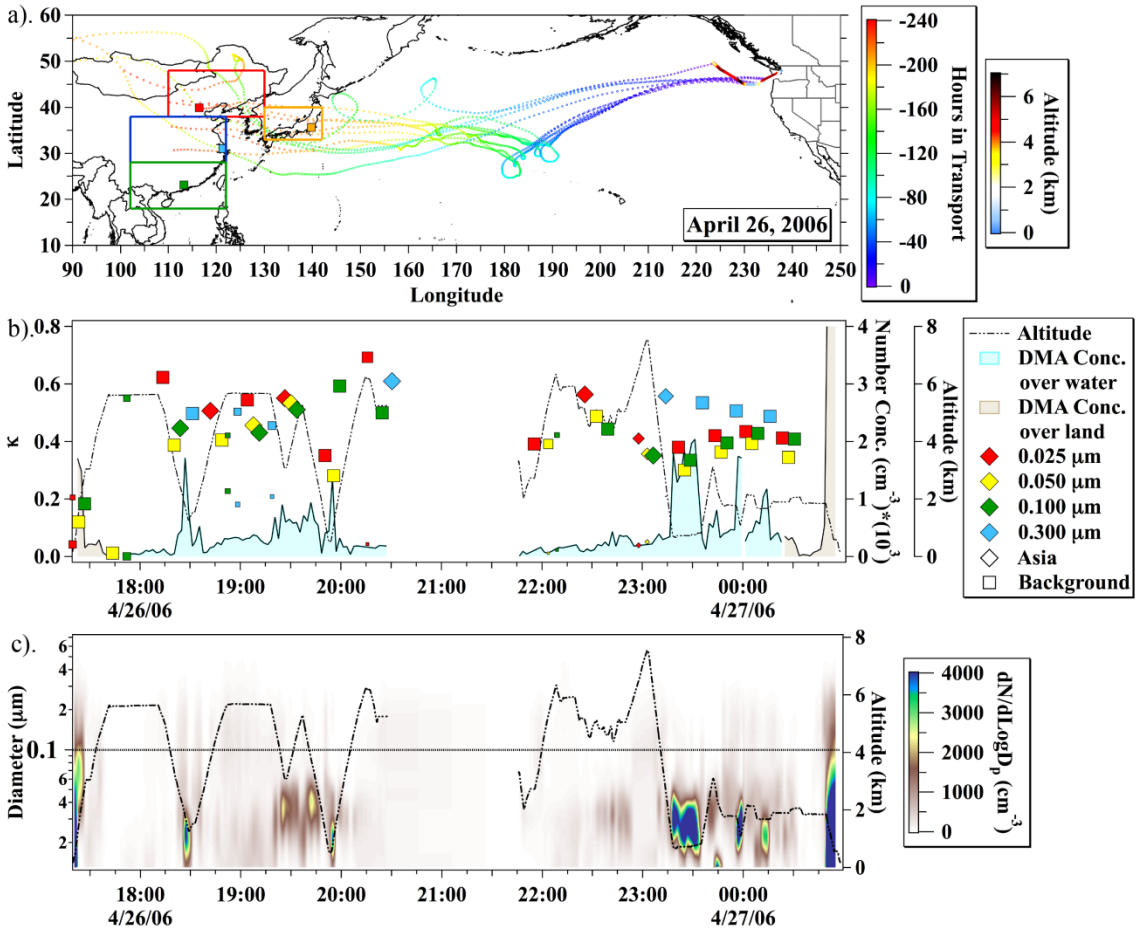

A-2. On April 26, 2006, the C-130 flew the same flight path out and back with the only difference being altitude. The C-130 lost the GPS signal midway through the flight.

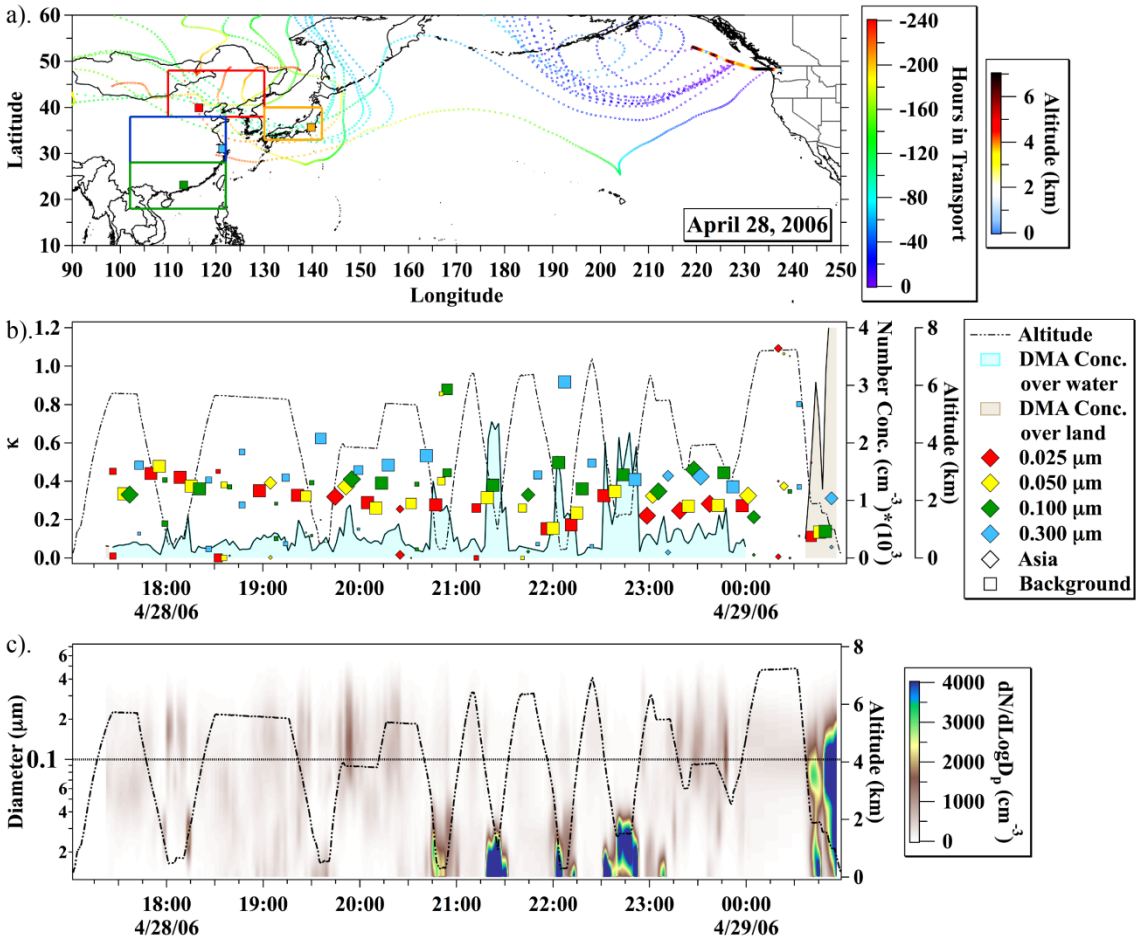

A-3. On April 28, 2006, the C-130 again flew an out and back pattern with the only difference being altitude. Within the marine boundary layer (MBL), nucleation was observed between 21:00 and 23:00 UTC. In addition, very hygroscopic aerosol with values close to the expected values for sulfuric acid was observed within the MBL at 21:00 and 22:00 UTC. The y-axis scale for □ in figure (b) was increased from 0.8 to 1.2

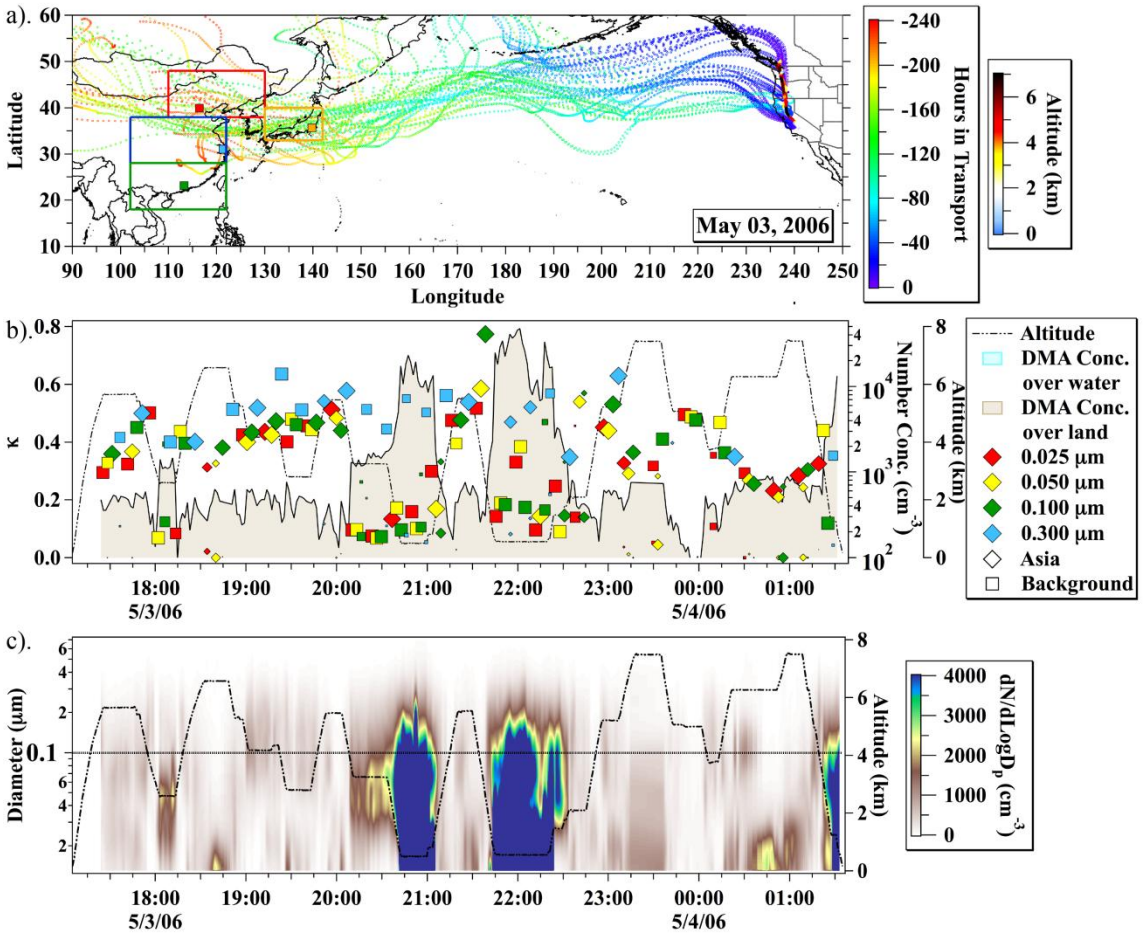

A-4. On May 03, 2006, the C-130 flew south along the Cascade Range and through the California Central Valley and return along the same flight path. Atmospheric profiles and low level flights were conducted over Sacramento at 20:45 and 22:00 UTC. A maximum number concentration of 47,264 cm^{-3} was measured near Sacramento and the number distribution was dominated by small particles. An aged aerosol layer was observed between 4 and 6 km. In figure (b) the y-axis for the number concentration is logarithmically spaced.

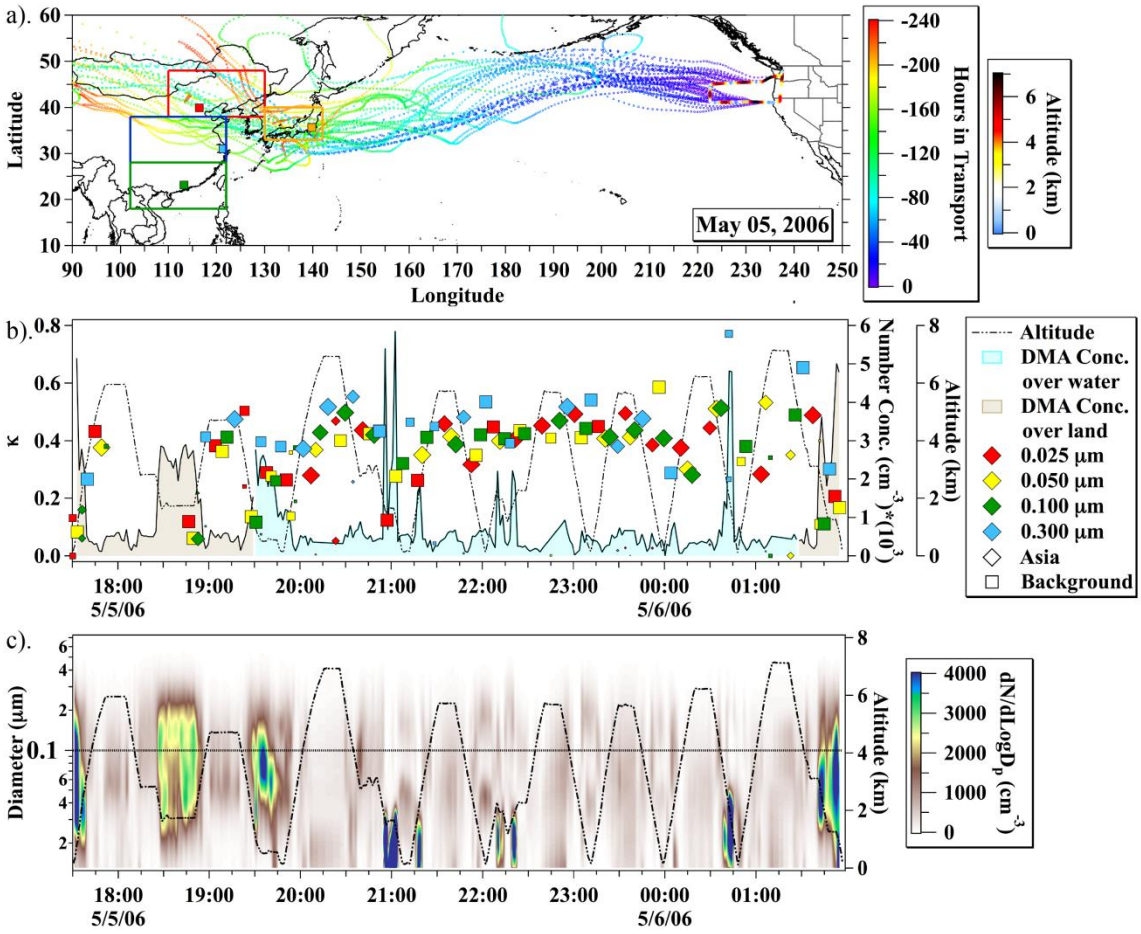

A-5. On May 05, 2006, the C-130 flew south along the Cascade Range before turning to the west towards the Pacific Ocean. Within the marine boundary layer (MBL) nucleation was observed between 21:00 and 22:00 UTC. However, in this instance the nucleation was only observed near the top of the MBL at 1.5 km.

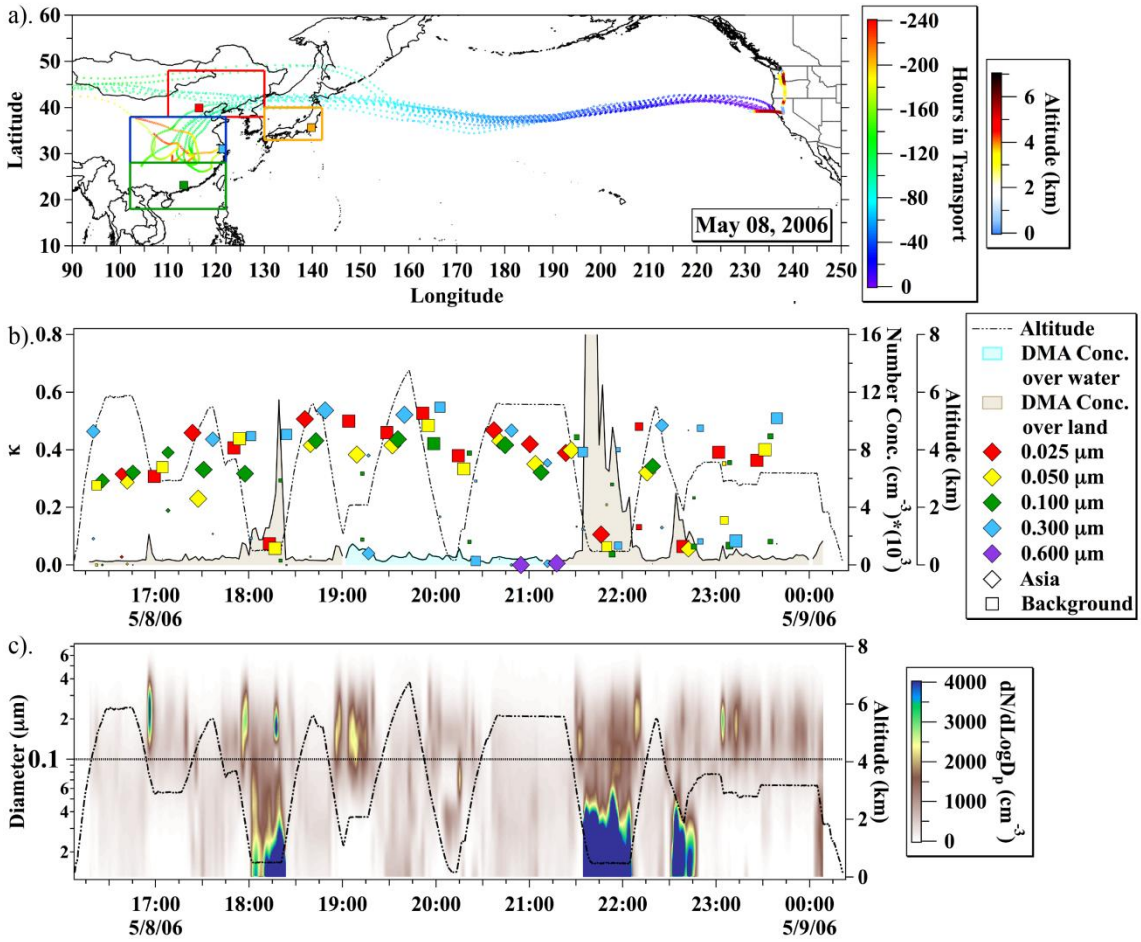

A-6. On May 08, 2006, the C-130 flew south along the Cascade Range and upon reaching Sacramento, CA turned to the west towards the Pacific Ocean. The aircraft returned upon the same path with only the altitude changing. The two profiles of the California Central Valley near Sacramento at 18:00 UTC (11:00 PT) and 21:45 UTC (14:45 PT) show the concentration increasing from 11500 cm^{-3} to 21000 cm^{-3}. An aged aerosol layer with a geometric mean diameter of the distribution greater than 0.100 µm was observed between 3 and 5 km.

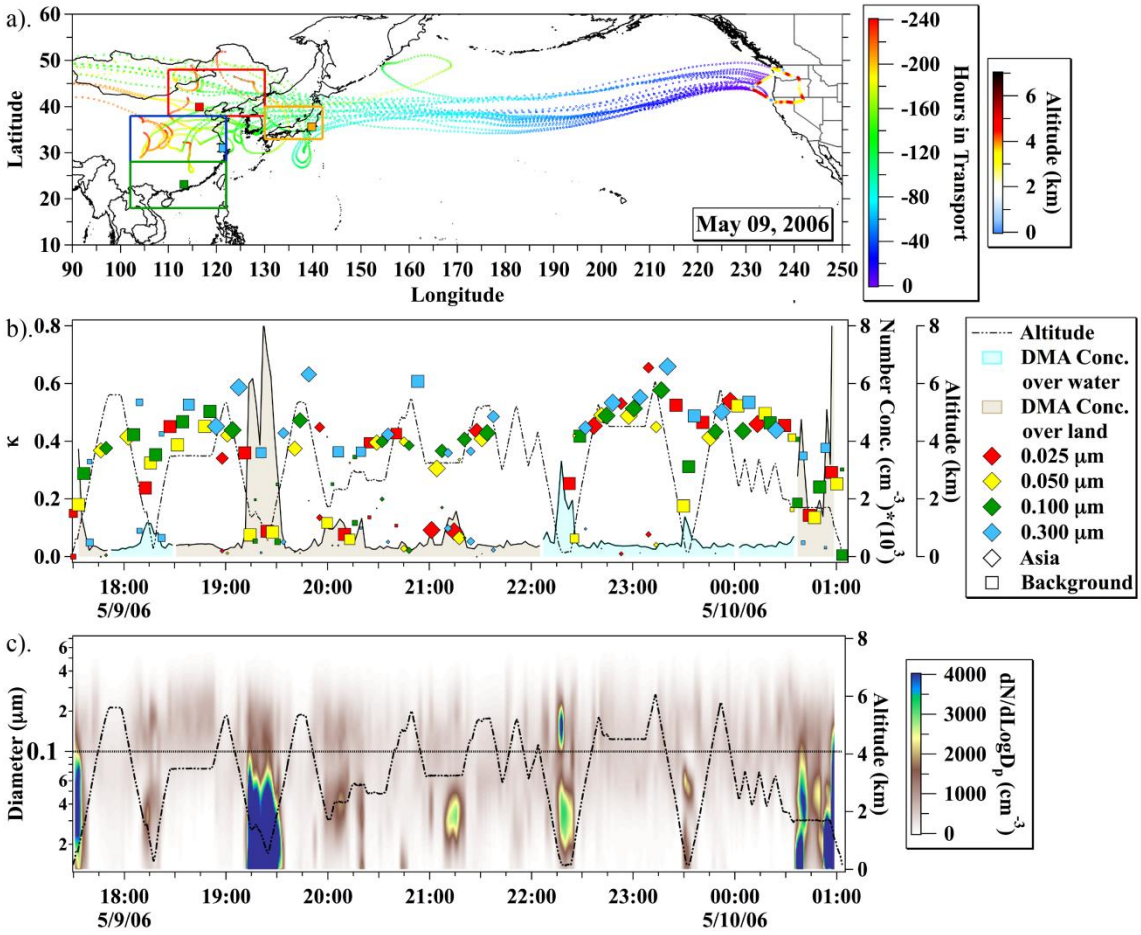

A-7. On May 09, 2006, after takeoff the C-130 flew northwest towards the Olympic Peninsula before turning around and flying back towards the Columbian Basin. Upon reach Richland, WA at 19:15 UTC an atmospheric profile was conducted. The C-130 then headed to the south and upon reaching Nevada turned back towards the Pacific Ocean. An aged aerosol layer was observed between 2 and 5 km.

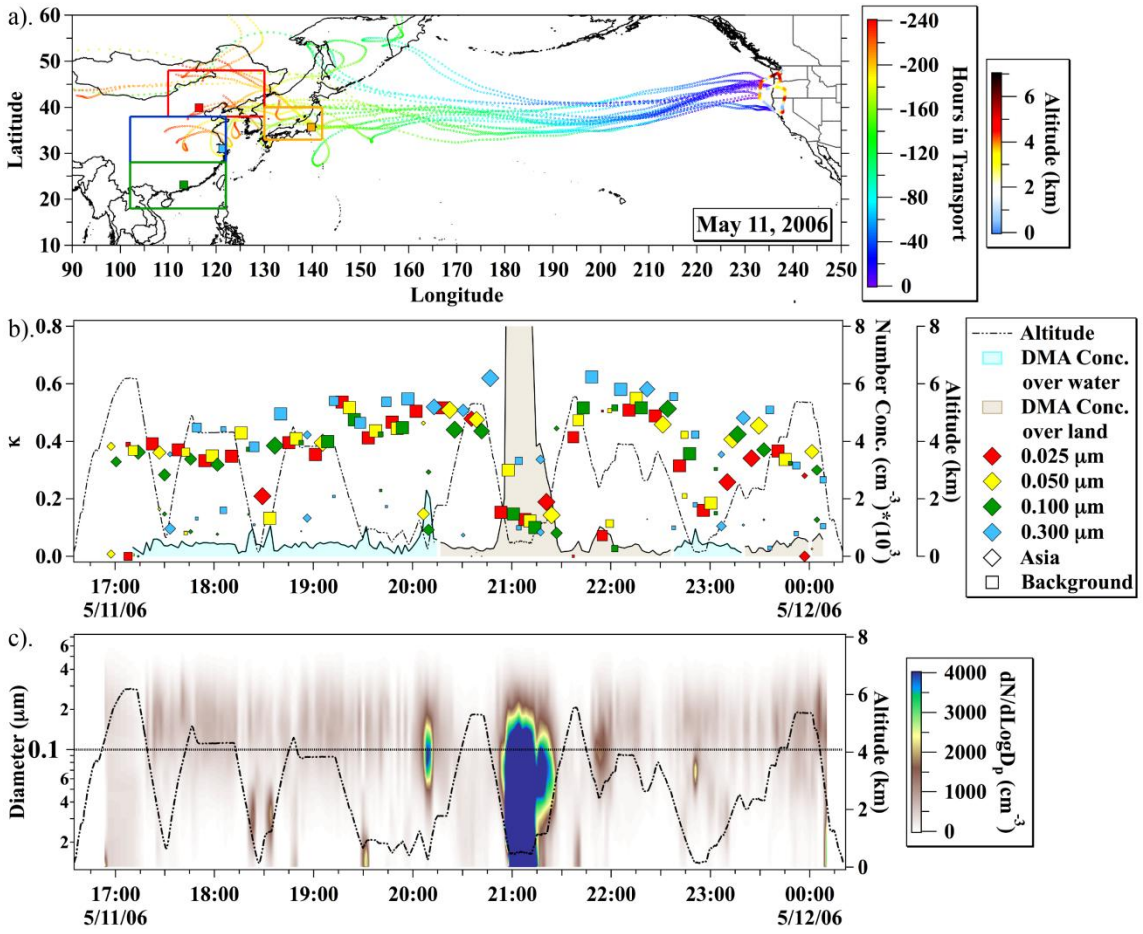

A-8. On May 11, 2006, the C-130 flew southwest towards the Pacific Ocean, then turned towards the south, and the southeast towards California. Just northwest of Sacramento an atmospheric profile was conducted at 21:00 UTC. The profile measured a maximum number concentration of 23,085 cm^{-3}. The C-130 then flew to the north along the Cascade Range. Over central Oregon the aircraft briefly jutted out over the Pacific Ocean before continuing back to Paine Field.

VITA

Name: Jason Michael Tomlinson

Address: Pacific Northwest National Laboratory

902 Battelle Boulevard

P.O. Box 999, MSIN: K9-24

Richland, WA 99352

Email Address: jason.tomlinson@pnl.gov

Education: B.S., Physics and Meteorology, Valparaiso University, 2002